University of Alberta

ELECTROCHEMICAL CHARACTERIZATION OF HYDROGEN EFFECTS ON THE PASSIVITY OF CARBON STEEL AND MICRO-ALLOYED STEEL

by

XIN PANG

A thesis submitted to the Faculty of Graduate Studies and Research in partial fulfillment of the requirements for the degree of Master of Science

In

MATERIALS ENGINEERING

Department of Chemical and Materials Engineering

Edmonton, Alberta

Fall 2003

National Library of Canada
Bibliothèque nationale du Canada

Acquisitions and Bibliographic Services
Acquisisitons et services bibliographiques

395 Wellington Street
Ottawa ON K1A 0N4
Canada

395, rue Wellington
Ottawa ON K1A 0N4
Canada

Your file Votre référence
ISBN: 0-612-87855-4
Our file Notre référence
ISBN: 0-612-87855-4

The author has granted a non-exclusive licence allowing the National Library of Canada to reproduce, loan, distribute or sell copies of this thesis in microform, paper or electronic formats.

L'auteur a accordé une licence non exclusive permettant à la Bibliothèque nationale du Canada de reproduire, prêter, distribuer ou vendre des copies de cette thèse sous la forme de microfiche/film, de reproduction sur papier ou sur format électronique.

The author retains ownership of the copyright in this thesis. Neither the thesis nor substantial extracts from it may be printed or otherwise reproduced without the author's permission.

L'auteur conserve la propriété du droit d'auteur qui protège cette thèse. Ni la thèse ni des extraits substantiels de celle-ci ne doivent être imprimés ou aturement reproduits sans son autorisation.

In compliance with the Canadian Privacy Act some supporting forms may have been removed from this dissertation.

Conformément à la loi canadienne sur la protection de la vie privée, quelques formulaires secondaires ont été enlevés de ce manuscrit.

While these forms may be included in the document page count, their removal does not represent any loss of content from the dissertation.

Bien que ces formulaires aient inclus dans la pagination, il n'y aura aucun contenu manquant.

Canadä

University of Alberta

Faulty of Graduate Studies and Research

The undersigned certify that they have read, and recommend to the Faculty of Graduate Studies and Research for acceptance, a thesis entitled Electrochemical Characterization of Hydrogen Effects on the Passivity of Carbon and Micro-alloyed Steels submitted by Xin Pang in partial fulfillment of the requirements for the degree of Master of Science in Materials Engineering.

Date: Aug. 28, 2003

University of Alberta

Library Release Form

Name of Author: Xin Pang

Title of Thesis: Electrochemical Characterization of Hydrogen Effects on the Passivity of Carbon Steel and Micro-Alloyed Steel

Degree: Master of Science

Year this Degree Granted: 2003

Permission is hereby granted to the University of Alberta Library to reproduce single copies of this thesis and to lend or sell such copies for private, scholarly or scientific research purposes only.

The author reserves all other publication and other rights in association with copyright in the thesis, and except as herein before provided, neither the thesis nor any substantial portion thereof may be printed or otherwise reproduced in any material form whatever without the author's prior written permission.

Xin Pang

151 John Street South, Apartment 9#
Hamilton, ONT L8N 2C3

Date: Aug. 28, 2003

Abstract

The effects of hydrogen injected into X70 micro-alloyed steel and A516-70 carbon steel on the passivity of these metals have been investigated by means of *in situ* electrochemical and photoelectrochemical measurements.

Experimental results show that hydrogen decreases the stability and thickness of the passive films on X70 steel, and thereby promotes its susceptibility to localized corrosion. An inconsistence of electrochemical and photoelectrochemical responses was firstly identified for the passive films on X70 steel, implying that the effects of hydrogen on the optical and electronic properties of the passive film are very complicated and are still far from fully understood. It was observed that elastic tensile stresses facilitate the anodic dissolution process, and increase the donor density of the passive films on A516-70 steel, resulting in a more negative open circuit potential and accelerated ion transfer rate of the steel, thereby produce a decreased corrosion resistance.

Acknowledgements

I hereby sincerely acknowledge the support of many people without whom I would never have been able to complete this thesis.

First, I am greatly indebted to my supervisor, Dr. Jingli Luo, who has gone beyond a mere thesis supervisor: by providing me with intellectual challenges, constant encouragements, and an appropriate research environment.

Yimin Zeng and Jianguo Yu, my group mates, deserve more than the traditional "thanks". They have generously offered invaluable help during my study and research. And I am especially grateful to Yimin Zeng for his full and selfless support in difficult times, and for his instructive comments and advices in writing this thesis.

I would also thank Yin Huang, and all the other group mates in the lab, for their friendship and for rescuing me whenever I needed help.

Many thanks to Adeyinka Adeleke who helped improve the English in this thesis.

Last but not least, I thank my love husband, Chao Shi, who is the person who has always been there for me. I gratefully thank him for his unconditional trust in me, and for putting up with me during stressful times.

I am very thankful for the financial support from the Natural Science and Engineering Research Council of Canada (NSERC), Syncrude Canada Ltd., Nova Chemicals, Dow Chemicals, and IPSCO.

Table of Contents

Chapter 1 Literature Review 1

1.1 Introduction 1

1.2 Hydrogen in Metals and its Resultant Deterioration 1

1.2.1 Entry of Hydrogen into Metals and Alloys 2

1.2.1.1 Entry of Hydrogen from the Gas Phase 2

1.2.1.2 Entry of Hydrogen from the Liquid Phase 3

1.2.1.3 Promoters and Inhibitors of Hydrogen Entry into Metals 4

1.2.2 State of Hydrogen in Metals and Alloys 5

1.2.3 Hydrogen Degradation of Metals and Alloys 7

1.2.3.1 Effects of Hydrogen upon Mechanical Properties 7

1.2.3.2 Effects of Hydrogen upon Corrosion Properties 9

1.3 Passive Films on Iron, Carbon Steel and Micro-Alloyed Steel 10

1.3.1 Fundamentals of Passivity 10

1.3.2 The Nature of Passive Films on Iron, Carbon Steel and Micro-Alloyed Steel 12

1.3.2.1 Iron Oxides 13

1.3.2.2 Passivity of Pure Iron 14

1.3.2.2.1 Structure Models of the Passive Film on Iron 14

1.3.2.2.2 Recent Studies on the Nature of the Passive Film on Iron 16

1.3.2.3 Passivity of Carbon Steel and Micro-Alloyed Steel 18

1.3.3 Effects of Hydrogen on Passive Films 19

1.4 Electronic Properties of Passive Films 20

1.4.1 Fundamentals of Semiconductor Electrochemistry 21

1.4.1.1 Energy Band Model 21

1.4.1.2 Semiconductor-Electrolyte Interface 22

1.4.1.2 Mott-Schottky Method 24

1.4.2 Electronic Properties of Passive Films 25

1.4.3 Effects of Hydrogen on the Electronic Properties of Passive Films 27

1.5 Summary 28

References 29

Chapter 2 Effects of Hydrogen on Composition and Structure of Passive Films.... 38
2.1 Introduction.... 38
2.2 Experimental Details.... 39
2.2.1 Materials and Solutions.... 39
2.2.2 Electrochemical Cell Setup.... 39
2.2.3 Electrochemical Measurements.... 40
2.2.3.1 Open Circuit Potential Decay.... 40
2.2.3.2 Pitting Potential Measurements.... 40
2.2.3.3 Galvanostatic Cathodic Reduction.... 40
2.2.3.4 AC Impedance Measurements.... 41
2.3 Main Results and Discussion.... 41
2.3.1 Open Circuit Potential Decay.... 41
2.3.2 Pitting Potential Measurements.... 42
2.3.3 Cathodic Current Reduction of Passive Films.... 45
2.3.4 AC Impedance Measurements.... 51
2.4 Summary.... 57
References.... 58

Chapter 3 Effects of Hydrogen on the Electronic Properties of the Passive Films.. 60
3.1 Introduction.... 60
3.2 Basics of Photoelectrochemical Spectroscopy Technique.... 61
3.3 Experimental Details.... 62
3.3.1 Materials and Solutions.... 62
3.3.2 Electrochemical Cell Setup.... 62
3.4 Main Results and Discussion.... 63
3.4.1 Photocurrents of Passive Films on X70 Micro-Alloyed Steel.... 63
3.4.2 Effects of Hydrogen on Passive Currents and Photocurrents of the Passive Films.... 67
3.5 Summary.... 74
References.... 75

Chapter 4 Effects of Elastic Stress and Hydrogen on Passivity of Carbon Steel..... 77
4.1 Introduction..... 77
4.2 Experimental Details..... 78
4.2.1 Materials and Solutions..... 78
4.2.2 Tensile Tests..... 79
4.2.3 Electrochemical Measurements..... 80
4.3 Main Results and Discussions..... 81
4.3.1 Effects of Elastic Tensile Stress on Anodic Dissolution..... 81
4.3.2 Effects of Elastic Tensile Stress on Passivity..... 85
4.3.2.1 Influences of the Elastic Tensile Stress Applied Before Passivation..... 86
4.3.2.2 Influences of the Elastic Tensile Stress Applied During Passivation..... 88
4.3.2.3 Influences of Elastic Tensile Stress on Passivity..... 89
4.3.3 Effects of Elastic Tensile Stress and Hydrogen on Passivity..... 91
4.3.3.1 Influences of the Elastic Tensile Stress Applied during Passivation..... 91
4.3.3.2 Influences of the Elastic Tensile Stress Applied During Passivation..... 93
4.3.3.3 Influences of Elastic Tensile Stress and Hydrogen on Passivity..... 94
4.4 Summary..... 95
References..... 96

Chapter 5 Conclusions and Future Work..... 98
5.1 Main Conclusions..... 98
5.2 Suggestions for Future Work..... 98

List of Tables

Chapter 1

Table 2-1. Theoretical thinning rates for the cathodic reductions of the passive films on iron and the values for density and molecular weight used for the calculation..... 49

Table 2-2. The cathodic charge consumed for reduction of the passive film formed under different conditions and corresponding calculated thickness. 51

Table 2-3. The values of R_s, R_f, C_f, CPE, R_{ct} for the passive films on specimens charged with various current densities. 54

Table 2-4. The values of R_s, R_f, C_f, CPE, R_{ct} for the passive films formed at different potentials without hydrogen charging..... 54

Table 2-5. The values of R_s, R_f, C_f, CPE, R_{ct} for the passive films formed at different potentials on the specimens charged with 10 A/m^2. 55

Chapter 4

Table 4-1. A516-70/A516-70M-01 standard specification for pressure vessel plates, carbon steel, for moderate- and lower-temperature service (Grade 70). 78

Table 4-2. The fitted values of R_s, R_p and CPE for different applied stresses..... 84

Table 4-3. Calculated N_D for the passive films formed under different stresses. 88

Table 4-4. Calculated N_D for the passive films on hydrogen-charged (80 A/m^2) specimens under different stresses. 93

List of Figures

Chapter 1

Figure 1-1. A schematic view of energy relations in gas-metal equilibrium for weak hydrogen traps..... 6

Figure 1-2. Hypothetical polarization diagram for a active-passive system with active, passive and transpassive regions..... 11

Figure 1-3. Schematic diagram of the energy levels of (a) an n-type semiconductor and (b) a p-type semiconductor. 22

Figure 1-4. Effect of varying the applied potential U on the band edges in the interior of an n-type semiconductor: (a) $U > U_{fb}$ (b) $U = U_{fb}$ (c) $U < U_{fb}$..... 23

Chapter 2

Figure 2-1. Schematic illustration of the electrochemical cell setup. 39

Figure 2-2. The variations of the U_{OC} with time for uncharged and charged specimens passivated at 0.6V for 2 hours..... 42

Figure 2-3. Polarization curve of X70 micro-alloyed steel in 0.3 M H_3BO_3 + 0.075 M $Na_2B_4O_7 \cdot 10H_2O$ buffer solution. The scan rate was controlled at 0.001 V/s. 43

Figure 2-4(a). Changes of U_p with the concentration of chloride ions in solution for hydrogen charged and uncharged specimens..... 44

Figure 2-4(b). Plots of U_p vs. $\ln([Cl^-])$..... 44

Figure 2-5. Galvanostatic reduction curves of specimens passivated at 0.2 V for 2 hours by a cathodic current of 0.1 A/m^2..... 46

Figure 2-6. Galvanostatic reduction curves of specimens passivated at 0.6 V for 2 hours by a cathodic current of 0.1 A/m^2..... 46

Figure 2-7. Schematic model for galvanostatic reduction of Fe_2O_3 in borate buffer of pH 8.4.[35] 47

Figure 2-8. Galvanostatic reduction curve for the uncharged specimen passivated at 0.2V for 2 hours. The specimen was reduced at 0.1 A/m^2 in the solution of pH 8.4. 49

Figure 2-9. Nyquist plots of impedance spectra measured (in points) at 0.2V and their simulated results (in lines). 52

Figure 2-10. Equivalent circuit[42] for the fitting of impedance data. 52
Figure 2-11. Charge transfer resistances of passive films on charged and uncharged specimen as a function of film formation potentials. 55
Figure 2-12. Ion diffusion resistances of passive films on charged and uncharged specimens as a function of film formation potentials. 55
Figure 2-13. Dependence of $1/C_f$ on the film formation potential for uncharged specimen and the one charged at 10 A/m^2. 56

Chapter 3

Figure 3-1. Schematic illustration of the photoelectrochemical excitation process[15] 61
Figure 3-2. Schematic illustration of the photoelectrochemical experimental setup. 63
Figure 3-3. Photocurrent spectra of the passive films formed on uncharged specimens at 0.6 V after different passivation time. 64
Figure 3-4. The time dependence of the photocurrent peak and shoulder values for the passive films formed on uncharged specimen at 0.6V. 65
Figure 3-5. Evaluation of E_g of the passive films on X70 steel formed at 0.6 V after different passivation time. 66
Figure 3-6. Changes of the passive current density with time for the passive film formed at 0.6 V. After 26.5 hours passivation, hydrogen charging was started and then stopped 1.5 hours later. 68
Figure 3-7. Photocurrent spectra of passive films formed at 0.6 V. After 26.5 hours passivation, hydrogen charging was started and then stopped 1.5 hours later. 69
Figure 3-8. Variations of the photocurrent peak and shoulder values with time. After 26.5 hours passivation, hydrogen charging was started and then stopped 1.5 hours later. 70
Figure 3-9. Evaluation of the E_g of the passive films formed at 0.6 V. After 26.5 hours passivation, hydrogen charging was started and then stopped 1.5 hours later. 71
Figure 3-10. Variation of passive current density with time for the passive film formed at 0.6 V. After 73 hours passivation, hydrogen charging was started and then stopped 3 hours later. 72

Figure 3-11. Variation of the photocurrent peak value for passive films with time. After 73 hours passivation, the hydrogen charging was started and then stopped 3 hours later. 72

Chapter 4

Figure 4-1. Shape and dimension (in 10^{-3} m) of specimens. 79
Figure 4-2. Schematic illustration of the experiment setup for stressing the specimens by applying a constant load during electrochemical measurements. 80
Figure 4-3. The stress-strain curve of the A516 steel specimen. 81
Figure 4-4. Open circuit potentials vs. time for A516 steel specimens in 0.5 M $NaHCO_3$ + 0.01 M NaCl solution. 82
Figure 4-5. The changes of open circuit potentials caused by different applied elastic tensile stresses for A516 steel specimens in 0.5 M $NaHCO_3$ + 0.01 M NaCl solution. 82
Figure 4-6. Equivalent circuit for A516 carbon steel at open circuit potential in 0.5 M $NaHCO_3$ + 0.01 M NaCl solution. 83
Figure 4-7. Impedance spectra for A516 carbon steel under various applied elastic tensile stresses in 0.5M$NaHCO_3$ +0.01MNaCl solution at open circuit potential. 83
Figure 4-8. The polarization curve of the uncharged stress-free specimen in 0.5 M $NaHCO_3$ + 0.01 M NaCl solution. 85
Figure 4-9. Current density vs. time curves for passive films on uncharged specimens passivated at - 0.1 V under different stress levels. 86
Figure 4-10. Mott-Schottky plots for the passive films formed at -0.1V for 1.5 hour where the specimens is under different stress levels. 87
Figure 4-11. Passive current density vs. time curve for A516 carbon steel at -0.1 V in 0.5M $NaHCO_3$+0.01 NaCl solution. During passivation, elastic tensile stress was induced. 89
Figure 4-12. The current density vs. time curves for the passive films on charged and uncharged specimens passivated at - 0.1 V under various stress levels. 92

Figure 4-13. Mott-Schottky plots for the passive films on hydrogen-charged specimens formed at -0.1V for 1.5 h under various stress levels. 93
Figure 4-14. Passive current density vs. time for A516 steel sample (hydrogen charged at 80 A/m^2 for 1h) at -0.1 V in 0.5 M $NaHCO_3$+ 0.01 M NaCl solution..... 94

List of Abbreviations

AES: auger electron spectroscopy

CPE: constant phase element

EXAFS: extended x-ray absorption fine structure

fcc: face-centered cubic

HAR: hydrogen absorption reaction

HER: hydrogen evolution reaction

PDF: point defect model

SCC: stress corrosion cracking

SCE: saturated calomel electrode

SIMS: secondary ion mass spectroscopy

STM: scanning tunneling microscopy

XANES: x-ray absorption near-edge spectroscopy

XPS: x-ray photoelectron spectroscopy

List of Symbols

a_0: Bohr radius (≈0.0529 nm)

A: area

B: a constant

C: capacitance

C_{dl}: double layer capacitance

C_f: capacitance of passive film

C_H: capacitance of Helmholtz layer

C_{sc}: capacitance of space charge layer

d: thickness

d_1: thickness of the outer layer of passive film

$\frac{d}{Q}$: thinning rate for cathodic reduction of passive film

e: electron charge

E_A: acceptor binding energy

E_b: binding energy between hydrogen and defects in materials

E_c: energy of the conduction band edge

E_D: donor binding energy

E_f: Fermi energy of semiconductor

E_g: band-gap energy

E_s: heat of the solid solution

E_v: energy of the valence band edge

F: Faraday constant

h: hole in semiconductor

i: current density

i_{cc}: critical current to achieve passivity

i_{charge}: cathodic hydrogen-charging current density

i_{corr}: corrosion current density

i_p: passive current density

i_{ph}: photocurrent

K: Boltzmann constant

M_w: molecular weight

N: number of free electrons

N_D: donor density

Q: cathodic charge

Q_0: cathodic charge used for the reduction of the outmost high valence oxide on the surface of passive film

Q_1: cathodic charge used for the reduction of the outer layer of passive film

r: roughness coefficient

r_s: radius of a sphere

R_{ct}: charge transfer resistance

R_f: ion diffusion resistance in passive film

R_p: polarization resistance

R_s: solution resistance

t : time

T: absolute temperature

U: electrode potential

U_f: film formation potential

U_{fb} : flat band potential of passive film

U_{oc}: open circuit potential

U_p: pitting potential

U_{pp}: passivation potential

ΔU: potential drop

ΔU_{dl}: potential drop in double layer

ΔU_H: potential drop in Helmholtz layer

ΔU_{sf}: potential drop due to surface state

V: volume

z: number of electrons used in reduction of 1 mole compound

Z_{CPE}: CPE impedance

Z_{img}: imaginary impedance

Z_{real}: real impedance

α : exponent of the CPE impedance

ε: strain

ε_0: vacuum permittivity (8.85419×10^{-14} F/m)

ε_{sc}: dielectric constant of space charge layer

ε_r: dielectric constant of passive film

ρ: density of a compound

σ_y: yield strength

$h\upsilon$: photon energy

Chapter 1 Literature Review

1.1 Introduction

How does the word "hydrogen" originate? It is derived from the Greek words **hydro** and **genes**, which together means "water forming". Written records indicate that Robert Boyle produced hydrogen gas as early as 1671 while experimenting with iron and acids. In 1766, Henry Cavendish[1] initially identified hydrogen as a distinct element.

Hydrogen is composed of a single proton and a single electron. It is the lightest and simplest element in the universe. It is very reactive and can be dissolved in a variety of metals and alloys. The interaction of hydrogen with metals has for long aroused considerable interest in both academics and various industrial organizations. The reason behind the success of its applications in these sectors is basically two-fold. The first is practical interest in the use of metal-hydrogen systems, such as the storage of hydrogen as a raw material in the production of chemicals or as a clean energy source. The second one concerns deleterious effects on the properties of materials, which are usually caused by the presence of hydrogen in the metal. Examples of the later include hydrogen embrittlement, hydrogen promoted stress corrosion cracking, brittle fracture, and corrosion. Since these problems give rise to dangers due to hydrogen degradation of materials, research on hydrogen based interactions are very necessary for control, for improvements and for possible new applications of hydrogen-metal systems. In this chapter, the omnipresent hydrogen entry into metallic systems and the resultant deterioration of the metal's properties will be reviewed. Emphasis is laid on the hydrogen effects on iron, carbon steel and micro-alloyed steel.

1.2 Hydrogen in Metals and its Resultant Deterioration

Hydrogen is the third most abundant element on the earth's surface. It is found primarily in water and organic compounds. It is estimated that 90% of the visible universe is composed of hydrogen. Materials under many circumstances may confront the possibility of hydrogen injection into the component. The entry of hydrogen into the metal phase constitutes a necessary step in the process resulting in degradation of metals.

1.2.1 Entry of Hydrogen into Metals and Alloys

Processes in which metals may absorb considerable amounts of hydrogen generated from the environment are summarized below:

1) in the petroleum and gas industries, or during the production and transportation of hydrogen, where materials are exposed to hydrogen gas.

2) during manufacturing operations such as welding, electroplating, phosphating and pickling. For example, water vapor and steam may decompose to hydrogen on hot surfaces of metallic materials during welding, steel making, heat-treatment or other manufacturing processes.

3) in a variety of industrial processes such as cathodic protection, wherein hydrogen production through Equation [1.1] acts as the cathodic reaction. Some of the hydrogen produced may enter the metal rather than evolving as a gas releasing to air.

$$H^{+} + e \rightarrow H \qquad [1.1]$$

1.2.1.1 Entry of Hydrogen from the Gas Phase

Hydrogen can be charged into metallic materials either from the gas phase or from the aqueous environment. Regardless of the route of production, hydrogen is dissolved in the metal in atomic form[2, 3], not in moleculous form. The dissociation of gaseous hydrogen takes place in an adsorption layer on the surface of the metal. The whole process can be divided into four consecutive steps: diffusion of the gas to the surface — adsorption on the surface including dissociation — penetration through the surface — diffusion into the bulk.

For the dissociative chemisorption (chemical adsorption) of hydrogen on transition metals, the heat of adsorption is related to the bond energies of M-H and H-H pairs. Transition metals, especially those of the Group VIII of the Periodic Table of the elements, have a considerable surface reactivity towards hydrogen. A strong interaction of hydrogen with iron atoms can be proved by Bond's calculations[4], which indicates that the energy of a Fe-H bond is 282 $kJ \cdot mol^{-1}$ while that of the Fe-Fe bond is approximately

70 kJ·mol^{-1}. This interaction produces a condition necessary (but not in itself sufficient) for the occurrence of many hydrogen-related effects in ferrous metals.

In gaseous hydrogen charging, the concentration of dissolved hydrogen in the metal obeys Sievert's law, *i.e.* the dissolved hydrogen concentration is directly proportional to the square root of the pressure of hydrogen gas.[5]

1.2.1.2 Entry of Hydrogen from the Liquid Phase

Over a century ago, Graham[6] reported the relatively easy absorption of large amounts of hydrogen into palladium and palladium-silver alloys. Later, he also showed that hydrogen could be introduced into such materials by electrochemical charging[7, 8].

The entry of hydrogen from aqueous solutions into the metal phase depends on many factors such as the surface conditions of the metal or alloy, the potential of the metal/electrolyte interface, the current density of hydrogen evolution, the pH of the electrolyte, the electrolyte composition, as well as impurities, temperature and pressure etc. Certain substances may strongly accelerate or impede this process. Due to the complexity of the metal/electrolyte boundary, the mechanism of the entry of hydrogen and the effect of promoters/inhibitors on this process has not been completely elucidated.

It is generally believed that the cathodic evolution of hydrogen from an aqueous solution proceeds in several successive stages. Depending upon the electrolyte, the overall hydrogen evolution reaction (HER) can be written:

$$2H_3O^+ + e^- \longrightarrow H_2 + 2H_2O \quad \text{(in acid solutions)} \qquad [1.2]$$

or

$$2H_2O + 2e^- \longrightarrow H_2 + 2OH^- \quad \text{(in alkaline solutions)} \qquad [1.3]$$

In the case of metals, which have the ability to absorb hydrogen, the HER occurs simultaneously with the hydrogen absorption reaction (HAR). Usually only a small part of the total quantity of hydrogen evolved is absorbed and finally enters into the metal. Among the list of many variables that determine the rate of hydrogen entry, the cathodic current density is one of the parameters, which critically affect the rate of hydrogen entry into metals. As far back as 1922, Bodenstein[9] demonstrated the permeation rate of

hydrogen through metallic membranes is directly proportional to the square root of the cathodic current density, which has also been confirmed by later studies[10-12].

1.2.1.3 Promoters and Inhibitors of Hydrogen Entry into Metals

It has been established for a long time that certain substances, even in small quantities, have a very marked effect in enhancing the entry of hydrogen into metals from both liquid and gaseous environments. These compounds are referred to as promoters of hydrogen entry. Species that seem to be most effective in promoting hydrogen entry are:

1) Compounds of certain elements of the V-A periodic Group (P, As, Sb) and the VI-A periodic Group (S, Se, Te);

2) Hg, Pb, Sn, CN^-, CNS^-, and halide anions;

3) Certain compounds of carbon: CS_2, CO, CON_2H_4, CSN_2H_4, and some other organic compounds.

The accelerating effect of promoters has been attributed to "poisoning" of the recombination reaction of the adsorbed hydrogen atoms into molecules[13-15], or a lowering of the M-H_{ads} bond energy[11, 16, 17], or the interaction of the promoter molecules with the electrons of the surface metal atoms[18]. Smialowski and Szklarska-Smialowska[19] were the first to postulate one of the current hypotheses that hydride formation of the promoter is an essential step in the process of hydrogen entry. Experiments[20] showing the influence of pH upon the promoter effect have been used to support the idea of the importance of the hydride-forming tendency of the most effective promoters. There are other concepts put forward to address the mechanism of promoter action. However, the experimental results obtained by different investigators conflict because of the complex conditions of metal/solution interfaces. The model of hydrogen entry into a metal together with the effect of promoters on this process still requires verification and further development.

On the other hand, some substances when added to the solution have just the opposite effect on the entry of hydrogen into metals. These are primarily polar organic compounds, whose molecules contain sulphur, nitrogen or oxygen atoms. One of the well-known and effective inhibitors of hydrogen entry is dibenzyl sulphoxide or, more precisely, the product of its cathodic reduction-dibenzyl sulphide[21, 22].

The mechanism of inhibitor action is not fully understood. However, it is generally believed that a strong chemisorption of the inhibitor molecules on the metal surface is necessary for inhibition of the entry of hydrogen. The inhibitor adsorbed there may affect hydrogen entry into the metal phase by one of or a combination of several of the mechanisms summarized below:

1) The inhibitor forms a compact layer on the metal surface or partially blocks the metal surface, which makes the transport of hydronium ions or water molecules to the metal surface more difficult. As a result, hydrogen atoms produced, which have no or only partial direct contact with the solid metal.

2) The inhibitor affects the process of the hydrogen evolution reaction, for example, the recombination rate of adsorbed hydrogen atoms, and thus decreases the hydrogen absorption reaction.

3) The inhibitor may weaken the strength of the bonding of the adsorbed hydrogen atoms to the metals surface atoms for example, by providing particular molecules with side-chain modifications having additional hydrogen bonding capability,

1.2.2 State of Hydrogen in Metals and Alloys

Hydrogen occupies interstitial sites in the metal lattice, forcing the nearest-neighbor metal atoms farther apart from each other, which causes an increase of volume of the nearest-neighbor shell of atoms. Hydrogen interacts with lattice imperfections such as vacancies, dislocations, impurities, grain boundaries, foreign atoms, high strain fields, second-phase particles, etc. in a non-ideal metal or alloy. Many of these defects interact with hydrogen more strongly than the host metal lattice, which results in local accumulation of hydrogen. Such sites inside the metals are called "hydrogen traps". The binding energy of hydrogen at these sites depends on the nature of the trapping and of the defects themselves, and it is usually of the order of a few tenths of eV.

In view of the importance of iron and steels in modern technology, the iron-hydrogen system has been give particular attention. It has been widely accepted that a hydride is not formed, or at least is unstable, in pure iron, carbon steel as well as low-alloy steels, while local accumulation of hydrogen in these materials has been reported. This is closely related to the extremely low solubility of hydrogen in iron at low temperatures.

Chan *et al.* [23] studied the effect of grain size and second phase particles on the trapping of hydrogen by various interfaces in iron, carbon steel and micro-alloyed steel. It was found that the hydrogen content of pure iron specimens depended on both the extent and the nature of grain boundaries. High angle boundaries held more hydrogen than those of low angle, and thus specimens with low angle grain boundaries were less susceptible to hydrogen damage. Moreover, inclusions and thermo-mechanical treatments also influence the hydrogen absorption in iron significantly. Below a critical volume fraction of inclusions no hydrogen-induced cracking occurred. Ferrite/pearlite and pearlite/pearlite colony interfaces in steel were found to trap hydrogen, whereas the ferrite/cementite interface within the pearlitic colonies had little effect on the hydrogen occlusivity.

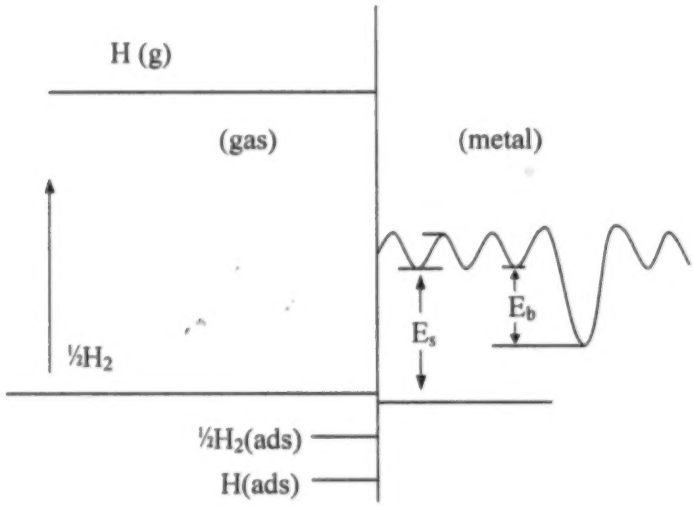

Figure 1-1. A schematic view of energy relations in gas-metal equilibrium for weak hydrogen traps.[24]

Figure 1-1 [24] shows a schematic view of energy relations in gas-metal equilibrium, including trapping. E_s is the heat of the solid solution while E_b is the binding energy between hydrogen and defects. Most traps can be classified into three categories: weak traps with $E_b < E_s$, moderate traps with $E_b \sim E_s$ and strong traps with $E_b > E_s$. Strong traps

behave irreversibly in the sense that the rate of escape of hydrogen is relatively small. In contrast, moderate or weak traps have appreciable escape rates and act reversibly under the same experimental conditions.

1.2.3 Hydrogen Degradation of Metals and Alloys

The detrimental effects of hydrogen have long been recognized in ferrous materials and subsequently in other metals and alloys. The ubiquity of the sources of hydrogen contributes to the importance of the problem.

1.2.3.1 Effects of Hydrogen upon Mechanical Properties

Hydrogen changes the cohesive forces between the host metal atoms. Several theoretical investigations[25, 26] show that the cohesive interactions are in fact decreased in many transition metals including palladium. As a result, the effort required to cause brittle cracking of a metal is decreased by hydrogen[27]. For the past six decades, a great amount of research has been dedicated to the influence of hydrogen on various mechanical properties. The severity and mode of the hydrogen damage depends on:

- source of hydrogen – external/internal,
- time of exposure,
- temperature and pressure,
- composition of solutions (*e.g.* acidic solutions, chloride ions),
- type of alloy and its history of processing, heat treatment, and surface treatment,
- number of defects in the metal,
- final treatment of the metal surface (*e.g.* galvanic nickel plating),
- level of residual and applied stresses.

Depending on the combination and number of the above variables, hydrogen damage may be classified as: internal cracks, blisters or voids in steels; hydrogen embrittlement, hydrogen induced cracking and high temperature hydrogen attack.

When sufficient hydrogen gathers at crystalline or metallurgical inhomogeneous sites, atomic hydrogen will recombine to form molecular H_2, causing internal cracking and blistering. Several authors[28-30] have investigated the generation of internal cracks and flaws by the introduction of large amounts of hydrogen. This large amount of excess

hydrogen can be accommodated in several ways: 1) out-gassing through the external surface; 2) interaction with, and trapping by, the metal lattice and imperfections such as inclusions and grain boundary etc.; and 3) recombination of dissolved hydrogen to molecular hydrogen at internal sites. Molecular hydrogen, resulting from the recombination at the internal sites, increases internal pressure. Consequently, internal flaws are introduced in the form of intergranular or transgranular cracks[31,32] or voids[33]. When these flaws are located near the external surfaces, surface blistering is often observed. The problem of blistering is especially prevalent in petroleum drilling and refining equipment, where sulfides and H_2S are common in the associated environment[34].

High temperature hydrogen attack is another major problem encountered in refineries, where hydrogen and hydrocarbon streams are handled under a pressure up to 20 MPa and a temperature of approximately 810 K. At an elevated temperature, hydrogen forms methane bubbles on the grain boundaries and in micro-voids of the material by reacting with the carbon of the steel. Expansion and joining of such bubbles resulting from methane pressure build-up could extend the voids into fissures, or even develop into major cracks. Hydrogen attack has been reported in plain carbon steel, low alloy steels and even some stainless steels operating above 473 K.

Hydrogen embrittlement is involved with seriously reduced ductility and load-bearing capacity of a metallic component resulted from the ingress of hydrogen, and the consequent cracking and catastrophic brittle failures of the susceptible material at stresses below the yield point. Hydrogen embrittlement occurs in a number of ways but the common features are an applied tensile stress and hydrogen dissolved in the metal. The most vulnerable materials to hydrogen embrittlement are high-strength steels, titanium alloys and aluminum alloys. Under certain circumstances, hydrogen embrittlement can be reversible. When environmental conditions are changed before the cracking occurs, so that hydrogen is no longer generated on the surface of the metal, hydrogen in the metal can re-diffuse from it, thereby restoring the ductility. One of the well-established hydrogen embrittlement mechanisms is the stress-induced hydride formation and cleavage mechanism supported by extensive experimental and theoretical evidence[35-38]. Another commonly cited hydrogen embrittlement mechanism is the de-cohesion model, which asserts that hydrogen lowers the cohesive strength of the solid and, consequently,

materials fail at lower applied stresses. Presently, the phenomenon of hydrogen embrittlement is not fully understood and its detection appears to be one of the most difficult aspects of the problem.

1.2.3.2 Effects of Hydrogen upon Corrosion Properties

Compared to the well documented damaging effects of hydrogen on the mechanical properties of various engineering materials, the phenomenon of hydrogen-promoted corrosion is much less studied and now drawing increasing research interest.

Hydrogen is known to accelerate both the general corrosion and localized corrosion of metals and alloys. It was reported that hydrogen absorbed on the surface of the metal could change the over-voltage of the electrode reactions, and thus promote general corrosion[39-41]. Moreover, many hydrogen-induced changes in the metal such as increased defects and internal stress[42-44], weakening of cohesive forces[25, 26], formation of microdefects, destabilization of passive films[45, 46] etc. also contribute to facilitate the general corrosion of hydrogen-containing metals. Since localized corrosion is usually considered to be more dangerous than uniform corrosion due to its insidious characteristics, the hydrogen effect on the resistance of metals to localized corrosion has received more attention.

Localized corrosion are the types of corrosion in which intense attack occurs at localized sites on the surface of a component whereas the rest of the surface is corroding at a much lower rate – either because of an inherent property of the component material or because of some environmental effect. Pitting and crevice corrosion are the two types of localized corrosion attack that are most commonly encountered in metals, and are also the major subject of research on localized corrosion. The resistance to localized corrosion varies greatly between different materials and is extremely dependent upon environmental factors. Typical examples of metallic materials prone to pitting corrosion are iron, stainless steels, copper alloys, nickel alloys and aluminum alloys. The most extensively investigated localized corrosion is the phenomenon of passivity breakdown in different metal/solution systems[47-50].

The most common mechanism of localized corrosion of iron, carbon steel and micro-alloyed steel is the localized breakdown of the passive films by chloride ions. Hydrogen

is reported to interact strongly with chloride ions and they act in combination to significantly damage the protectiveness of passive films. Published literature has shown that hydrogen decreases the stability of the passive films on stainless steels[51] and ferritic steels[52] as well as increases the corrosion rates of austenitic stainless steels[53, 54], iron-based and nickel-based amorphous alloys[55]. It was also found that hydrogen increases the pitting susceptibility of type 310 and 304 stainless steel[56, 57], pure nickel[33], and pure iron[58]. However, no consensus has been reached as to how hydrogen behaves in passive films, and hence the mechanism responsible for the hydrogen deterioration of corrosion resistance of materials remains to be investigated further.

1.3 Passive Films on Iron, Carbon Steel and Micro-Alloyed Steel

Passivity has been the subject of intense investigation for over one century, in view of the important role it plays in the corrosion behavior of metals and alloys. Hydrogen injected into materials with passive characteristics will subsequently change the structure and composition of the passive film, affecting their corrosion resistance significantly[59, 60].

1.3.1 Fundamentals of Passivity

Some normally active metals and alloys, in certain environments, lose their chemical reactivity and become extremely corrosion-resistant. This phenomenon, termed passivity, is observed in chromium, iron, nickel, titanium, and many of their alloys. For the majority of metals, passivity is caused by the spontaneous formation of an adherent oxide layer in a specific environment. These films, which usually are not thicker than a few nanometers, act as a reactivity barrier between the metal surface and the corrosive environment.

The phenomenon of passivity is best illustrated by the polarization curve, or the current-potential behavior of the metal, having the general shape shown in Figure 1-2 [61]. At relatively low potential values, within the "active" region, the behavior is linear as it is for normal metals. With increasing potential, the anodic current density decreases promptly to a very low value, charactering the "passive" region, in which the current density remains independent of potential. Finally, at still higher potential values, the current density again increases due to further oxidation in the "transpassive" region.

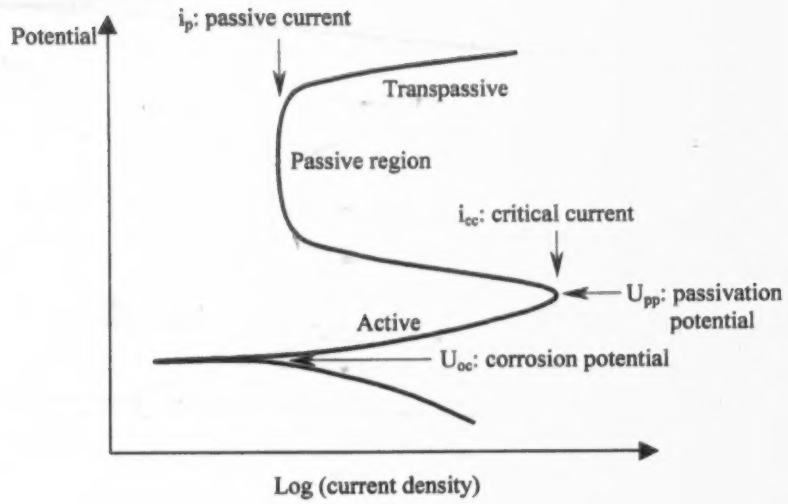

Figure 1-2. Hypothetical polarization diagram for an active-passive system with active, passive and transpassive regions.[61]

For a metal that passivates, its corrosion rate can be significantly reduced by keeping the potential of the metal in the passive region. The current required to shift the potential in the anodic direction from the corrosion potential E_{corr} can be several orders of magnitude greater than the current necessary to maintain the potential within the passive region. At the potential value of E_{pp}, the current peaks as shown in Figure 1-2. In order to achieve passivity, the critical current density (i_{cc}) must be exceeded, and the anodic potential must then be maintained in the passive region without allowing it to fall back in the active region or getting into the transpassive region, where the protective oxide film can break down. It follows that although a high current density may be required to produce passivation ($> i_{cc}$), only a small current density is needed to maintain it, and that in the passive region the corrosion rate is small due to the low passive current density (i_p).

The role of alloying elements in anodic dissolution and passivation was described by Marcus[62]. It was concluded that elements that enhance passivation are elements characterized by high metal-oxygen bond strength and low metal-metal bond strength, and the high metal-oxygen bond strength is necessary for stability of the passive film.

The low metal-metal bond strength favors rapid nucleation and growth of the oxide by facilitating the breakage of surface metal-metal bonds involved in the early stages of passivation. Based on this concept, elements such as Al, Ti and Cr are passivity promoters, while Mo, W, Ta and Nb act as dissolution moderators or blockers as they possess high metal-metal bond strength. It is obvious that promoters or passivators will be the main constituents of the passive film, whereas dissolution blockers will tend to remain at the film/substrate interface where they can restrain the dissolution process.

The formation of passive films is initially governed by the potential–pH–diagram, and later by relative reaction rates. Local activation of the passive film can be induced by mechanical or chemical breakdown of the film. An overview of the phenomenon of passivity and its breakdown can be obtained from a series of review papers[47, 63-65].

In situ methods used to investigate the structure of passive films include X-ray scattering, diffraction, and Mössbauer spectroscopy. Since *ex situ* measurements complicate the situation by the possibility of structural changes after removing a film from the passivating environment, *in situ* techniques are preferred for characterizing passive films. However, since the thickness of passive films formed at low-to-moderate temperatures is usually less than 10^{-8} m, it is experimentally difficult to investigate the structure by traditional X-ray diffraction. Lately, new *in situ* techniques (scanning tunneling microscopy, STM, X-ray scattering using synchrotron radiation, and extended X-ray absorption fine structure, EXAFS) have been used to study the structure of thin oxide films. So far, the investigations on the structure of passive films are still insufficient and the long-standing controversy regarding the chemical and crystallographic nature of the film remains unsolved.

1.3.2 The Nature of Passive Films on Iron, Carbon Steel and Micro-Alloyed Steel

The passivity of metals has been actively investigated for almost two centuries[66-68]. The exact chemical composition and structure of the passive films on metals and alloys, however, remain unsolved due to the difficulties in scrutinizing the film *in situ*[69-72].

Iron, carbon steel and micro-alloyed steel are universally used for all kinds of structures mainly by virtue of their relatively low price and excellent properties. In view of the importance of their application in modern technology, the nature of passive films

on iron, carbon steel and micro-alloyed steel is given particular attention, especially in the environment of buffer solutions.

1.3.2.1 Iron Oxides

Surface analysis and electrochemical studies[73-76] have shown that passive films on iron, carbon steel and micro-alloyed steel mainly consist of iron oxides or iron hydroxides. Although the composition and structure of anodic oxide films differs from that of the bulk oxide, crystallographic examination of the iron oxides can offer informative insight into the nature of the passive film on iron, carbon steel and micro-alloyed steel.

Iron can be at oxidation state II or III in the form of Fe^{2+} or Fe^{3+} in its oxides. Based on this fact, iron oxides tend to be somewhat non-stoichiometric. The common iron oxides are: ferrous oxide FeO, hematite γ-Fe_2O_3, maghemite γ-Fe_2O_3, and magnetite Fe_3O_4. When water is involved, several oxyhydroxides are possible: goethite γ-FeOOH, akaganeite γ-FeOOH, and lepidocrocite γ-FeOOH.

Fe_3O_4 is an oxide with structural formula $[Fe^{2+}(Fe^{3+})_2O_4]$ having the spinel structure. The structure of Fe_3O_4 consists of a closed-packed fcc oxygen lattice with the divalent Fe^{2+} in tetrahedral coordination and the trivalent Fe^{3+} in octahedral coordination with oxygen ions. There are 32 O^{-}ions in a unit cell. The structure may also be seen as layered sheets of $[Fe^{2+},Fe^{3+}]$ between closed-packed sheets of oxygen ions. The octahedral sites are larger than the tetrahedral sites, and there are twice as many octahedral sites occupied as tetrahedral sites.

The spinel structure is interesting because it may contain vacancies as a regular part of the crystal. For example, if magnetite is oxidized, Fe^{2+} will turn into Fe^{3+}. If all Fe^{2+} is converted into Fe^{3+}, charge balance requires a net formula of $Fe_{21.67}O_{32}$ per unit cell and this means that 2.33 sites must be vacant – thus we obtain what is called a defect spinel. In a way, the composition is now $Fe_{21.67}Vac_{2.33}O_3$, with many vacancies in its structure. For the same reason, when Fe^{3+} in magnetite is reduced to Fe^{2+}, oxygen vacancies emerge as an integral part of the structure. The anhydrous iron oxide γ-Fe_2O_3 (maghemite) also has a defect spinel structure with hematite stoichiometry.

1.3.2.2 Passivity of Pure Iron

The passive film on iron has been widely[73, 74, 77-99] studied in near-neutral borate buffer solution by many researchers using various techniques, *e.g.*, *in situ* electrochemical methods, radiotracer measurements, Mössbauer spectroscopy, electromodulated reflectance, Raman spectroscopy, electro-ellipsometry, *ex situ* Auger, x-ray photoelectron spectroscopy (XPS), secondary ion mass spectrometry (SIMS) and electron diffraction techniques. The work of Nagayama and Cohen[74, 78] established some fundamental understandings of the procedures. However, discrepancies exist in the literature as to how to interpret the results and what they indicate regarding the structure and composition of the passive film on iron.

1.3.2.2.1 Structure Models of the Passive Film on Iron

The composite layer model comprising an inner layer of magnetite and an outer layer of ferric oxide has been suggested from thermodynamic considerations[100, 101] and cathodic reduction experiments[78] on the film. Nagayama and Cohen[78] studied the anodic oxidation of iron in a pH 8.4 borate buffer solution, and found that in the passive potential region the film consists of an inner "Fe_3O_4" layer and an outer "γ-Fe_2O_3" layer, whose total thickness varies linearly with potential from 1.0×10^{-9} to 3.0×10^{-9} m. At higher potentials, the presence of some hexavalent iron in the γ-Fe_2O_3 layer is suggested, which constitutes the outermost part of the film having a defect structure of the general formula $Fe_x^{6+}\cdot Fe_{2-2x}^{3+}\cdot\square_x\cdot O_3$. Results from further studies[74] concluded that the passivation potential is governed by the reaction[74]

$$\gamma - Fe_2O_3 + 6H^+ + 2e^- \longrightarrow 2Fe^{2+} + 3H_2O \qquad [1.4]$$

The observation of two reduction plateaus, which underlies the two-layer model, has been frequently reported in galvanostatic experiments on the passive film on iron[78, 102, 103]. The first plateau is generally attributed to reduction of the outer layer and the second to reduction of the inner layer. Nagayama and Cohen identified the first plateau to be the reduction of γ-Fe_2O_3 to Fe^{2+} with near 100 percent current efficiency (Reaction [1.4]),

and the second plateau to be the reduction of Fe_3O_4 to Fe with a low current efficiency (Reaction [1.5]).

$$Fe_3O_4 + 4H_2O + 8e^- \longrightarrow 3Fe + 8OH^- \qquad [1.5]$$

Since then a number of investigations[74, 79-85, 87-89, 104-114] have been conducted to study the nature and stability of the passive film on iron by the technique of cathodic galvanostatic reduction. This study provides quantitative information on the chemical composition of the film, provided that the exact reduction mechanism is known. In most work, the results have been interpreted by assuming the presence of a two-layer film consisting of an inner layer of Fe_3O_4 and an outer layer of γ-Fe_2O_3, while different reduction mechanism may be proposed.

Studies on the structure and composition of the passive film on iron were conducted using a variety of *in situ* techniques, for example, Mössbauer spectroscopy[115-117], X-ray absorption spectroscopy[118-120], and surface enhanced Raman spectroscopy[121-123]. In contrast, these measurements were interpreted as showing that the passive film is amorphous and/or similar to Fe hydroxides or oxyhydroxides. The result is inconsistent with passive films composed of discrete layers.

An alternative explanation to the galvanostatic reduction results was given in which the film is assumed to be a single layer of γ-Fe_2O_3. In this case, the two reduction waves are attributed to reduction of Fe_2O_3 first to Fe^{2+} and then to Fe(0)[92, 113]. By means of cathodic reduction combined with ellipsometry, Sato *et al.*[104] deduced that the anodic oxide film on iron in neutral solution is a layer of partially hydrated iron (III) oxide rather than a composite layer of magnetite and ferric oxide. Additional evidence[108, 124-128] was later presented in which all the iron in the anodic oxide film was considered to be ferric, and a model that consists of a barrier (inner) layer of anhydrous γ-Fe_2O_3 next to the metal phase and a deposit (outer) layer of hydrous ferric oxide next to the solution phase was proposed. According to their cathodic reduction investigations[128] using a borate solution of pH 6.35, no magnetite layer is present and all the iron in the passive film is iron (III). Oxygen in the film is estimated from the ellipsometric thickness to be in excess of the stoichiometric ferric oxide, hence hydrogen may be associated with excess oxygen to

form bound water. The average composition is represented as $Fe_2O_3 \cdot 0.4H_2O$ or $Fe_2O_3 \cdot 1.4FeOOH$, in which the hydrogen may be replaced partly with an iron-ion vacancy. The barrier layer was potential dependent and its thickness at steady state was proportional to the overpotential of the layer formation. The deposit layer, which was stable only in the neutral and basic pH range, appeared to differ in thickness with different passivation processes and also with different solution environments such as pH and anion.

The passive film formed in an extended range of potential in a borate solution of pH 8.42 was also studied by Sato and his colleagues[129]. Composition depth profiles of passive films on iron have been obtained by means of cathodic reduction combined with ellipsometry and chemical analysis. In few investigations, a solid-state reduction reaction has been proposed in which Fe_2O_3 is reduced to a lower valent oxide[104, 130].

Based on the data presented in the literature, it is evident that structural and compositional examinations of the passive film on iron can be interpreted differently depending on whether a single-layer or a two-layer structure is assumed for the passive film. Two-layer models tend to favor a simple electrochemical reductive dissolution mechanism, whereas single-layer models lead to a two-step mechanism, which involves conversion of the oxide to lower valent species. Despite these discrepancies in the iron passivity, it appears that, from a thermodynamic point of view, the ferric oxide film cannot form without the concurrent formation of some Fe_3O_4 (or Fe^{2+} ion), although the interface/boundary between layers may not be very rigid. In other words, the co-existence of Fe^{3+} and Fe^{2+} in the passive film on iron should be justifiable.

1.3.2.2.2 Recent Studies on the Nature of the Passive Film on Iron

To clarify some ambiguous aspects of the reduction mechanism of iron passive films, studies using model substrates with well-defined composition were initiated. Thin sputter-deposited oxide films have been suggested as a model system for natural passive films[131, 132]. Davenport and Schmuki *et al.*[97, 133-136] have studied the mechanism of cathodic dissolution of iron oxides using sputter-deposited thin-film samples with *in situ* XANES (X-ray absorption near-edge spectroscopy). In borate buffer solution, the XANES spectra showed that no formation of metallic iron took place during the

reduction. As the chemical dissolution reaction has been ruled out[136], reactions [1.4] and [1.6] were considered to be the dominant reactions during galvanostatic reduction of the iron oxide.

$$Fe_3O_4 + 8H^+ + 2e^- \longrightarrow 3Fe^{2+}(aq) + 4H_2O \qquad [1.6]$$

In recent years, a growing number of investigations on passivity of Fe and Fe base alloys using modern *in situ* techniques such as XANES and STM (scanning tunneling microscopy) have been carried out[97,98, 136, 137-142], in an effort to elucidate the influence of solution chemistry on the nature of the passive film on Fe and Fe-Cr alloys. The XANES method allows monitoring of time-dependent changes taking place in the sample during electrochemical experiments, whereby information on both the amount of sample dissolution and changes in the valence state of the material can be gained. XANES studies on the electrochemical behavior of Fe and thin, sputter-deposited films of Fe_2O_3 in borate buffer (pH 8.4), phosphate buffer (pH 8.4) and in 0.1 M NaOH revealed that the reactions taking place during reduction of the passive film on iron are significantly different for all three electrolytes. In borate buffer (pH 8.4), reduction leads to a complete dissolution of the passive film. In alkaline solution, no dissolution takes place, but, instead, the passive film is converted into a lower-valent oxide/hydroxide film during reduction. Similarly, in phosphate buffer (pH 8.4), there is no dissolution in a direct step to low cathodic potentials, but the resulting reduction product is metallic iron. In an alkaline phosphate-containing solution, conversion into metallic iron is possible in a direct reduction step to a potential in the stability region of Fe^0; at intermediate potentials, a ferrous layer is formed in the reduction reaction. The presence of phosphate species in the electrolyte enables the further reduction of this ferrous layer to Fe^0 at lower potentials. The origin and detailed mechanism of different reduction behavior in various solutions, however, have not been completely resolved in the XANES investigations.

More recently, *in situ* and *ex situ* XANES data suggest that the film is either amorphous or spinel (similar to Fe_3O_4 or γ-Fe_2O_3)[137, 143, 144], or a nanocrystalline microstructure with numerous defects[144]. It was suggested that the film structure is based on Fe_3O_4 [143], but with cation vacancies on octahedral and tetrahedral sites (80% and 66%

occupancies, respectively) and with cations occupying octahedral interstitial sites (12% occupancy). STM[145] examination also showed that the passive film on Fe has a crystalline structure.

1.3.2.3 Passivity of Carbon Steel and Micro-Alloyed Steel

As far as corrosion properties are concerned, carbon steel and micro-alloyed steel show similar behavior to that of pure iron, since the passive films on them are also mainly composed of Fe_3O_4 and γ-Fe_2O_3[146-149]. Compared to pure iron and stainless steels, few studies have been carried out on the corrosion behavior of carbon steel and micro-alloyed steel. Salvarezza *et al.*[150] have studied the passive film growth, electrodissolution and pitting corrosion of prepassivated carbon steel in dilute NaOH solutions containing Na_2SO_4 by using potentiostatic and potentiodynamic techniques, and proposed two kinetic reaction models implying different passive film growth mechanisms to describe the passive film growth, the electrodissolution process through the passive film and pitting corrosion. XPS results[151] show that different oxide and sulfur structures were developed during the electrochemical oxidation of 1018 carbon steel in concentrated acid media. The analysis indicated that, during film growth, H_2O and/or hydroxyl groups are incorporated into the film structure. XPS depth profile analyses for the film showed that the ratio of Fe to S and Fe to O increases from film surface to film/carbon steel interface. Auger electron spectroscopy (AES) and XPS analysis[152] also showed that a crucial role is played by passive film formation on DIN 34CrNiMo6 steel with respect to both wear-accelerated corrosion processes and surface mechanical phenomena. Depending on the nature of the solution, passive carbon steel exhibits either subsurface cracking or plastic flow accompanied by wear.

Quite a lot of research work[153-156] has been dedicated to inhibitors for corrosion prevention of carbon steels and micro-alloyed steels, both of cathodic and anodic processes, as well as to hydrogen absorption and hydrogen permeation through steel, but only very few investigations on hydrogen-promoted corrosion of steels have been reported, and systematic investigation is still needed.

1.3.3 Effects of Hydrogen on Passive Films

Since the passive film formed on metals and alloys protects the metal from corrosion, the effects of hydrogen on passivity of the metal play an important role in the processes that lead to hydrogen-promoted corrosion.

Hydrogen is considered to be present as protons[33, 157] in a passive film. Because of a strong coulombic interaction between the hydrogen and oxygen ions, some of the protons combine with oxide ions or hydroxyl ions to form hydroxyl ions or water according to the following reactions:

$$H^+ + O^{2-} \rightarrow OH^- \qquad [1.7]$$

$$H^+ + OH^- \rightarrow H_2O \qquad [1.8]$$

These processes compete with metal ions for oxygen ions and hence lower the average oxidation state of the metal ions. As a result, the passive film formed with the presence of hydrogen in the bulk becomes thinner and thereby contains less oxide. Cathodic galvanostatic reduction experimental results[158] showed that much less cathodic charge was consumed to reduce passive films on iron for hydrogen charged specimens than that used for uncharged specimen. This simply indicates that a lower average valence state of iron ions may be present in the hydrogen-containing passive films. Thinner passive films on hydrogen charged specimens than that on uncharged ones were found by SIMS analysis[159].

Hydrogen in metals would affect the properties of the passive films formed on the surface and consequently affect the corrosion behavior of the metals. The effects of hydrogen in type 310 stainless steel on the disorder of passive films and pitting susceptibility have been investigated by Luo *et al.*[57, 160]. It was found that hydrogen decreased the breakdown potential, facilitated the pitting initiation and increases the pit density and growth rate. Several researchers also reported that hydrogen decreased the passivity of iron and steel and promoted their pitting[2, 161, 162]. It is believed[32] that the increase in OH^-/O^{2-} ratios in passive films accelerated pit initiation because of a decrease in the mean cationic valence. Another researcher[57] attributed the increase in pitting

susceptibility to the formation of localized proton clusters around defects in the passive film. Oriani *et al.*'s work[33] showed that pitting induction time of nickel was shortened when hydrogen was present in nickel. Similar effects of hydrogen on pitting susceptibility of 304 stainless steel were also presented by Yashiro *et al.*[56]. It was found by Song *et al.*[163] that with the increase in the content of hydrogen-containing species in passive films, the substitution of OH^- by Cl^- was promoted, which made the film prone to breakdown in chloride-containing solutions. Some researchers[164, 165] have also reported that a passive film on stainless steel exhibits a duplex character with an inner region enriched in chromium oxide and an outer region enriched in iron oxide. Recently, Qin *et al.*[60] also found that chemical nature and thickness of the passive films on AISI 310 stainless steel were affected significantly by the presence or absence of hydrogen in the bulk of the samples.

In summary, hydrogen has been found to accelerate the corrosion rate of metallic materials, increase their susceptibility to localized corrosion, and destabilize the passive films on them. Despite the different approaches employed and the existence of conflicting results in the literature, the deterioration of the passive films caused by hydrogen ingress has been explained mainly in terms of the following mechanisms: hydrogen may 1) change the average valence state of cations in a passive film; 2) increase the ratio of OH^-/O^{2-} in a passive film; 3) decrease the film thickness.

1.4 Electronic Properties of Passive Films

Electron transfer through the passive film is crucial for passivation and for the corrosion behavior of the metal. Measurement of the electronic characteristics of the passive film implicitly yields valuable information on the elusive mechanism of the protection of the film. Electronically, many anodically formed passive films (*e.g.* Cu, Ti, Fe, Fe/Cr etc.) exhibit semiconductive behavior[166]. Thus their electronic properties can be investigated with techniques borrowed from ideal semiconductor electrochemistry, *e.g.* photoelectrochemistry and capacitance measurements of the Mott-Schottky type[167], despite the fact that passive films often show considerable deviations from ideal semiconductor behavior because of its small thickness, non-ideal crystalline structure

(amorphous or highly defective), mobile doping species, and doping levels close to degeneracy[167].

1.4.1 Fundamentals of Semiconductor Electrochemistry

It is instructive to first gain some fundamental knowledge of semiconductor electrochemistry related to this research, before we plunge into the effect of hydrogen on electronic properties of passive films.

1.4.1.1 Energy Band Model

Due to the extremely large number of atoms that must be considered, the electronic structure of the semiconductors is typically discussed in terms of energy bands. The valence band is the highest occupied energy band and the conduction band is the lowest unoccupied band. It is the difference in energy between the upper edge of the valence band and the lower edge of the conduction band (termed the band gap) that determines the properties of the material. For insulators, the band gap is so large that electrons cannot be promoted from the valence band to the conduction band. However, for semiconductors, the band gap is not as large, and electrons can be promoted into the conduction band, leaving a positively charged hole (h^+) in the valence band.

Electrons can be excited to the conduction band either thermally or photochemically. However, the addition of a different element into the semiconductor (termed doping) can also generate charge carriers (*i.e.* electrons or holes) in the semiconductor. For example, the addition of P into Si introduces occupied energy levels into the band gap close to the lower edge of the conduction band, thereby allowing facile promotion of electrons into the conduction band Figure 1-3(a).[168] The addition of Al introduces vacant energy levels into the band gap close to the upper edge of the valence band, which allows facile promotion of electrons from the valence band Figure 1-3(b).[168] This leads to the formation of holes in the valence band. Undoped semiconductors are called intrinsic semiconductors. Doped semiconductors in which the dominant charge carriers are electrons are called n-type semiconductors, whereas those in which holes are the majority charge carriers are p-type semiconductors.

Another important concept of energy band model is the Fermi level, which is defined as the energy level at which the probability of occupation by an electron is ½. For an

intrinsic semiconductor the Fermi level lies at the mid-point of the band gap. For an n-type semiconductor, the Fermi level lies just below the conduction band, whereas for a p-type semiconductor it lies just above the valence band (also see Figure 1-3 [168]).

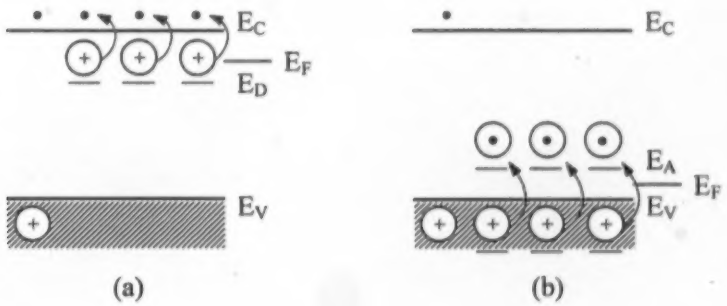

Figure 1-3. Schematic diagram of the energy levels of (a) an n-type semiconductor and (b) a p-type semiconductor.[168]

1.4.1.2 Semiconductor/Electrolyte Interface

When the semiconductor is immersed in the electrolyte, the electrochemical potential of the two phases must be the same at equilibrium. The electrochemical potential of the solution is determined by the redox potential of the electrolyte solution, and redox potential of the semiconductor is determined by the Fermi level. Movement of charge between the semiconductor and the electrolyte is required in order to equilibrate the two phases, by which movement a region termed the space charge field is formed. For an n-type semiconductor electrode at open circuit, the Fermi level is typically higher than the redox potential of the electrolyte, and hence electrons will be transferred from the electrode into the solution. Therefore, there is a positive charge associated with the space charge region, and this is reflected in an upward bending of the band edges. Since the majority charge carrier of the semiconductor has been removed from this region, this region is also called the depletion layer. For a p-type semiconductor, the depletion layer exhibits downward bending in the band edges.

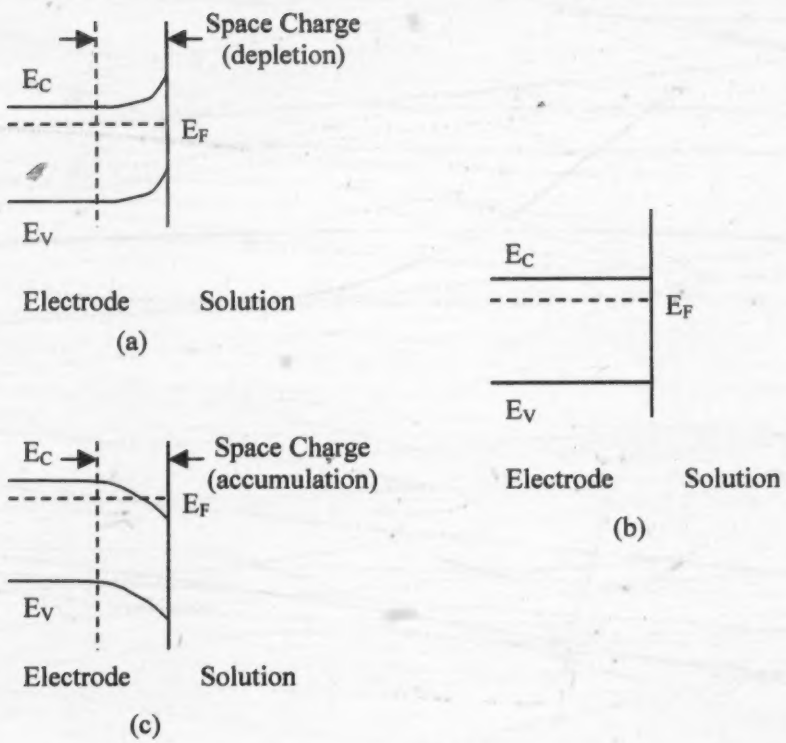

Figure 1-4. Effect of varying the applied potential U on the band edges in the interior of an n-type semiconductor: (a) $U > U_{fb}$ (b) $U = U_{fb}$ (c) $U < U_{fb}$.[168]

As the Fermi level changes with the applied potential, the magnitude and direction of band bending, varies with the applied potential. There are three different situations to be considered. Take an n-type semiconductor for example, at potentials positive of the flat band potential the depletion region arises (Figure 1-4 (a)). At certain potentials, the Fermi energy lies at the same energy as the solution redox potential. There is no net transfer of charge, and hence there is no band bending. This potential is therefore referred to as the flat band potential, U_{fb} (Figure 1-4 (b)). At U_{fb} the depletion layer disappears and there is no electric field within the passive film. At negative potentials of the flat band, an accumulation region arises, which corresponds to an excess of the majority charge carrier (electrons) in the space charge region (Figure 1-4(c)).

1.4.1.3 Mott-Schottky Method

The Schottky barrier model[169-172] was first proposed to deal with semiconductor/metal contact, and is now also used to for the semiconductor/electrolyte interface. The potential drop ΔU of an electrolyte/semiconductor contact can be expressed by:

$$\Delta U = \Delta U_{sc} + \Delta U_{sf} + \Delta U_{dl} \qquad [1.9]$$

where ΔU_{dl} is the potential drop in the double layer, ΔU_{sc} is the potential drop in space charge layer, and ΔU_{sf} is related to the surface state.

In most cases, the concentration of the electrolyte solution is high. Thus, the potential drop in the diffuse layer can be neglected and $\Delta U_{dl} = \Delta U_H$, where ΔU_H is the potential drop in the Helmholtz layer. For an n-type semiconductor, assuming no surface states, the space charge capacitance C_{sc} is given by the differentiation of q_{sc} vs. U (q_{sc}: the charge amount in the space charge region, U: the applied anodic potential):

$$C_{sc} = \frac{\partial q_{sc}}{\partial U} = \frac{1}{2}(2\varepsilon_0\varepsilon_{sc}eN_D)^{1/2}(U - U_{fb} - \frac{kT}{e})^{1/2} \qquad [1.10]$$

or

$$\frac{1}{C_{sc}^{\ 2}} = \frac{2}{eN_D\varepsilon_0\varepsilon_r}(U - U_{fb} - \frac{kT}{e}) \qquad [1.11]$$

where ε_0 is the permittivity of free space (8.85419×10^{-12} F/m), ε_r is the dielectric constant (relative permittivity), ε_{sc} is the dielectric constant of the space charge layer, e the charge of electron, U the applied potential, N_D the donor or acceptor density, k is the Boltzmann constant and T is the absolute temperature. Equations [1.10] and [1.11] are called Mott-Schottky relationship. For the Mott-Schottky measurements of passive films, the acquired capacitance C of the electrode is related to C_{sc} and C_H by Equation [1.12]:

$$\frac{1}{C} = \frac{1}{C_{sc}} + \frac{1}{C_H} \qquad [1.12]$$

In most cases, the C_H is much larger than C_{sc}[173, 174, 170]. Hence,

$$\frac{1}{C^2} \approx \frac{1}{C_{sc}^{\ 2}} = \frac{2}{eN_D\varepsilon_0\varepsilon}(U - U_{FB} - \frac{KT}{e}) \qquad [1.13]$$

In Mott-Schottky experiments, the electrode capacitance is measured as the potential scans in the anodic direction, by which a $1/C^2$ vs. U plot is produced.

1.4.2 Electronic Properties of Passive Films

The electronic properties of the passive film on iron were studied over the past decade in numerous investigations using capacitance and photocurrent techniques as well as measurements of electron-transfer reactions with defined red/ox couples added to the electrolyte. From capacitance measurements[96, 167], it is clear that the oxide film behaves as a highly doped n-type semiconductor. Generally, the capacitive behavior shows three different regions: at low potentials, a Mott-Schottky type of behavior is observed; at higher potentials, a deviation or a plateau is found, which has been interpreted as dielectric behavior or the presence of a deep donor species; at even higher potentials, the capacitance increases with potential; this has been attributed, for example, to the contribution of the conversion layer.

The presence of two donor levels in the passive film on iron has been attributed by Stimming[175] to the octahedral or tetrahedral sites in the spinel structure. The donors are Fe^{2+} ions which occupy part of the octahedral and tetrahedral sites. This implies that the stoichiometry of the film differs slightly from γ-Fe_2O_3 (all Fe^{3+} sites are occupied).

Different authors have investigated the passive film on Fe with photocurrent spectroscopy[99, 176-179]. In general, the photocurrent spectra can be interpreted using an ideal crystalline semiconductor approach, which yields an indirect band gap of 1.9 eV. During an extensive investigation of iron in pH 8.4 borate buffer, it was found that the band-gap energy is potential-dependent in the potential region 0-0.3V versus the saturated calomel electrode, followed by a nearly constant value of 1.9 eV at higher potentials. It was further observed by Gärtner that the photocurrent at a constant wavelength shows an exponential potential dependence that cannot be described using

the classical model and the behavior $i_{ph} \propto U_{appl}^{0.5}$ was predicted. Therefore, the potential dependence of the photocurrent was interpreted in terms of a field-aided escape from deep states according to a Poole-Frenkel mechanism[180]. Above a potential of 0.7 V, the photocurrent started to decrease with potential, which may be ascribed to the contribution of surface or localized states in the electron-hole recombination kinetics.

The photoinhibition of passivity breakdown was first reported by Lenhart *et al.* [181] for nickel in 1987 and then was observed by various studies on iron[182, 183], stainless steels[184-186] and copper alloys[187, 188]. Schmuki and Bohni[182] have observed that a monochromatic (3.25×10^{-7} m) illumination of iron in borate buffer pH 8.4 leads to a very strong increase in its pitting corrosion resistance. Mott-Schottky analysis and photocurrent transient measurements indicated that illumination during passivation leads to modifications in the electronic properties of the passive films—specifically to an increase of the bulk doping—and the surface state density. The cause for the decreased pitting susceptibility is attributed, by the author[182], to light induced changes in the passive film properties during passivation, rather than the change in the electric field distribution within the passive film[64].

It appears from recent photo-electrochemical studies that thin amorphous oxide films on metals differ in their electronic properties from the corresponding crystalline bulk oxides. In many cases the bandgap energy of passive oxide films can deviate from that of bulk oxides by up to 10% [189]. For amorphous oxide films with a high concentration of localized donor and acceptor states, the term bandgap should be replaced by the mobility gap, which is delimited by two sharp mobility edge E_c and E_v in the mobility gap which can be determined from photo-electrochemical measurements of passive oxide films. However, for simplicity, the term bandgap is still used in most papers even for amorphous films.

Previous work[190, 191] showed that the passive film formed on carbon steel in chromate solution is an n-type semiconductor. Mott-Schottky measurements[192] show that passive film formed on A516-70 carbon steel is an n-type semiconductor with a highly disordered nature, which exhibits a strong frequency dependence of the capacitance behavior. In chromate solution, a thicker space-charge layer, a lower donor density and a more

positive flat-band potential appear in the formed film, which is more stable than that formed in the bicarbonate solution.

In a word, some controversy exists on the detailed nature of the passive film on iron, carbon steel and micro-alloyed steel, even though it represents by far the most extensively studied passive metal system. Since the characteristics of the film depend on many passivation parameters, at least some of the controversy may be due to different experimental conditions.

1.4.3 Effects of Hydrogen on the Electronic Properties of Passive Films

It is now understood that hydrogen exists as atomic hydrogen in the dissolved state in metallic components and is similar to interstitial solute atoms such as carbon, as far as diffusional and solubility characteristics are concerned[5]. Much experimental information and theoretical considerations demonstrate that in transition metals the electron accompanying the proton of the dissociated hydrogen enters the s and d-bands of the host metal changing the density of states at the Fermi surface and causing shifts of the energy bands.

Presently, few investigations were reported on the effects of hydrogen on the electronic properties of passive films. The passive films on type 310 stainless steel are found to exhibit n-type semiconductivity[57, 160]. Observed hysteresis in the capacitance-potential curve and Urbach tail in the photocurrent spectra indicate that the passive films are highly defective. A photoelectrochemical study[160, 193] has shown that hydrogen could increase the disorder degree of the passive film on AISI 310 stainless steel, which is one of the reasons that hydrogen increases the pitting susceptibility. It is also reported[159] that the presence of hydrogen caused an inversion of the semiconducting type of the passive film on 310 stainless steel from p-type to n-type, which was more susceptible to pitting. The shortening of pitting induction times as charging current density increases was related by Yu *et al.*[194] to the increased donor density caused by hydrogen charging. The effects of hydrogen on the electronic properties and the stability of passive films deserve further investigation.

1.5 Summary

Under certain circumstances hydrogen entry into metals and alloys can be facilitated in a number of ways. The hydrogen dissolved in metal and alloys, even in a small quantity, affects the mechanical, corrosion, electrical, and optical properties of the material significantly. The ubiquity of the sources of hydrogen contributes to the importance of hydrogen degradation problems of metallic materials.

Recently, hydrogen-promoted corrosion, *i.e.* the increased susceptibility to corrosion (both general and localized) due to the presence of dissolved hydrogen, has attracted increasing research interest. Most of the related investigations thus far have been concentrated on hydrogen deterioration of the protectiveness of passive films on iron and steels. According to the literature on the passivity of iron, carbon steel and micro-alloyed steel, it appears that:

1) Discrepancies exist in the literature with regard to the structure and composition of the passive film on iron, carbon steel and micro-alloyed steel, whereas the co-existence of Fe^{3+} and Fe^{2+} in the films is generally accepted.

2) The influence of dissolved hydrogen on the composition, structure and properties of the passive film is complex and not completely understood. This partly arises from the open question on the nature and structure of the passive film itself, whereas the adverse nature of the effects is well recognized.

With the advance of modern technology, new surface analysis techniques (both *in situ* and *ex situ*) have been employed in investigating the elusive composition and structure of passive films. Despite this effort, agreement is yet to be established. Furthermore, the mechanism of hydrogen promoted corrosion is still far from clarified. Only a few researchers have reported the effects of hydrogen on the corrosion behavior of metals[194, 195].

The objective of the present work is to further clarify hydrogen induced changes in composition and properties of the passive films on carbon steel and micro-alloyed steel, as well as the interplay between hydrogen and other detrimental factors such as aggressive ions (*e.g.* Cl^-) and elastic tensile stresses, which in combination with hydrogen promote the corrosion of these metals.

References

1. J. C. Maxwell, *Electrical Researches of the Honourable Henry Cavendish*, Frank Cass & Co., (1967).
2. D. Beachem, *Met. Trans.*, **3**, 437 (1972).
3. M. Ruda, D. Farks and J. Abrita, *Physical Review B*, **54**, 9765 (1996).
4. G. C. Bond, *Catalysis by Metals*, Academic Press, New York (1962).
5. R. A. Oriani, in *Proc. Conf. Fundamental Aspects of Stress Corrosion Cracking*, Houston: Natl. Assoc. Corros. Eng., p. 32 (1969).
6. T. Graham, *Phil. Trans. Roy. Soc.(London)*, **156**, 415 (1866).
7. T. Graham, *Phil. Mag.*, **36**, 63 (1868).
8. T. Graham, *Proc. Roy. Soc. (London)*, **16**, 422 (1868).
9. M. Bodenstein, *Z. Electrochem.*, **28**, 517 (1922).
10. W. Raczynski, *Arch. Hutnictwa*, **3**, 59 (1958).
11. J. O'M Bockris, J. McBreen and L. Nanis, *J. Electrochem. Soc.*, **112**, 1025 (1965).
12. T. Zakroczymski, Z. Szklarska-Smialowska and M. Smialowski, *Werkstoffe u. Korrosion*, **26**, 617 (1975).
13. A. H. M. Aten and F. M. Zieren, *Rec. Trav. Chim.*, **49**, 641 (1930).
14. W. Beck, A. L. Glass and E. Taylor, *J. Electrochem. Soc.*, **112**, 53 (1965).
15. T. P. Radhakrishnan and L. L. Shreir, *Electrochim. Acta*, **11**, 1007 (1966).
16. L. D. Kovba and I. A. Bagotskaya, *Zhurn. Fiz. Khim.*, **37**, 161 (1963).
17. J. F. Newman and L. L. Shreir, *Corros. Sci.*, **9**, 631 (1969).
18. M. Smialowski and Z. Szklarska-Smialowska, in *The 17th Meeting of CITCE*, Tokyo, (1966).
19. M. Smialowski and Z. Szklarska-Smialowska, *Rocz. Chem.*, **29**, 85 (1955).
20. J. F. Newman and L. L. Shreir, *Corros. Sci.*, **9**, 631 (1969).
21. G. Trabanelli, F. Zucchi, G. Gullini and V. Carassiti, *Brit. Corr. J.*, **4**, 267 (1969).
22. K. Schwabe and W. Leonard, *Chem. Ing. Techn.*, **38**, 59 (1966).
23. S. L. I. Chan, M. M. Martinez and A. J. Charles, in *International Congress on Metallic Corrosion*, National Research Council of Canada, Ottawa, Ontario, Canada, p. 237 (1984).

24. H. H. Johnson and R. W. Lin, in *Hydrogen Effects in Metals*, I. M. Bernstein and A. W. Thompson, Editors, p. 3, The Metallurgical Society of AIME, New York (1981).
25. M. S. Daw and M. I. Baskes, *Phys. Rev. B*, **29**, 6443 (1984).
26. T. McMullen, M. J. Stott and E. Zaremba, *Phys. Rev. B*, **35**, 1076 (1987).
27. R. A. Oriani, *Ann. Rev. Mater. Sci.*, **8**, 327 (1978).
28. I. M. Bernstein, *Met. Trans.*, **1**, 3143 (1970).
29. A. S. Teteman and W. D. Robertson, *Trans. AIME*, **224**, 775 (1962).
30. I. M. Bernstein and B. B. Rath, *Met. Trans.*, **4**, 1545 (1973).
31. T. Shibata and T. Takeyama, *Corrosion*, **33**, 243 (1977).
32. S. I. Pyun, C. L. and R. A. Oriani, *Corros. Sci.*, **33**, 437 (1992).
33. M. E. Armacanqui and R. A. Oriani, *Corrosion*, **44**, 696 (1988).
34. C. D. Kim, in *Vol. 11, Metals Handbook (9th ed.)*, p. 245, ASM International, Metal Park, OH (1986).
35. D. G. Westlake, *Trans. ASM*, **62**, 1000 (1969).
36. H. K. Birnbaum, *J. Less-Common Met.*, **104**, 31 (1984).
37. D. S. Shih, I. M. Robertson and H. K. Birnbaum, *Acta Metall.*, **36**, 111 (1988).
38. J. Lufrano, P. Sofronis and H. K. Birnbaum, *Journal of the Mechanics & Physics of Solids*, **46**, 1497 (1998).
39. R. N. Iyer and H. W. Pickering, *Annu. Rev. Mater. Res.*, **20**, 299 (1990).
40. A. Srhiri, M. Etman and F. Dabosi, *Electrochim. Acta*, **41**, 429 (1996).
41. J. Bockris and D. Drazic, *Electrochim. Acta*, **7**, 293 (1962).
42. H. P. Dhar, P. E. Conway and K. M. Joshi, *Electrochim. Acta*, **18**, 789 (1973).
43. H. W. Pickering, *Corros. Sci.*, **29**, 325 (1989).
44. P. Forchhammer and H. J. Engell, *Werkst. Korros.*, **20**, 457 (1969).
45. H. S. Isaacs, U. Bertocci and J. Kruger, in *Advances in Localized Corrosion*, S. Smialowska, Editor, NACE, Houston (1990).
46. M. Osawa and M. Hasegawa, *Trans. ISIJ*, **21**, 464 (1981).
47. H. J. Engell, *Electrochim. Acta*, **22**, 987 (1977).
48. H. Böhni, *Langmuir*, **3**, 924 (1987).
49. F. Hine and K. Komai, in *Localized Corrosion*, K. Yamakawa, Editor, Elsevier, London (1988).

50. H. H. Strehblow, in *Corrosion Mechanisms in Theory and Practice*, p. 201, Dekker, New York (1995).
51. M. Hasegawa and M. Osawa, *Corrosion*, **36**, 67 (1980).
52. M. Hasegawa and M. Osawa, *Corrosion*, **39**, 115 (1983).
53. A. A. Seys, M. J. Brabers and A. A. Van Haute, *Corrosion*, **30**, 47 (1974).
54. L. J. Qiao and J. L. Luo, *Corrosion*, **54**, 281 (1998).
55. R. Nishimura, *Mater. Sci. Eng.*, **25**, 1074 (1991).
56. H. Yashiro, B. Pound, N. Kumagai and K. Tanno, *Corros. Sci.*, **40**, 781 (1998).
57. Q. Yang, L. J. Qiao, S. Chiovelli and J. L. Luo, *Corrosion*, **54**, 628 (1998).
58. P. Schmuki and H. Bohni, *J. Electrochem. Soc.*, **139**, 1908 (1992).
59. J. G. Yu, C. S. Zhang, J. L. Luo and P. R. Norton, *J. Electrochem. Soc.*, **150**, B68 (2003).
60. Z. Qin, P. R. Norton and J. L. Luo, *British Corrosion Journal*, **36**, 33 (2001).
61. P. R. Roberge, *Handbook of Corrosion Engineering*, 1140, McGraw-Hill Professional, (1999).
62. P. Marcus, *Corros. Sci.*, **36**, 2155 (1994).
63. N. Sato, *Corros. Sci.*, **31**, 1 (1990).
64. D. D. Macdonald, *Pure & Applied Chemistry*, **71**, 951 (1999).
65. J. W. Schultze and M. M. Lohrengel, *Electrochim. Acta*, **45**, 2499 (2000).
66. N. Cabrera and N. F. Mott, *Reports on Progress in Physics*, **12**, 163 (1948).
67. N. Sato and M. Cohen, *J. Electrochem. Soc.*, **111**, 512 (1964).
68. D. D. Macdonald, *Pure & Applied Chemistry*, **71**, 951 (1999).
69. S. Mischler, A. Vogel, H. J. Mathieu and D. Landolt, *Corros. Sci.*, **32**, 925 (1991).
70. R. Kirchheim, B. Heine, H. Fischmeister, S. Hofmann, H. Knote and U. Stolz, *Corros. Sci.*, **29**, 899 (1989).
71. V. Maurice, W. P. Yang and P. Marcus, *J. Electrochem. Soc.*, **145**, 909 (1998).
72. D. Costa, W. P. Yang and P. Marcus, *Mat. Sci. Forum*, **185-188**, 325 (1995).
73. S. C. Tjong and E. Yeager, *J. Electrochem. Soc.*, **128**, 2251 (1981).
73. M. Nagayama and M. Cohen, *J. Electrochem. Soc.*, **110**, 670 (1963).
75. K. Kuroda, B. D. Cahan, G. Nazri, E. Yeager and T. E. Mitchell, *J. Electrochem. Soc.*, **129**, 2163 (1982).

76. B. D. Cahan and C. T. Chen, *J. Electrochem. Soc.*, **129**, 474 (1982).

77. K. E. Heusler, K. G. Weil and K. F. Bonhoeffer, *Z.phys. Chem. N. F.*, **15**, 149 (1958).

78. M. Nagayama and M. Cohen, *J. Electrochem. Soc.*, **109**, 781 (1962).

79. N. Sato and M. Cohen, *J. Electrochem. Soc.*, **111**, 512 (1964).

80. N. Sato and M. Cohen, *J. Electrochem. Soc.*, **111**, 519 (1964).

81. N. Sato and M. Cohen, *J. Electrochem. Soc.*, **111**, 624 (1964).

82. J. L. Ord, *J. Electrochem. Soc.*, **113**, 213 (1966).

83. N. Sato and M. Cohen, *J. Electrochem. Soc.*, **114**, 585 (1967).

84. N. Sato, *Electrochim. Acta*, **12**, 1135 (1967).

85. C. L. Foley, J. Kruger and C. J. Bechtoldt, *J. Electrochem. Soc.*, **114**, 994 (1967).

86. J. G. N. Thomas and T. J. Nurse, *Br. Corros. J.*, **2**, 13 (1967).

87. R. V. Moshtev, *Ber. Bunsenges. phys. Chem.*, **72**, 452 (1968).

88. S. Haruyama, K. Ogura and K. Nagasaki, *J. Electrochem. Soc. Japan*, **37**, 38 (1969).

89. L. I. Freiman and Y. M. Kolotyrkin, *Protection of Metals*, **5**, 113 (1969).

90. R. P. Frankenthal, *Electrochim. Acta*, **16**, 1845 (1971).

91. A. Rauscher, H. Konno and M. Nagayama, *Electrochim. Acta*, **22**, 823 (1977).

92. K. Ogura and K. Sato, *Electrochim. Acta*, **25**, 857 (1980).

93. Tong E. Pou, Oliver J. Murphy, Vneica Young and John O'M. Bockris, *J. Electrochem. Soc.*, **131**, 1243 (1984).

94. Z. Szklarska-Smialowska and W. Kozlowski, *J. Electrochem. Soc.*, **131**, 499 (1984).

95. K. Azumin, T. Ohtsuka and N. Sato, *J. Electrochem. Soc.*, **134**, 1352 (1987).

96. M. J. Kloppers, F. Bullucci and R. M. Latanision, *Corrosion*, **48**, 229 (1992).

97. A. J. Davenport, J. A. Bardwell and C. M. Vitus, *J. Electrochem. Soc.*, **142**, 721 (1995).

98. S. Virtanen, P. Schmuki, A. J. Davenport and C. M. Vitus, *J. Electrochem. Soc.*, **144**, 198 (1997).

99. J. S. Kim, E. A. Cho and H. S. Kwon, *Corros. Sci.*, **43**, 1403 (2001).

100. H. Gohr and E. Lange, *Naturwissenschaften*, **43**, 12 (1956).

101. H. Gohr and E. Lange, *Z. Elektrochem. Ber Bunsenges. phys. Chem.*, **61**, 1292 (1957).

102. S. Haruyama and T. Tsuru, *Corros. Sci.*, **16**, 623 (1976).

103. D. Rahner and W. Forker, *Z. Phys. Chem.*, **18**, 344 (1978).

104. N. Sato, K. Kudo and T. Noda, *Corros. Sci.*, **10**, 785 (1970).

105. K. Ogura, *J. Electroanal. Chem.*, **79**, 149 (1977).

106. G. M. Schmid and N. Hacherman, *J. Electrochem. Soc.*, **109**, 1096 (1962).

107. K. Ogura, S. Haruyama and K. Nagasaki, *J. Electrochem. Soc. Japan*, **37**, 102 (1969).

108. N. Sato and K. Kudo, *Electrochim. Acta*, **16**, 447 (1971).

109. K. Ogura and N. Hackerman, *J. Electrochem. Soc.*, **120**, 1638 (1973).

110. A. Agius and J. Siejka, *J. Electrochem. Soc.*, **120**, 1019 (1973).

111. K. Ogura and N. Hackerman, *J. Electrochem. Soc.*, **121**, 1013 (1974).

112. K. Ogura and K. Sato, in *The 4th International Symposium on Passivity*, The Electrochemical Society, p. 463 (1978).

113. K. Ogura and T. Majima, *Electrochim. Acta*, **23**, 1361 (1978).

114. K. Ogura and T. Majima, *Electrochim. Acta*, **24**, 325 (1979).

115. W. E. O'Grady, *J. Electrochem. Soc.*, **127**, 555 (1980).

116. J. Eldridge and R. W. Hoffman, *J. Electrochem. Soc.*, **135**, 955 (1989).

117. Cs. Vértes, M. L. Varsányi, A. Vértes, W. Meisel and P. Gütlich, *Electrochim. Acta*, **38**, 2253 (1993).

118. M. Kerkar, J. Robinson and A. J. Forty, *Faraday Discuss. Chem. Soc.*, **89**, 31 (1990).

119. G. G. Long, J. Kruger, D. R. B.ack and M. Kuriyama, *J. Electroanal. Chem.*, **150**, 603 (1983).

120. R. W. Hoffman, in *Passivity of Metals and Semiconductors*, M. Froment, Editor, p. 147, Elsevier Science Publishers B. V., Amsterdam (1983).

121. L. J. Oblonsky and T. M. Devine, *Corros. Sci.*, **37**, 17 (1995).

122. J. C. Rubim and J. Dünnwald, *J. Electroanal. Chem.*, **258**, 327 (1989).

123. J. Gui and T. M. Devine, *Corros. Sci.*, **32**, 1105 (1991).

124. N. Sato, K. Kudo and T. Noda, *Z. Phys. Chem. N. F.*, **98**, 271 (1975).

125. N. Sato, *Corros. Eng. (Tokyo) (Boshoku Gijutsu)*, **23**, 535 (1974).

126. N. Sato, T. Noda and K. Kudo, *Electrochim. Acta*, **19**, 471 (1974).

127. T. Noda, K. Kudo and N. Sato, *J. Jpn. Inst. Met.*, **37**, 951 (1973).

128. N. Sato, K. Kudo and T. Noda, *Electrochim. Acta*, **16**, 1909 (1971).

129. N. Sato, K. Kudo and R. Nishimura, *J. Electrochem. Soc.*, **123**, 1419 (1976).

130. C. T. Chen and B. D. Cahan, *J. Electrochem. Soc.*, **129**, 17 (1982).

131. K. Sugimoto, M. Seto, S. Tanak and N. Hara, *J. Electrochem. Soc.*, **140**, 1586 (1993).

132. S. Virtanen, P. Schmuki, H. Bohni, P. Vuoristo and T. Mantyla, *J. Electrochem. Soc.*, **142**, 3067 (1995).

133. A. J. Davenport, H. S. Isaacs, J. A. Bardwell, B. MacDougall, G. S. Frankel and A. G. Schrott, *Corros. Sci.*, **35**, 19 (1993).

134. A. J. Davenport, M. Sansone, J. A. Bardwell, A. J. Aldykiewicz Jr., M. Taube and C. M. Vitus, *J. Electrochem. Soc.*, **141**, L6 (1994).

135. P. Schmuki, M. Büchler, S. Virtanen, H. Böhni, R. Müller and L. J. Gauckler, *J. Electrochem. Soc.*, **142**, 3336 (1995).

136. P. Schmuki, S. Virtanen, A. J. Davenport and C. M. Vitus, *J. Electrochem. Soc.*, **143**, 574 (1996).

137. A. J. Davenport and M. Sansone, *J. Electrochem. Soc.*, **142**, 725 (1995).

138. L. J. Oblonsky, A. J. Davenport, M. P. Ryan, H. S. Isaacs and R. C. Newman, *J. Electrochem. Soc.*, **144**, 2398 (1997).

139. P. Schmuki, S. Virtanen, A. J. Davenport and C. M. Vitus, *J. Electrochem. Soc.*, **143**, 3997 (1996).

140. P. Schmuki, M. Büchler, S. Virtanen, H. S. Isaacs, M. P. Ryan and H. Böhni, *J. Electrochem. Soc.*, **146**, 2097 (1999).

141. P. Schmuki, S. Virtanen, H. S. Isaacs, M. P. Ryan, A. J. Davenport, H. Bohni and T. Stenberg, *J. Electrochem. Soc.*, **145**, 791 (1998).

142. P. Schmuki S. Virtanen, M. Büchler, H. S. Isaacs, *J. Electrochem. Soc.*, **146**, 4087 (1999).

143. M. F. Toney, A. J. Davenport, L. J. Oblonsky, M. P. Ryan and C. M. Vitus, *Physical Review Letters*, **79**, 4282 (1997).

144. A. J. Davenport, L. J. Oblonsky, M. P. Ryan and M. F. Toney, *J. Electrochem. Soc.*, **147**, 2162 (2000).

145. M. P. Ryan, R. C. Newman and G. E. Thompson, *J. Electrochem. Soc.*, **142**, L177 (1995).

146. M. Ergun and A. Y. Turan, *Corros. Sci.*, **32**, 1137 (1991).

147. K. Videm and A. M. Koren, *Corros. Sci.*, **49**, 746 (1993).

148. Y. F. Cheng and J. L. Luo, *Bulletin of Electrochemistry*, **17**, 97 (2001).

149. Y. F. Cheng, C. Yang and J. L. Luo, *Thin Solid Films*, **416**, 169 (2002).

150. R. C. Salvarezza, D. V. Vásquez Moll and A. J. Arvia, *Electrochim. Acta*, **32**, 1421 (1987).

151. E. Sosa, R. C. Sierra, M. T. Oropeza, F. Hernández, N. Casillas, R. Tremont, C. Cabrera and I. González, *Electrochim. Acta*, **48**, 1665 (2003).

152. S. Mischler, A. Spiegel, M. Stemp and D. Landolt, *Wear*, **251**, 1295 (2001).

153. N. Hackerman and A. C. Makrides, *Ind. Eng. Chem.*, **46**, 523 (1954).

154. J. M. Bastidas, J. L. Polo and E. Cano, *Journal of Applied Electrochemistry*, **30**, 1173 (2000).

155. J. M. Bastidas, J. L. Polo, E. Cano and C. L. Torres, *Journal of Materials Science*, **35**, 2637 (2000).

156. S. Muralidharan, B. Ramesh Babu, S. Venkatakrishna Iyer and S. Rengamani, *Journal of Applied Electrochemistry*, **26**, 291 (1996).

157. P. Ruetschi and R. Giovanoli, *J. Electrochem. Soc.*, **135**, 2663 (1988).

158. J. G. Yu, J. L. Luo and P. R. Norton, *Electrochim. Acta*, **47**, 1527 (2002).

159. M. Z. Yang, J. L. Luo, Q. Yang, L.J. Qiao, Z. Qin and P. R. Norton, *J. Electrochem. Soc.*, **146**, 2107 (1999).

160. Q. Yang and J. L. Luo, *J. Electrochem. Soc.*, **148**, B29 (2001).

161. R. Troiano, *Trans ASM*, **52**, 54 (1960).

162. G. Bianchi and A. Cerquetti, *Corros. Sci.*, **10**, 19 (1970).

163. R. H. Song, S. Pyun and R. A. Oriani, *J. Electrodhem. Soc.*, **137**, 1703 (1990).

164. H. H. Sthehblow, *Surf. Interface Anal.*, **12**, 363 (1988).

165. N. E. Hakiki, M.Da Cunha Belo, A. M. P. SimÔes and M. G. S. Perreira, *J. Electrochem. Soc.*, **145**, 3821 (1998).

166. P. Schmuki, *Journal of Solid State Electrochemistry*, **6**, 145 (2002).

167. M. H. Dean and U. Stimming, *J. Electroanal. Chem.*, **228**, 135 (1987).

168. A. W. Bott, *Current Separations*, **17**, 87 (1998).

169. N. Cabrera, and N. F. Mott, *Reports on Progress in Physics*, **12**, 267 (1948).

170. U. Stimming, in *Passivity of Metals and Semiconductors*, M. Froment, Editor, p. 477, Elsevier Science Publishers B. V., Amsterdam (1983).

171. N. F. Mott, E. A. Davis, in *Electronic Processes in Non-Crystalline Materials*, Clareno, Editor, Oxford (1979).

172. H. Gerischer, *Corros. Sci.*, **29**, 257 (1989).

173. Cahan B D, Chen C T, J Electrochem Soc., Vol.129 (1982), pp474

174. Koenig U, Schultze J W, Solid State Ionics 53-56 (1992), pp255

175. U. Stimming, PhD Thesis, Freie Universität Berlin (1979).

176. A. D. Paola, F. D. Quarto and C. Sunseri, *Corros. Sci.*, **26**, 935 (1986).

177. P. C. Searson, R. M. Latanision and U. Stimming, *J. Electrochem. Soc.*, **135**, 1358 (1988).

178. K. Azumi, T. Ohtsuka and N. Sato, *J. Electrochem. Soc.*, **133**, 1326 (1986).

179. T. O. Burleigh and R. M. Latanision, *J. Electrochem. Soc.*, **134**, 135 (1987).

180. H. H. Poole, *Philos. Mag.*, **33**, 112 (1916).

181. S. Lenhart, M. U. Macdonald and D. D. Macdonald, *Electrochim. Acta*, **32**, 1739 (1987).

182. P. Schmuki and H. Böhni, *Electrochim Acta*, **40**, 775 (1995).

183. D. F. Heaney and D. D. Macdonald, *J. Electrochem. Soc.*, **146**, 1773 (1999).

184. D. D. Macdonald, E. Sikora, M. W. Balmas and R. C. Alkire, *Corros. Sci.*, **38**, 137 (1997).

185. C. B. Breslin, D. D. Macdonald, E. Sikora and J. Sikora, *Electrochim. Acta*, **42**, 127 (1997).

186. D. D. MacDonald, E. Sikora, M. W. Balmas and R. C. Alkire, *Corros. Sci.*, **38**, 97 (1996).

187. H. Brookes, M. Vasquez and D. D. Macdonald, *Corrosion*, **55**, 343 (1999).

188. C. B. Breslin and D. D. Macdonald, *Electrochim. Acta*, **44**, 643 (1998).

189. J. W. Schultze and L. Elfenthal, *J. Electroanal. Chem.*, **204**, 153 (1986).

190. Y. F. Cheng and J. L. Luo, *Electrochim. Acta*, **44**, 2947 (1999).

191. Y. F. Cheng and J. L. Luo, *Electrochim. Acta*, **44**, 4795 (1999).

192. Y. F. Cheng and J. L. Luo, *Applied Surface Science*, **167**, 113 (2000).

193. Q. Yang, M. Z. Yang and J. L. Luo, in *Proceedings of the 8th International Symposium on Passivity of Metals and Semiconductors, Vol.99-42, Corrosion Monograph Series*, The Electrochemical Society, p. 214 (2000).

194. J. G. Yu, J. L Luo and P. R. Norton, *Applied Surface Science*, **177**, 129 (2001).

195. Q. Yang and J. L. Luo, *Thin Solid Films*, **371**, 132 (2000).

Chapter 2 Effects of Hydrogen on Composition and Structure of Passive Films

2.1 Introduction

With increasing research interest on hydrogen-promoted corrosion, investigations have been conducted on the effect of hydrogen on the passive film formed on variety of metals[1-3], especially on stainless steel[4-6] and pure iron[7, 8].

Despite all these efforts, a general mechanistic theory has not been achieved to encompass quantitative factors and critical parameters governing the detrimental effects of hydrogen on passive films. This mainly arises from the unanswered questions concerning the nature of the passive film and the complexity of detrimental hydrogen effects. For example, different compositions and structures have been suggested for passive films on iron to explain the cathodic reduction curves of the passive film[9-14], and divergence exists regarding the electrochemical reactions responsible for the reduction of the film. Data addressing the first arrest of the reduction curve is also lacking. Thus no conclusive opinion has been obtained about the cathodic reduction mechanism, and consequently the chemical composition and structure, of the hydrogen containing passive film. Yu *et al.*[14, 15] have attributed the decreased stability of the passive film on iron to the possible thinning and increased hydration degree of the passive film due to hydrogen-charging but quantitative evaluations of these processes are yet to be released. The study in this chapter is aiming to provide a semi-quantitative explanation for the effects of hydrogen on the corrosion behavior of the passive film.

X70 micro-alloyed steel is now widely used in many industries, usually under cathodic protection. The action of cathodic protection is one of the main sources of hydrogen generation in metal and alloys. However, little work has been done to study the passive film on such materials. In this chapter, *in situ* electrochemical methods have been employed to explore the effect of hydrogen on the passive film of X70 micro-alloyed steel. It is anticipated that this will help to advance the understanding of the mechanism by which hydrogen influences the properties of passive film.

2.2 Experimental Details

2.2.1 Materials and Solutions

X70 steel (0.04%C, 1.46%Mn, 0.003%S, 0.008%P, 0.24%Si, 0.22%Cu, 0.1%Ni, 0.05%Cr, 0.073%Nb, 0.2%Mo, 0.028%Al, 0.024%Ti, in wt%, and the balance Fe), from IPSCO Inc., was used as the electrode material in the experiments. The specimens were cut into 0.02 × 0.02 × 0.001 m^3 coupons. Both surfaces of each specimen were mechanically ground down to 600-grit emery paper and degreased with acetone before the experiments.

0.1 M NaOH + 150 ppm As_2O_3 solution was used to charge hydrogen at designed cathodic current densities. The test electrolyte solution was 0.3 M H_3BO_3 + 0.075 M $Na_2B_4O_7 \cdot 10H_2O$ at pH 8.4. All solutions were prepared with analytical grade reagents and deionized water.

2.2.2 Electrochemical Cell Setup

In the electrochemical experiments, a Devanathan type[16] cell (Figure 2-1) was employed for the measurements, with the specimen separating a hydrogen-charging compartment from a measurement compartment. The area on each side of the specimen exposed to the charging and test solutions is about 1.2 × 10^{-4} m^2.

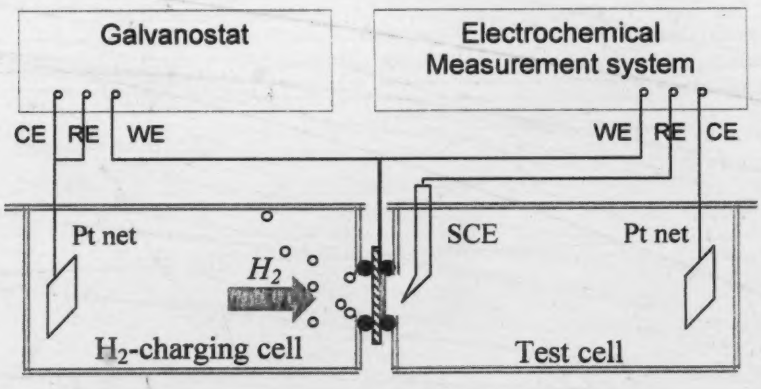

Figure 2-1. Schematic illustration of the electrochemical cell setup.

WE: working electrode, RE: Reference electrode, CE: counter electrode.

The potential of the working electrode was measured with respect to a saturated calomel electrode (SCE). In the present work, all potentials are referred to the SCE scale. In both compartments of the Devanathan cell, platinum nets were used as the counter electrodes. Prior to each run, the test side of working electrode was held at -1.0 V for 10 minutes to achieve a completely electro-reduced surface in the electrolyte. Potential dynamic and static measurements were recorded with an EG&G Instrument Model 273 Potentiostat. All measurements were carried out at ambient temperature in quiescent solutions. All the electrochemical measurements were performed at least twice, in order to verify the reproducibility of the results. Some experiments were repeated even 7 to 8 times to get consistent results.

2.2.3 Electrochemical Measurements

2.2.3.1 Open Circuit Potential Decay

The open circuit potential (U_{OC}) decay was measured after the specimens had been passivated for 2 hours at a desired constant film formation potential. For the hydrogen charged case, the charging was started in the charging compartment after the passivation was initiated in the measurement compartment for 1 hour, and was then kept concurrent with the passivation for another 1 hour. Both charging and passivation were interrupted upon the start of measurements of the variations of the U_{OC} of the specimens with time.

2.2.3.2 Pitting Potential Measurements

The U_p was determined from potentiodynamic polarization curve measurements in solutions containing various chloride ion concentrations. The potential was scanned towards the anodic direction at a rate of 3.3×10^{-4} V/s from the potential of -0.1 V to the U_{OC}. The potential corresponding to an abrupt increase in current was taken as the U_p. For the hydrogen charged case, hydrogen was charged into the entry side for 1 hour first and then the potential scanning was started with concurrent hydrogen charging.

2.2.3.3 Galvanostatic Cathodic Reduction

For the cathodic current reduction experiments, the interference of dissolved oxygen in the solution with oxide reduction was eliminated by bubbling nitrogen through the test

solution before the specimen was exposed and throughout the testing. The specimen was first passivated at the desired potential for 2 hours, and then the cathodic reduction at -0.1 A/m^2 was commenced in the same electrolyte solution immediately after the passivation was completed. The variation of electrode potential with time was recorded. For the hydrogen charged case, the charging was started after the specimen had been passivated for 1 hour and was kept concurrent with the passivation for another 1 hour.

2.2.3.4 AC Impedance Measurements

The electrochemical impedance response was studied for of the passive film on X70 steel formed at various film formation potentials under a constant hydrogen charging current density. The specimen was initially passivated at 0 V for 1 hour followed by the impedance measurement, and then the potential was stepped 0.1 V higher anodically for the next measurement cycle, *i.e.*, 1 hour passivation + impedance measurement. The potential stepping and measurement cycle was continued until the potential reached 0.7 V. For the hydrogen charged case, the charging was started 1 hour before the passivation at 0 V and was kept concurrent until the experiments were ended at a potential of 0.7 V. For all the impedance measurements, the frequency was scanned logarithmically from 10,000 Hz to 0.01 Hz with eight points per decade. The peak-to-peak amplitude of the AC signal was 0.01 V.

2.3 Main Results and Discussion

2.3.1 Open Circuit Potential Decay

The change of electrode potential with time was traced after the interruption of applied anodic polarization at 0.6 V for 2 hours, and the results are plotted in Figure 2-2. The U_{OC} decays until a static potential is reached. For the charged specimens, a rapid drop in the potential was observed and after 500 seconds steady values in the vicinity of -0.3 V were reached, while for the uncharged specimen the potential underwent gradual decrease and finally reached a relatively stable value of about -0.2 V after 2000 seconds. It is generally accepted that the potential decay of the specimens at open circuit can be derived from the dissolution of the passive film upon the interruption of the applied film formation potential. The longer the elapsed time that occurs before the

potential reached a steady value, the more stable is the film. The rapid potential decay rate and lower steady value of the potential for the charged specimens show clearly that a less stable passive film was formed on the hydrogen charged specimens. The lower steady potential for hydrogen containing specimen also indicates that a higher dissolution rate of the specimen occurs at equilibrium state than that of uncharged electrode.

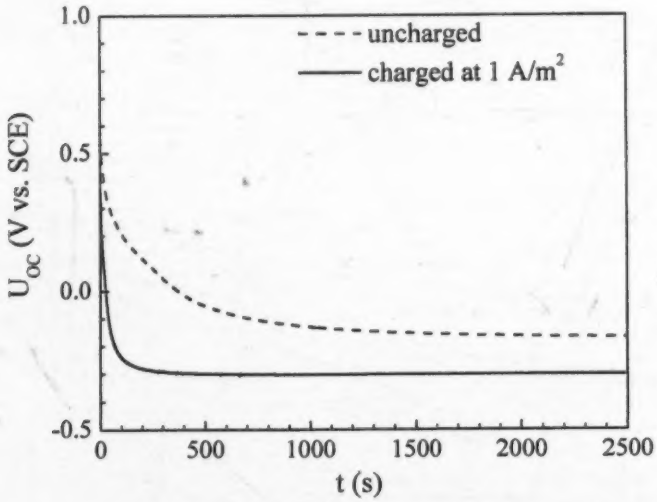

Figure 2-2. The variations of the U_{OC} with time for uncharged and charged specimens passivated at 0.6V for 2 hours.

2.3.2 Pitting Potential Measurements

The anodic polarization curve for X70 micro-alloyed steel is presented in Figure 2-3. The result shows that X70 steel exhibits passivity behavior in the potential range from U_{OC} to 0.9 V in 0.3 M H_3BO_3 + 0.075 M $Na_2B_4O_7 \cdot 10H_2O$ buffer solution.

In order to investigate the effect of hydrogen on the pitting breakdown process, the pitting potentials (U_p) were measured for the passive film on uncharged and charged specimens exposed to solutions containing various concentrations of chloride ions. Figure 2-4(a) shows the variation of the U_p with the concentration of chloride ions for the specimen uncharged and charged with 1 A/m^2. It is shown that the U_p changes linearly

with the logarithm of Cl^- concentration for the passive film on both uncharged specimens and those charged at 1 A/m^2.

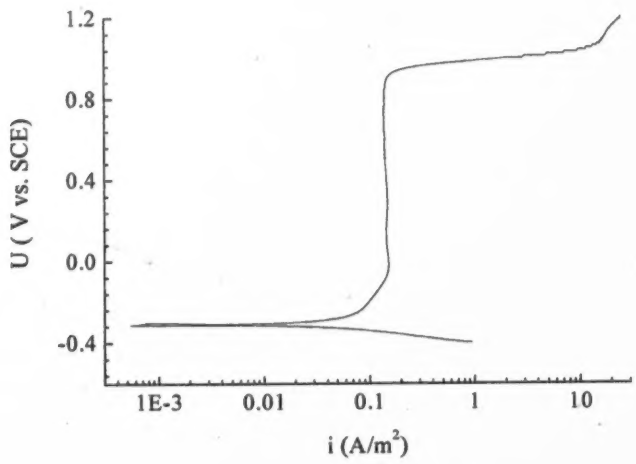

Figure 2-3. Polarization curve of X70 micro-alloyed steel in 0.3 M H_3BO_3 + 0.075 M $Na_2B_4O_7 \cdot 10H_2O$ buffer solution. The scan rate was controlled at 0.001 V/s.

The slopes characterizing the linear dependence of U_p on the logarithm of Cl^- concentrations are given by linear fitting of the data in the U_p versus ln([Cl^-]) plot Figure 2-4(b):

Uncharged: $$\frac{dU_p}{d\lg([Cl^-])} = -0.3 \qquad [2.1]$$

Hydrogen-charged: $$\frac{dU_p}{d\lg([Cl^-])} = -0.2 \qquad [2.2]$$

It can be seen that U_p decreases with increasing concentration of chloride ions for both cases and the hydrogen decreased the value of U_p at all chloride ion concentrations below 0.1 M, especially at relative low Cl^- concentrations, indicating that the hydrogen strongly facilitates the pitting corrosion and localized breakdown of the passive film.

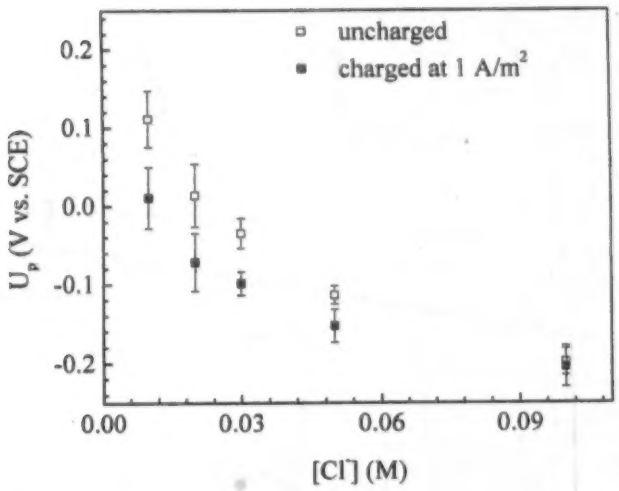

Figure 2-4(a). Changes of U_p with the concentration of chloride ions in solution for hydrogen charged and uncharged specimens.

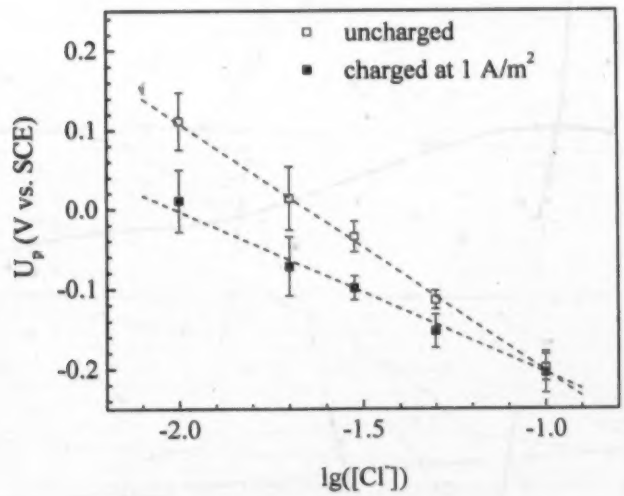

Figure 2-4(b). Plots of U_p vs. ln([Cl^-]).

Theories have been proposed to interpret the critical U_p and describe the breakdown in terms of the chemical or electrochemical reaction[17-21] occurring between the passive film and aggressive anions (Cl^-) adsorbed on it. Passivity breakdown could be incurred by

the displacement of adsorbed chloride ions with adsorbed oxygen at local sites[22]. The displacement results in an increase in the exchange current density for metal dissolution, and pit initiation at favored sites was therefore observed to occur at a well-defined potential corresponding to the critical U_p[22]. The competition for adsorption at the oxide/electrolyte interface between hydroxyl ions and aggressive anions, such as the chloride ions, was also related to the pit initiation potential by Bird *et al.*[19]. As the Cl^- adsorption grows stronger, the U_p becomes more negative. Higher Cl^- concentration in the solution would facilitate the adsorption, and thus give rise to lower U_p. For hydrogen charged specimens, lower pH value in the vicinity of the hydrogen-containing passive film may be present, due to the oxidation of hydrogen at the electrode/solution interface[23], or the hydrolysis of more dissolving metal ions produced by hydrogen-enhanced passive film dissolution[24,25]. With the depletion of OH^-, *i.e.*, lower pH value, more Cl^- ions will migrate to the site to maintain electrical neutrality and be adsorbed on the film surface. In other words, hydrogen enhances the localized acidification leading to pitting[26,27]. In addition to this fact, hydrogen may result in highly disordered passive film with increased defects and inhomogeneity[8, 28, 29], and thus favor the non-uniform adsorption mechanism of chloride ions. This was proposed by Heusler[30] to explain passivity breakdown which at the same time provide more weak points at which pitting may arise[31].

A possible thinning of the passive film may be caused by hydrogen, as Ogura and Kaneko[31] pointed out that an indispensable condition for pit initiation is that the passive film is thinned before pitting occurs. During anodic film growth, the electric field within the passive film was found to be of the order of 10^{10} V/m^2. According to Sato[32], this electric field exerts significant electrostriction on the film and yields high internal compressive stresses in the film. Under the same film formation potential, higher field strength is present in a thinning passive film. As a result, higher internal stress would arise in a thinner passive film, making it susceptible to the mechanical breakdown of passivity. The lower U_p of hydrogen-containing passive films may infer a possible thinning effect induced by hydrogen charging.

2.3.3 Cathodic Current Reduction of Passive Films

Galvanostatic reductions of the passive films formed at 0.2 and 0.6 V on X70 steel

charged with hydrogen at various current densities were performed at -0.1 A/m^2. The consumed charges as a function of potential are shown in Figure 2-5 and Figure 2-6, respectively.

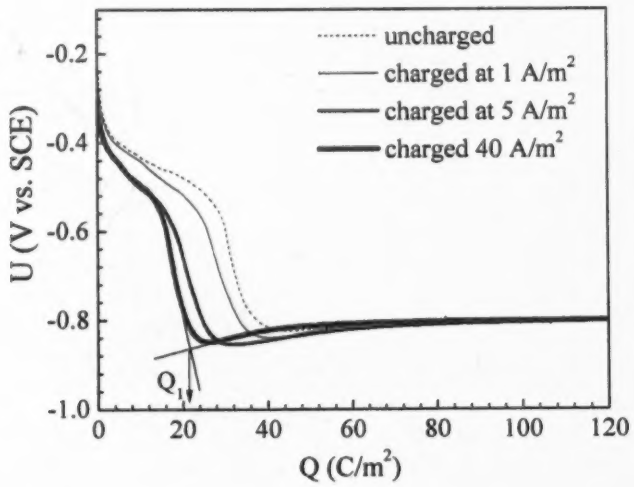

Figure 2-5. Galvanostatic reduction curves of specimens passivated at 0.2 V for 2 hours by a cathodic current of 0.1 A/m^2.

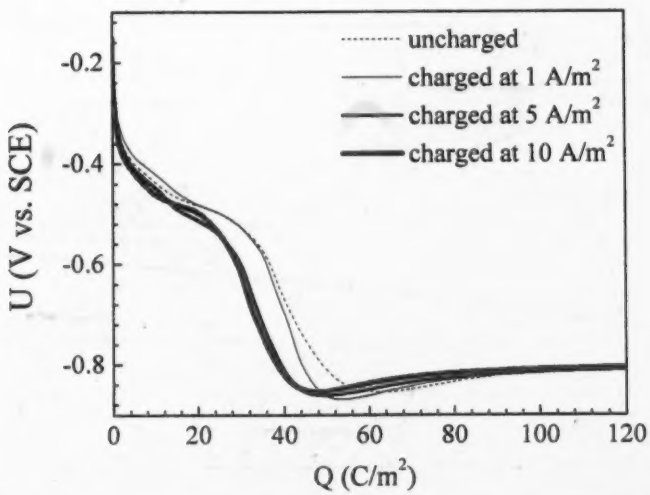

Figure 2-6. Galvanostatic reduction curves of specimens passivated at 0.6 V for 2 hours by a cathodic current of 0.1 A/m^2.

For both charged and uncharged specimens, two plateaus appear in the curves obtained, which are located at around -0.54 V and -0.84 V, respectively. This phenomenon is similar to the behavior of the film on iron[10,14]. According to the duplex layer model postulated by Nagayama and Cohen[9], the anodically passivated iron in a boric acid/borate buffer solution at a pH of 8.41 is covered with an oxide film consisting of an inner Fe_3O_4 and outer γ-Fe_2O_3 layer. The first plateau of the reduction curve is commonly attributed to the reduction of the external film layer and the second to the reduction of the internal layer, in view of reducing the film from the oxide/solution interface inward[9, 33, 34].

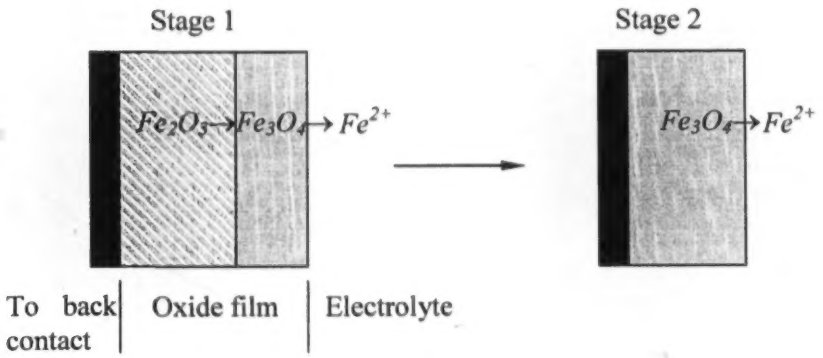

Figure 2-7. Schematic model for galvanostatic reduction of Fe_2O_3 in borate buffer of pH 8.4.[35]

Schmuki *et al.*[35] have studied the cathodic dissolution of sputter-deposited iron oxide layers as model systems for the nature passive film on iron with the *in situ* XANES method, and suggested that during the reduction of a single layer film of Fe_2O_3, a solid-state transformation $Fe_2O_3 \rightarrow Fe_3O_4$ reaction occurs prior to the reductive dissolution of Fe_3O_4 to Fe^{2+} ions in solution, as illustrated in Figure 2-7. The galvanostatic reduction results obtained in the present work are interpreted in terms of this two-stage scheme. The following expression[36] is used to calculate the film thickness (d):

$$d = \frac{QM_w}{zF\rho r} \qquad [2.3]$$

where Q is the cathodic charge consumed to reduce a film of thickness d, M_w = molecular weight of the compound undergoing reduction, z = number of electrons used, F = Faraday constant, ρ = density of the compound, r = roughness coefficient. Theoretical thinning rates, $\frac{d}{Q}$, for different cathodic reactions calculated are listed in Table 2-1. The roughness factor employed is 1.2.[37]

Table 2-1. Theoretical thinning rates for the cathodic reductions of the passive films on iron and the values for density and molecular weight used for the calculation

Compound	Type of reaction	M_w (kg/mol)	ρ (kg/m^3)	Thinning rate $(\frac{m}{C/m^2})$
γ-Fe_2O_3	$Fe_2O_3 \rightarrow 2Fe^{2+}$	0.15969	5.24×10^3	1.32×10^{-10}
γ-Fe_2O_3	$Fe_2O_3 \rightarrow \frac{2}{3}Fe_3O_4$	0.15969	5.24×10^3	3.95×10^{-10}
Fe_3O_4	$Fe_3O_4 \rightarrow 3Fe^{2+}$	0.23154	5.18×10^3	1.93×10^{-10}

According to Schmuki *et al.*'s two-stage reduction scheme, the charge consumed in the reduction of the whole Fe_2O_3 layer of the passive film is divided into two parts: one for the reduction of the whole layer of Fe_2O_3 to Fe_3O_4, and the other for the reduction of the whole layer of Fe_3O_4 to Fe^{2+} (in solution). Thus the thickness d_1 of the external Fe_2O_3 layer of the passive film can be calculated, using the thinning rate given in Table 2-1, by Equation [2.4]:

$$d_1 = \frac{Q_1}{1/1.93+1/3.95} = 1.30Q_1 \qquad [2.4]$$

where Q_1 (as defined[10] in Figure 2-5) is the total amount of charge consumed to reduce the Fe_2O_3 layer of thickness d_1.

The values of d_1 calculated using Equation [2.4] turn out to be in the range of 5×10^{-9} ~ 8×10^{-9} m, which is larger than the value ($\leq 5\times10^{-9}$ m) generally acknowledged for the

passive film on iron in borate buffer[9, 38, 39]. This excessive consumption of cathodic charge could be ascribed to reduction to Fe^{2+} from an oxidation state higher than Fe^{3+}. Several authors[9, 40, 41] have presumed the occurrence of highly oxidized iron compound in passive films. According to Nagayama and Cohen[9, 40, 41], the outermost portion of the film is a cation-deficient structure such as $Fe_x^{6+} \cdot Fe_{2-2x}^{3+} \cdot \square_x \cdot O_3$. Konno and Nagayama[40], using XPS, found an average valence of iron in the film equal to 3.59 and claimed that in the outermost film layer the average oxidation degree significantly exceeds that of Fe^{3+}.

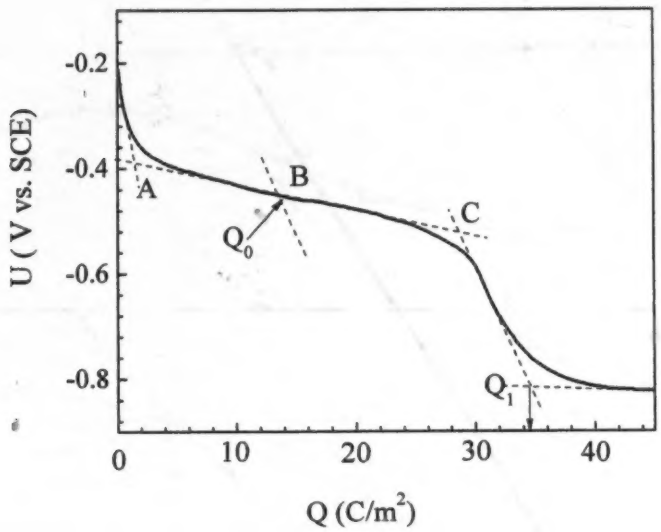

Figure 2-8. Galvanostatic reduction curve for the uncharged specimen passivated at 0.2V for 2 hours. The specimen was reduced at 0.1 A/m^2 in the solution of pH 8.4.

Taking this into consideration, a modification of the two-stage reduction scheme (Figure 2-7) of Fe_2O_3 is proposed, as illustrated in Figure 2-8. The charge Q_0 consumed during the very early stage on a reduction curve is assumed to correspond to the reduction of the high valence oxide on the surface, which presumably has a negligible thickness. Thus the passive film thickness can be derived from Q_1 reduced by Q_0. The value of Q_0 is determined graphically from the reduction curves[13]. Tangents are drawn to the curve at its inflection points. The line AC is bisected at point B, whose abscissa gives the value of

Q_0 (which corresponds to E_1 in the literature[13]). In Table 2-2, calculated values are given for the passive film formed under different film formation potential (U_f) and hydrogen-charging current density (i_{charge}). Equation [2.4] was used for the thickness calculation by replacing Q_1 with $Q_1 - Q_0$. The thickness obtained falls into a rather reasonable range.

Table 2-2. The cathodic charge consumed for reduction of the passive film formed under different conditions and corresponding calculated thickness.

U_f (V)	i_{charge} (A/m^2)	Q_0 (C/m^2)	Q_1 (C/m^2)	d_1 $\times 10^9$ (m)
0.2	0	14	35	2.7 ± 0.1
	1	13	32	2.5 ± 0.2
	5	9	26	2.2 ± 0.3
	10	8	23	2.0 ± 0.2
	25	9	23	1.8 ± 0.3
	40	8	22	1.8 ± 0.3
0.6	0	17	50	4.3 ± 0.1
	1	17	48	4.1 ± 0.2
	5	16	47	4.0 ± 0.2
	10	15	42	3.5 ± 0.3
	25	15	42	3.5 ± 0.3
	40	15	42	3.5 ± 0.2

It follows from the data in Table 2-2 that hydrogen charging resulted in a thinner external Fe_2O_3 layer, and thence a lower passive film thickness. The thinning effect was enhanced by increasing hydrogen charging current density and saturated at an i_{charge} of about 10 A/m^2. Passive films formed at a more positive potential were thicker and less thinned, as a 25.9 % decrease in thickness d_1 was observed for the passive film formed at 0.2 V and 18.6 % for the film passivated at 0.6 V due to hydrogen charging of 10 A/m^2.

Another noticeable effect of hydrogen-charging lies in the difference between reduction curves of passive films formed at the two potentials. As shown in Figure 2-5 and Figure 2-6, the reduction curves for both potentials look roughly the same, except

that lower Q_0 and Q_1 values were present on reduction curves of films passivated at 0.2 V than those for 0.6 V. In addition, hydrogen charging decreased Q_0 for reduction curves of 0.2 V much less than it did for films formed at 0.6 V. It is seen clearly that in Figure 2-6, the first plateaus of reduction curves for uncharged and charged specimens are positioned very closely, while in Figure 2-5 the first plateaus of charged specimens are positioned with separation, indicating that less cathodic charge needed to reduce the outmost high valence iron ions. Therefore it can be inferred that the hydrogen charged into the electrodes could have reduced the high valence of iron element in the film, in addition to decreasing the film thickness.

It was found through all the cathodic reduction experiments in duplicate, that the largest experimental error for Q_0 and Q_1 are 0.8 and 3 C/m^2, respectively, thus the total error for the calculated film thickness is less than 5×10^{-10} m. Therefore, the trend of thinning effect of hydrogen ingression, indicated by the d_1 data in Table 2-2, is reliable, especially with relatively high hydrogen charging current densities. And the beneficial influence of passivating potential on the film thickness is evident as well.

2.3.4 AC Impedance Measurements

The effect of hydrogen on the ion transportation and capacitance of the passive film was also investigated by means of impedance measurements. Figure 2-9 shows the Nyquist plots measured at 0.2 V for the specimens charged with different current density as well as the uncharged ones. The curve takes a shape of depressed semicircle with the center of the circle below the real axis. It is obvious that charging decreased the diameter of the semi-circle markedly. It was observed that the more charging current density, the more decrease and depression in diameter appeared.

The analysis of the impedance data was carried out using the non-linear least squares fitting Levenberg-Marquardt algorithm and the equivalent circuit model in Figure 2-10,[42] where R_s means the solution resistance, R_{ct} represents the charge transfer resistance of interfaces of metal/film and film/solution, C_f is the capacitance of passive film and R_f the resistance of ion diffusion in the passive film, and CPE is related to the "double layer capacitor", whose impedance is

$$Z_{CPE} = A(j\omega)^{-\alpha} \qquad [2.5]$$

where the constant $A = 1/C_{dl}$ (C_{dl}: the double layer capacitance) and the exponent α is less than one. The simulated results were plotted in Figure 2-9 together with the experiment results.

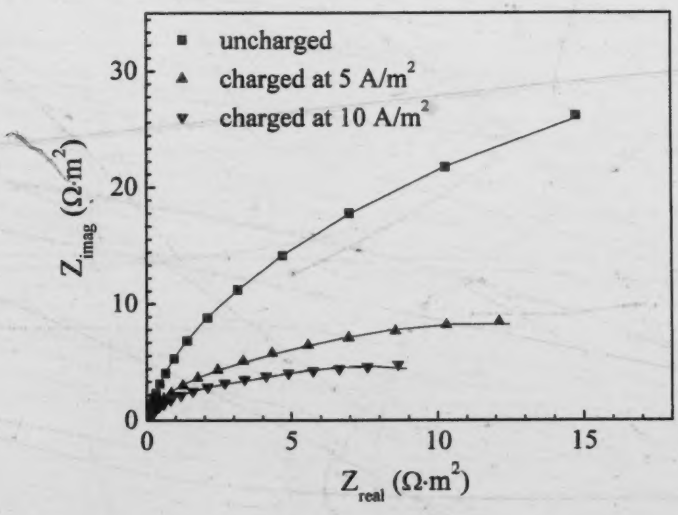

Figure 2-9. Nyquist plots of impedance spectra measured (in points) at 0.2V and their simulated results (in lines).

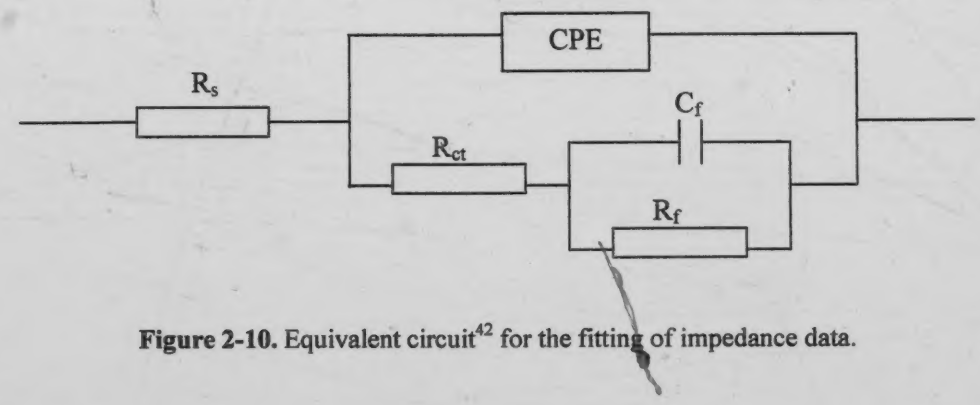

Figure 2-10. Equivalent circuit[42] for the fitting of impedance data.

Table 2-3. The values of R_s, R_f, C_f, CPE, R_{ct} for the passive films on specimens charged with various current densities.

U_f (V)	i_{charge} (A/m^2)	R_s (Ω)	R_f ($\Omega \cdot m^2$)	C_f (F/m^2)	CPE		R_{ct} ($\Omega \cdot m^2$)
					C_{dl} (F/m^2)	α	
	0	97.4	30.1	0.34	0.32	0.94	81.3
	1	97.1	10.3	0.55	0.30	0.94	16.7
0.2	5	100.8	8.0	0.97	0.31	0.93	12.2
	10	106.7	6.2	1.20	0.29	0.93	8.9
	25	100.8	6.3	1.26	0.28	0.94	8.5
	0	99.0	32.7	0.27	0.22	0.94	93.6
	1	119.4	10.3	0.48	0.22	0.93	15.6
0.6	5	116.9	8.3	1.03	0.22	0.93	11.1
	10	114.3	6.9	1.08	0.22	0.92	9.7
	25	113.0	6.5	1.17	0.21	0.92	9.2

Table 2-4. The values of R_s, R_f, C_f, CPE, R_{ct} for the passive films formed at different potentials without hydrogen charging.

U_f (V)	R_s (Ω)	R_f ($\Omega \cdot m^2$)	C_f (F/m^2)	CPE		Rct ($\Omega \cdot m^2$)
				C_{dl} (F/m^2)	α	
0	110.5	19.5	0.99	0.49	0.94	50.5
0.1	111.3	18.8	0.94	0.43	0.95	59.2
0.2	112.1	16.9	0.81	0.38	0.95	58.7
0.3	112.6	16.8	0.77	0.35	0.95	61.5
0.4	112.7	16.6	0.75	0.32	0.95	65.4
0.5	112.8	17.5	0.68	0.29	0.95	69.2
0.6	113.0	16.7	0.65	0.26	0.95	72.1
0.7	113.2	15.0	0.61	0.25	0.95	70.3

Table 2-5. The values of R_s, R_f, C_f, CPE, R_{ct} for the passive films formed at different potentials on the specimens charged with 10 A/m^2.

U_f (V)	R_s (Ω)	R_f ($\Omega \cdot m^2$)	C_f (F/m^2)	CPE		R_{ct} ($\Omega \cdot m^2$)
				C_{dl} (F/m^2)	α	
0	131.4	4.4	2.31	0.50	0.89	6.0
0.1	133.6	4.9	1.78	0.38	0.91	6.6
0.2	134.6	5.6	1.71	0.32	0.92	6.9
0.3	135.2	5.9	1.43	0.28	0.92	6.7
0.4	135.8	6.1	1.25	0.26	0.91	6.5
0.5	136.6	6.5	1.16	0.23	0.91	6.5
0.6	137.0	7.0	1.21	0.21	0.91	6.8
0.7	138.1	6.9	1.06	0.21	0.89	6.9

The coincidence of the experimental data with the simulated results underlies the validity of the equivalent circuit for characterizing the passivated electrode. The parameter of each element in the equivalent circuit (Figure 2-10) was calculated by simulation for passive films formed under different conditions, and the results are listed in Table 2-3, Table 2-4 and Table 2-5. Hydrogen effects on some major parameters of the passive film were analyzed in Figure 2-11 - Figure 2-13. It is shown that hydrogen increases the film capacitance, and decreases the resistance to charge transfer and ion diffusion of the passive film.

Only the results of one typical experiment set are demonstrated in this section (the impedance measurements). The reason is that certain errors were found to be yielded by Non-linear Least Squares Fitting of the experimental data with controlled goodness of fit (fit error $\leq$ 1%); in order to avoid the confusion between the fitting errors and the experimental ones, exact values of the experimental errors from the experiments in repetition are not listed. Experiments were repeated 3-4 times and similar results, having the same trends of hydrogen effects as analyzed hereafter, were observed.

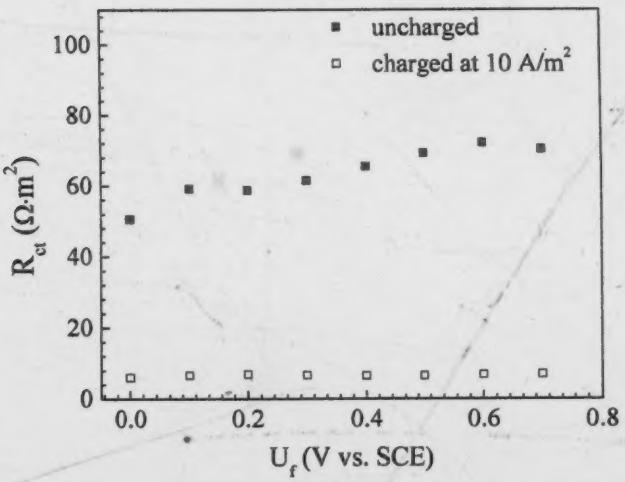

Figure 2-11. Charge transfer resistances of passive films on charged and uncharged specimen as a function of film formation potentials.

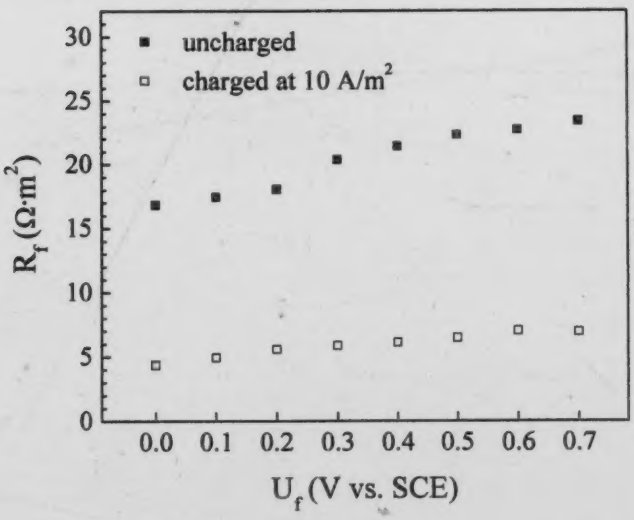

Figure 2-12. Ion diffusion resistances of passive films on charged and uncharged specimens as a function of film formation potentials.

The influence of film formation potential on charge transfer resistance is

demonstrated in Figure 2-11, where different trends for charged and uncharged specimens were observed. For the uncharged case, the charge transfer resistance increased with film formation potential, indicating an increasing stability and thickness of the film with potential. Whereas for the charged specimen, whose charge transfer resistances were significantly lower than those for the uncharged specimen, no big difference was identified among the charge transfer resistances at different potentials. Thus it can be inferred that hydrogen charging has a deleterious effect on the stability of the passive film, which overrides the beneficial influence of increasing potentials on the stability and thickness of the film. This effect was further borne out by the decrease of ion diffusion resistance of the passive film. As was shown in Figure 2-12, hydrogen facilitates the ion diffusion and transport process in the passive film and thus decreases the stability of the passive film. The value of capacitance of the passive film is related to the film thickness d and the relative permittivity ε_r of the film, as is given in the definition of capacitance:

$$C = \frac{\varepsilon_r \varepsilon_0 S}{d} \qquad [2.6]$$

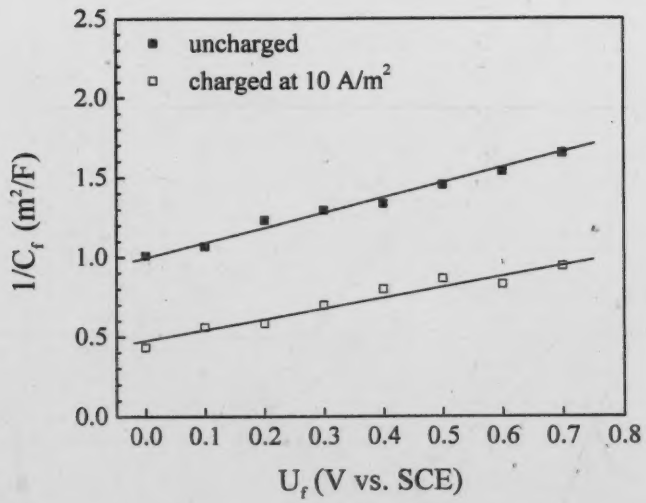

Figure 2-13. Dependence of $1/C_f$ on the film formation potential for uncharged specimen and the one charged at 10 A/m^2.

Figure 2-13 shows the variation of the reciprocal of capacitance of the passive film as a function of film formation potential for both charged and uncharged cases. A linear increase in $1/C_f$ can be seen as the potential goes up from 0 to 0.7 V for both the charged and uncharged specimens, suggesting a thickening of the passive film with increasing potentials and/or a decrease in ε_r due to the compositional change (possibly the decreasing Fe^{2+}/Fe^{3+} ratio[7]) in the film with rising film formation potentials. Similarly, the higher capacitance for the charged specimen than the uncharged one might imply a thinning of the passive film and/or an increase in the dielectric constant ε_r of the film due to hydrogen charging. Thus we can infer that hydrogen charged into the passive film may reduce part of Fe^{3+} ions into Fe^{2+}, resulting a increase in Fe^{2+}/Fe^{3+} ratio in the film and consequently an increased ε_r. Moreover, a smaller slope of the line for the charged specimen than that for the uncharged specimen suggests that the increasing potential thickens the passive film on uncharged specimen more than it does the charged specimen, thus indicating further that the passive film on a charged specimen might be thinner than that on an uncharged specimen passivated at the same potential.

2.4 Summary

(1) The hydrogen-containing passive film on X70 exhibits a higher open circuit decay rate and lower static potential after decay. In borate buffer solutions containing chloride ions, hydrogen causes deterioration in the stability of the passive film on X70 steel and results in a decrease of the U_p.

(2) Two reduction plateaus, at around -0.54 V and -0.84 V, respectively, appear in the charged and uncharged passive films on X70 steel. Hydrogen results in a decrease in thickness of the outer Fe_2O_3 layer in the passive film. The thinning effect was enhanced by increasing hydrogen charging current density and stabilized at an i_{charge} of about 10 A/m^2. Passive films formed at the high potential of 0.6 V have a thicker Fe_2O_3 layer than that formed at 0.2 V. The thinning effect by hydrogen is less obvious on the film formed at 0.6 V than that formed at 0.2 V.

(3) Hydrogen has a noticeable effect on the impedance response of the passive film on X70 steel. Within the film formation potential range, hydrogen significantly decreases the charge transfer resistance. The charge transfer resistance of hydrogen-

containing passive films formed under various potentials exhibits a constant low value. At a passive potential, increasing hydrogen content decreases the ion transportation resistance and increases the capacitance of passive films.

References

1. Y. F. Cheng and J. L. Luo, *Applied Surface Science*, **167**, 113 (2000).
2. Y. F. Cheng and J. L. Luo, *Bulletin of Electrochemistry*, **17**, 97 (2001).
3. E. Sikora and D. D. Macdonald, *Electrochim. Acta*, **48**, 69 (2002).
4. H. Yashiro, B. Pound, N. Kumagai and K. Tanno, *Corros. Sci.*, **40**, 781 (1998).
5. J. L. Luo and Q. Yang, *J. Electrochem. Soc.*, **148**, B29 (2001).
6. Q. Yang and J. L. Luo, *Electrochimi. Acta*, **45**, 3927 (2000).
7. S. I. Pyun, C. L. and R. A. Oriani, *Corros. Sci.*, **33**, 437 (1992).
8. J. G. Yu, J. L Luo and P. R. Norton, *Applied Surface Science*, **177**, 129 (2001).
9. M. Nagayama and M. Cohen, *J. Electroanal. Chem.*, **109**, 781 (1962).
10. M. Nagayama and M. Cohen, *J. Electrochem. Soc.*, **110**, 670 (1963).
11. N. Sato, K. Kudo and T. Noda, *Corros. Sci.*, **10**, 785 (1970).
12. N. Sato, K. Kudo and T. Noda, *Electrochim. Acta*, **16**, 1909 (1971).
13. K. Ogura and K. Sato, *Elelctrochimi. Acta*, **25**, 857 (1980).
14. J. G. Yu, J. L. Luo and P. R. Norton, *Elelctrochimi. Acta*, **47**, 1527 (2002).
15. J. G. Yu, C. S. Zhang, J. L. Luo and P. R. Norton, *J. Electroanal. Chem.*, **150**, B68 (2003).
16. M. A. V. Devanathan and Z. Stachurski, *Roy. Soc. Proc. Ser. A*, **270**, 90 (1962).
17. H. H. Strehblow and B. Titze, *Corros. Sci.*, **17**, 461 (1977).
18. A. Saraby-Reintjes, *Elelctrochimi. Acta*, **30**, 403 (1985).
19. H. E. H. Bird, B. R. Pearson and P. A. Brook, *Corros. Sci.*, **28**, 81 (1988).
20. M. Ergun and A. Y. Turan, *Corros. Sci.*, **32**, 1137 (1991).
21. A. D. Davydov, *Elelctrochimi. Acta*, **46**, 3777 (2001).
22. H. Böhni and H. H. Uhlig, *J. Electrochem. Soc.*, **116**, 906 (1969).

23. L. Li, J. L. Luo, J. G. Yua, Y. M. Zeng, B. T. Lu and S. H. Chen, *Eletrochemistry Communications*, **5**, 396 (2003).
24. L. J. Qiao and J. L. Luo, *Corrosion*, **54**, 281 (1998).
25. J. G. Yu, J. L. Luo and P. R. Norton, *Elelctrochimi. Acta*, **47**, 4019 (2002).
26. M. G. Alvarez and J. R. Galvele, *Corros. Sci.*, **24**, 27 (1984).
27. J. R. Galvele, R. M. Torresi and R. M. Carranza, *Corros. Sci.*, **31**, 563 (1990).
28. Q. Yang, L. J. Qiao, S. Chiovelli and J. L. Luo, *Corrosion*, **54**, 628 (1998).
29. Y. F. Cheng and J. L. Luo, *Electrochim. Acta*, **44**, 2947 (1999).
30. K. E. Heusler and L. Fischer, *Werkst. Korros.*, **27**, 550 (1976).
31. K. Ogura and M. Kaneko, *Corros. Sci.*, **23**, 1229 (1983).
32. N. Sato, *Elelctrochimi. Acta*, **16**, 1683 (1971).
33. A. Rauscher, H. Konno and M. Nagayama, *Electrochim. Acta*, **22**, 823 (1977).
34. S. Haruyama and T. Tsuru, *Corros. Sci.*, **13**, 275 (1973).
35. P. Schmuki, S. Virtanen, A. J. Davenport and C. M. Vitus, *J. Electrochem. Soc.*, **143**, 574 (1996).
36. Z. S. Smialowska and W. Kozlowski, *J. Electrochem. Soc.*, **131**, 499 (1984).
37. M. G. S. Ferreira and J. L. Dawson, *J. Electrochem. Soc.*, **132**, 760 (1985).
38. T. Ohtsuka and A. Ohta, *Materials Science and Engineering A*, **198**, 169 (1995).
39. K. Aramaki and T. Shimura, *Corros. Sci.*, in Press (2003).
40. H. Konno and M. Nagayama, in *Vol. The Electrochemical Society Monograph Series*, R. P. Frankenthal and J. Kruger, Editors, p. 585, Princeton, NJ (1978).
41. C. T. Chen, B. D. Cahan and E. Yeager, Case Western Reserve University, Technical Report no. 48, (1979).
42. Y. M. Zeng, J. L. Luo and P. R. Norton, *J. Electroanal. Chem.*, in Press (2003).

Chapter 3 Effects of Hydrogen on the Electronic Properties of Passive Films

3.1 Introduction

It has already been well recognized that the electronic properties of passive films on metals play an important role in the film formation, breakdown and pitting initiation processes. Furthermore, as passive films on many metals exhibit semiconductive behavior, the semiconductive properties of passive films have to be considered while studying the processes occurring on and within a passive film. Therefore, the electronic properties of passive films inevitably make a major subject of studies attempting to address the role of hydrogen in corrosion. However, divergence exists in analyzing the effects of hydrogen on the electronic properties of passive films[1,2] with no conclusive mechanisms being established.

It has been reported that most passive films on stainless steels behave like n-type semiconductor, which is more resistant to general corrosion[3, 4] than a p-type film, as indicated by Sato[5]. Pyun *et al.*[6, 7] found that hydrogen increases the anodic current of the film on iron, which further shows that the effect of hydrogen on the passive current is reversible. In other words, after the cessation of hydrogen charging, the passive current will return to the original value before hydrogen charging. Based on this fact, the main question that poses concern to researchers is related to whether the effect of hydrogen on the electronic and optical properties of the passive film is also reversible or not. To date, no reports have been published to address this problem.

Photoelectrochemical measurement has been presented by many researchers[8-14] as a very useful *in situ* technique for studying the electronic and optical properties of passive films on a variety of metallic materials. This is based on the recognition of the fact that even thin passive films consist of their own phase with specific properties. In contrast to intensive interests on the passive films on iron and stainless steels, few investigations have been done on the passive film on micro-alloyed steels. These materials have been widely used as pipeline materials in industry, in most cases, under cathodic protection. The objective of the present work is to investigate the effects of hydrogen on the

electronic and optical properties of the passive films on X70 micro-alloyed steel by potentiostatic and photo-electrochemical measurements, in an attempt to clarify the reversibility of the hydrogen effects.

3.2 Basics of Photoelectrochemical Spectroscopy Technique

Photoelectrochemical Spectroscopy is one of the most powerful *in situ* techniques for investigating a passive film. Its applications have been widely recognized by both researchers and engineers to study solar cells based on the principle of converting light into electric power. Recent research showed that it is a very interesting *in situ* technique for the study of passivity, giving that the passive film formed on many metals exhibits semiconductive properties.

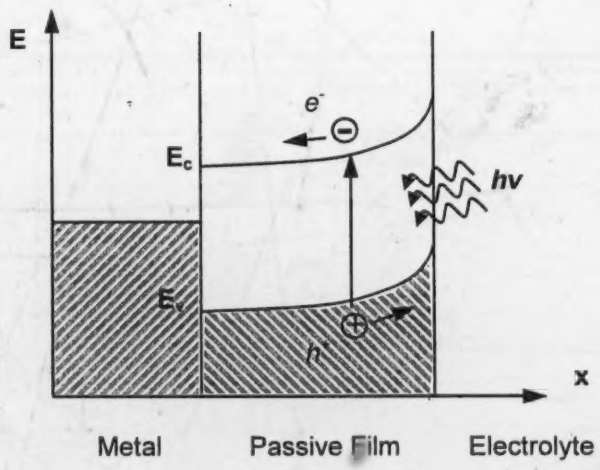

Figure 3-1. Schematic illustration of the photoelectrochemical excitation process.[15]

A schematic representation of the electronic excitation process in an illuminated n-type passive film is given in Figure 3-1 [15], as it is generally accepted that the passive film on iron and steels has n-type semiconducting behavior. When a semiconductor is placed in contact with an electrolyte, a region known as the space-charged layer is produced. For an n-type semiconductor at positive potentials, the band edges curve upward forming a depletion layer. When the passive film is exposed to radiation of sufficient energy,

electrons can be promoted to the conduction band, leaving positively charged holes in the valence band. With the electric field in the depletion region, the separation of the charge occurs by movement of a hole towards the interface while the electron moves in the other direction. As a result of this, anodic photocurrent is introduced in the circuit, which can be detected experimentally in the external circuit as discussed in the next section.

3.3 Experimental Details

3.3.1 Materials and Solutions

The X70 micro-alloyed steel (0.04%C, 1.46%Mn, 0.003%S, 0.008%P, 0.24%Si, 0.22%Cu, 0.1%Ni, 0.05%Cr, 0.073%Nb, 0.2%Mo, 0.028%Al, 0.024%Ti, in wt%, and the balance Fe), supplied by IPSCO, was used for in this work. The specimens were cut into $0.02 \times 0.02 \times 0.001$ m^3 coupons. Both test surfaces were mechanically ground down to 600-grit emery paper and degreased with acetone before carrying out the experiments. The specimen areas exposed to the charging and test solutions are about 1.2×10^{-4} m^2. The test electrolyte solution was 0.3 M H_3BO_3 + 0.075 M $Na_2B_4O_7 \cdot 10H_2O$ at pH 8.4, and 0.1M NaOH + 150 ppm As_2O_3 was used as the charging electrolyte. Addition of As_2O_3 in the charging solution is basically to inhibit the hydrogen recombination reaction, and thereby promotes the entry of hydrogen atoms into metals[16]. All solutions were prepared with analytical grade reagents and deionized water.

3.3.2 Electrochemical Cell Setup

Measurements were made in a Devanathan type cell (see Chapter 2 Figure 2-2) at room temperature, with one compartment for hydrogen charging and the other for electrochemical measurements. The hydrogen-charging was carried out by the constant cathodic current method in the hydrogen-charging cell, while the electrochemical measurements were conducted in the other cell. In the system, a SCE was used as the reference electrode and two platinum nets (0.05×0.02 m) were used as counter electrodes, one in each compartment. Potentials used in this paper are all given with respect to the SCE scale. All the electrochemical and photoelectrochemical measurements were performed at least twice to verify the reproducibility of the results.

Figure 3-2 shows the experimental setup for potentiostatic and photocurrent measurements. Potentiostatic measurements were recorded using a Gamry CMS system. In the photo-electrochemical experiments, a 75 W Xenon arc lamp was used as the light source. Light in the wavelength (λ) range from 2×10^{-7} to 9×10^{-7} m was cast on the specimens from a digital monochromator scanning at a rate of 1.21×10^{-9} m/s, in order to establish the electronic excitation process in the illuminated passive film. Photocurrent spectra were obtained by plotting the photocurrent measured against the photon energy $h\nu$ of the incident monochromatic light ($h\nu = 1240/\lambda$, where the $h\nu$ is in eV and λ is in 10^{-9} m). Improved signal-to-noise ratio was achieved by using a lock-in amplifier in the photocurrents measurements. The reference channel frequency of the lock-in amplifier was 30 Hz, which is also the frequency of the light chopper. All photocurrent data in this work were normalized to 1 W lamp output. All the electrochemical and photoelectrochemical measurements were performed at least twice to obtain consistent results. The error bar/range of the experimental results shows the range of experimental data produced by different sets of experiment.

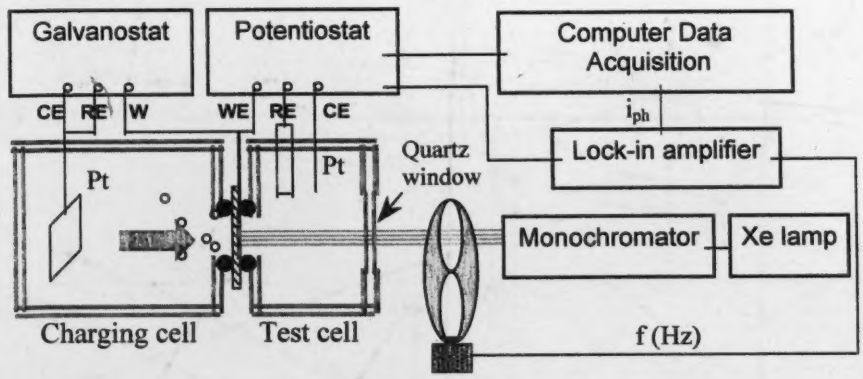

Figure 3-2. Schematic illustration of the photoelectrochemical experimental setup.

3.4 Main Results and Discussion

3.4.1 Photocurrents of Passive Films on X70 Micro-alloyed Steel

As shown in the anodic polarization curve in Figure 2-3, the X70 micro-alloyed steel exhibits passivity behavior in the potential range from the open circuit potential to around

0.9 V in 0.3 M H_3BO_3 + 0.075 M $Na_2B_4O_7 \cdot 10H_2O$ buffer solution. For comparison, a passive film on the uncharged X70 micro-alloyed steel specimen was first formed potentiostatically at 0.6 V for various lengths of times, and the photocurrent spectra of the films were measured. The results are shown in Figure 3-3 and Figure 3-4.

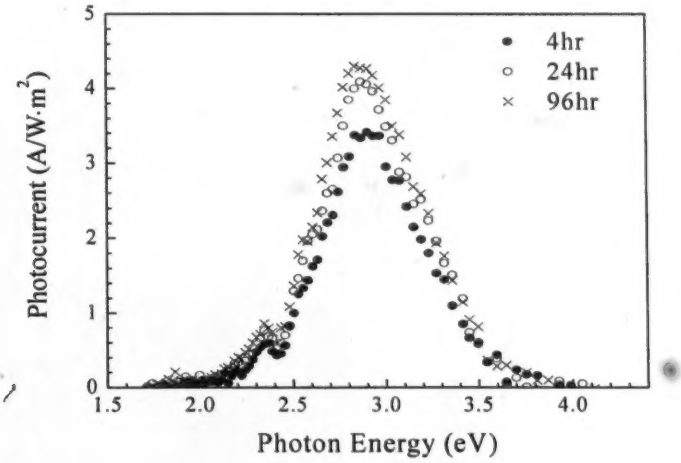

Figure 3-3. Photocurrent spectra of the passive films formed on uncharged specimens at 0.6 V after different passivation time.

As shown in Figure 3-3, by decreasing λ or increasing photon energy, the photocurrent first became measurable at incident photon energy of approximately 2.06 eV. Subsequently, it exhibited a shoulder at 2.37 eV, and subsequently increased to a peak value at 2.90 eV before it started to decrease and finally diminished at high enough photon energy. The anodic photocurrent of the film infers that the passive film formed on X 70 micro-alloyed steel is an n-type semiconductor. For different lengths of passivation times, the position of the shoulder and peak on the photocurrent spectra did not change, remaining at 2.37 eV and 2.90 eV. Figure 3-4 shows the time dependence of the photocurrent peak and shoulder values for the passive film formed at 0.6 V. It is observed that the photocurrent peak and shoulder values of the film gradually increase with time. However, the time effect becomes rather insignificant after 24 hours of passivation. The experiment was repeated and similar results were obtained. The error bars in Figure 3-4

demonstrate the range of experimental data produced on different samples. Experimental results were normalized to the same photocurrent background of an uncharged specimen.

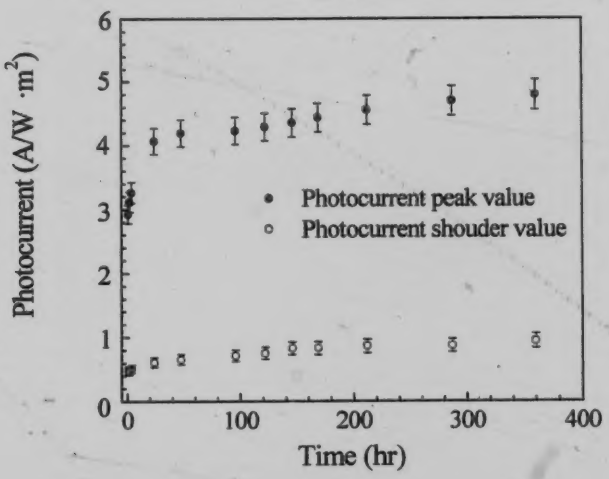

Figure 3-4. The time dependence of the photocurrent peak and shoulder values for the passive films formed on uncharged specimen at 0.6V.

In order to obtain the band gap energy of the passive films on X70 micro-alloyed steel, the following relationship was employed:

$$i_{ph}h\nu = B(h\nu - E_g)^2 \qquad [3.1]$$

where E_g is the band gap energy of the semiconductor, $h\nu$ is the incident photon energy, and B is a constant. The photocurrent spectra in Figure 3-3 were re-plotted in terms of $(i_{ph}\cdot h\nu)^{0.5}$ vs. $h\nu$, as shown in Figure 3-5. Data in the range of 2.45 – 2.85 eV were linearly fitted. For the film formed at 0.6 V for 4 hours, the Equation $(i_{ph}h\nu)^{0.5} = -0.097+0.045h\nu$ was produced, defining the linearly fitted line whose intersection with the abscissa gives an E_g of the film as 2.153 eV. For the film formed at 0.6 V for 24 hours, the linearly fitted equation was $(i_{ph}h\nu)^{0.5} = -0.11+0.049h\nu$,

which yields an E_g of 2.146 eV for the passive film. An E_g of 2.146 eV was obtained for the film formed at 0.6 V for 96 hours from the linearly fitted equation of $(i_{ph}h\nu)^{0.5} = -0.11+0.052h\nu$.

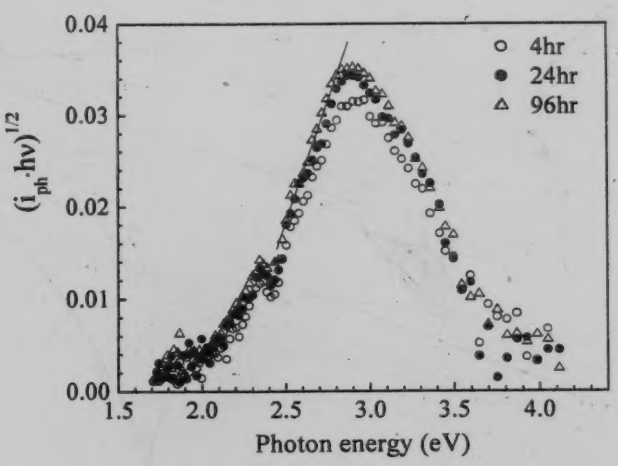

Figure 3-5. Evaluation of E_g of the passive films on X70 steel formed at 0.6 V after different passivation time.

Previous work showed[17-19] that the passive film on iron is composed primarily of Fe_3O_4 and γ-Fe_2O_3. Accordingly, the generation of the photocurrents of the passive film on iron involves two processes[18] with the first process involving d-d transition (corresponding to the photocurrent shoulder on the photoelectrochemical spectra), i.e., the electronic excitation from Fe^{3+} band to Fe^{2+} band. The second process is termed p-d transition (corresponding to the photocurrent peak on the photoelectrochemical spectra), i.e., the excitation from the valence (O_{2p}) to the conduction band (Fe_{3d}). At film formation potential of 0.6 V, the passive films on X70 micro-alloyed steel formed in alkaline solution are mainly composed of ferric and ferrous oxides. Our experimental results show that the shoulder and peak on photocurrent spectra for the passive films on X70 micro-alloyed steel appear at around the same positions of photon energies as for the films on iron in buffer solution. Therefore, it is reasonable to assume that the passive

films on X70 micro-alloyed steel should also be mainly composed of Fe_3O_4 and γ-Fe_2O_3 with an electronic band structure similar to that of the passive film on iron. The results also show that a longer film formation time gives rise to a slightly lower E_g value of the passive film. This may be related to a relatively high concentration of Fe^{3+} and O^{2-} ions in the passive film after a long film formation time. It has been established that factors used in determining the E_g of the passive film include the film composition, defect and donor or acceptor concentrations etc. A long film formation time is generally believed to be beneficial to the "integrity" or "quality" of a film. The higher concentration of Fe^{3+} and O^{2-} in the film, arising from a longer passivating time, would favor the electronic excitation processes from valence band (Fe^{3+} and O_{2p}) to conduction band (Fe^{2+}), i.e., the E_g may decrease with increasing Fe^{3+} and O^{2-} concentrations in the passive film as it grows "better".

The time effect on the photocurrent of the passive film can be explained as follows. With the elapse of film formation time, especially in the initial stage of the film formation, the passive film gradually becomes thicker, with a homogenous and less defective structure. In a passive film, the photo-generated holes or electrons have low mobility. As the film becomes more uniform with time, the movement of charge carriers is less impeded by defects and the mobility of holes or electrons increases. Moreover, as highlighted above, an increase in the film formation time in the initial stage of passivation would cause a relatively rapid increase in Fe^{3+} and O^{2-} concentrations in the film, which benefits the absorption of incident photon. After a long time passivation, the passive film reaches a steady state in the buffer solution and the time effect on the growth of the film and its photocurrent would be much less pronounced.

3.4.2 Effects of Hydrogen on Passive Currents and Photocurrents of the Passive Films

To investigate the effects of hydrogen on anodic passive current and photocurrent of the passive films on X70 micro-alloyed steel, the test side of the specimen was first pre-passivated for 26.5 hours, and then hydrogen-charging was conducted on the other side of the specimen at 2 A/m^2 for 1.5 hours before it was stopped, while the passivation of the test side was continued. During the whole procedure, the test side of the specimen was

kept under potentiostatic control at a passivating potential of 0.6 V in the borate buffer solution, with *in situ* passive currents and photoelectrochemical measurements being carried out concurrently on this side.

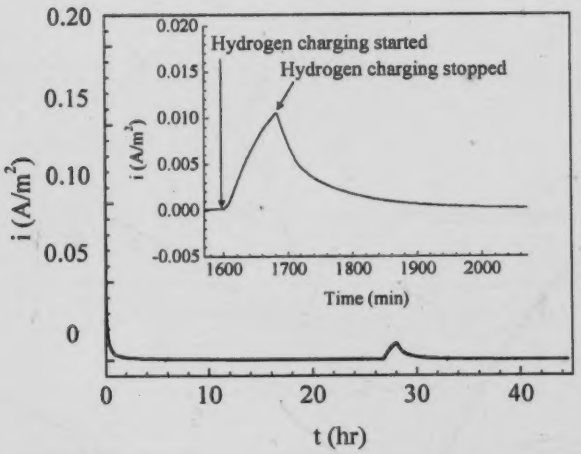

Figure 3-6. Changes of the passive current density with time for the passive film formed at 0.6 V. After 26.5 hours passivation, hydrogen charging was started and then stopped 1.5 hours later.

Figure 3-6 shows the variation of anodic current densities with time, caused by the hydrogen-charging. Three stages are involved in the anodic passive current density vs. time (i-t) curve of the working electrode. In the first stage, after 26.5 hours of pre-passivation at 0.6 V, the current density gradually dropped from 0.20 A/m^2 to 4.0×10^{-4} A/m^2, as the passive film formed on the test side of specimen grew thicker and more compact. The second stage appeared when hydrogen was charged into the specimen after the steady-state passive current was attained. However, the anodic current density did not ascend immediately until the hydrogen charging had started for 8~10 minutes. This time lag between the hydrogen-charging and the anodic current response can be attributed to the diffusion process during which hydrogen generated on the other side of the specimen proceeds to permeate the electrode. After that, the anodic current density went up quite rapidly, and finally reached a value of 1.25×10^{-2} A/m^2 in 1.5 hours. In the third stage, the current density started to decrease due to the cessation of hydrogen charging, with a

three-minute time lag occurring again, which may also be attributed to the diffusion process in the specimen. It took around 8 hours for the anodic current to recover to the steady value, which is close to the one before the commencement of hydrogen charging.

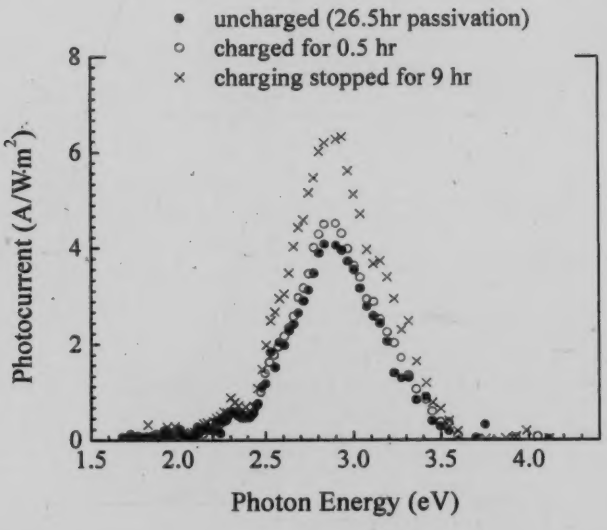

Figure 3-7. Photocurrent spectra of passive films formed at 0.6 V. After 26.5 hours passivation, hydrogen charging was started and then stopped 1.5 hours later.

Figure 3-7 shows the concurrent change of photocurrent with time caused by the hydrogen charging. The anodic photocurrent of the film obtained after hydrogen charging started infers that the hydrogen-containing passive film on X70 micro-alloyed steel is still an n-type semiconductor. With the hydrogen charging, a shoulder and a peak were still present on the photocurrent spectra at about 2.37 eV and 2.90 eV respectively, which implies that hydrogen does not change the nature of photon-induced electronic excitation (the d-d and p-d transitions) processes in the passive film. However, the magnitude of the photocurrent generated is increased by the hydrogen charging and the effect becomes fairly noticeable upon incident photon energies within 2.6~3.3 eV, with a maximum increase occurring at 2.90 eV. The surprising observation was that, after the hydrogen charging was stopped, the photocurrent shoulder and peak of the film continued to rise,

while the anodic passive current density decreased and resumed to the steady value of uncharged state. Figure 3-8 shows the variations of the photocurrent peak and shoulder values with time for the passive film formed on hydrogen charged specimen. Experiments were repeated after which the results were also normalized to give the error range shown in Figure 3-8. The photocurrent peak and shoulder values of the film continually increased with time and were enhanced by hydrogen. After the cessation of hydrogen charging and total removal of the charging circuit, the photocurrent of the film continually went up and then stabilized at a high level with the subsequent increase of passivating time.

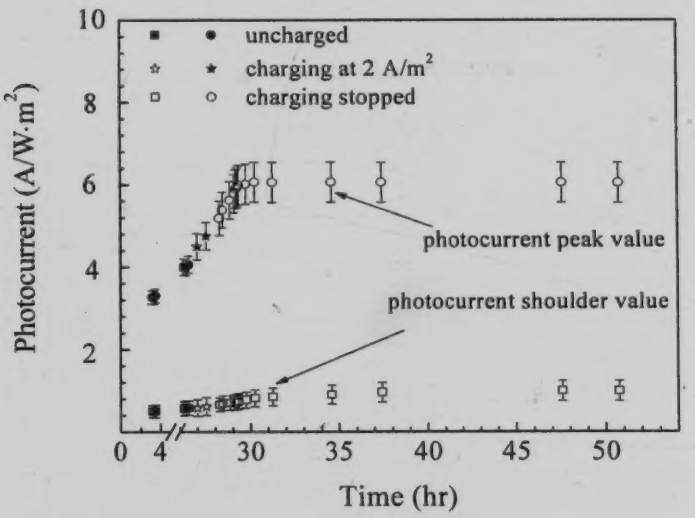

Figure 3-8. Variations of the photocurrent peak and shoulder values with time. After 26.5 hours passivation, hydrogen charging was started and then stopped 1.5 hours later.

Figure 3-9 demonstrates the $(i_{ph}\cdot h\nu)^{0.5}$ vs. $h\nu$ plots converted from the photocurrent spectra in Figure 3-7 according to Equation [3.1]. Linear fitting of the data in the range of 2.45 ~ 2.85 eV gives a linear equation of $(i_{ph}h\nu)^{0.5} = -0.11+0.050h\nu$ and an E_g of 2.15 eV for the passive film formed at 0.6 V for 26.5 hours. In the same manner, equation of $(i_{ph}h\nu)^{0.5} = -0.11+0.053h\nu$ and an E_g of 2.16 eV were obtained for the film that has

undergone hydrogen charging at 2 A/m^2 for 0.5 hour. For the passive film that was continually passivated for another 9 hours after the hydrogen charging was stopped, a linearly fitted equation of $(i_{ph}h\nu)^{0.5} = -0.14+0.064h\nu$ was obtained and the E_g of the film was calculated to be 2.17 eV.

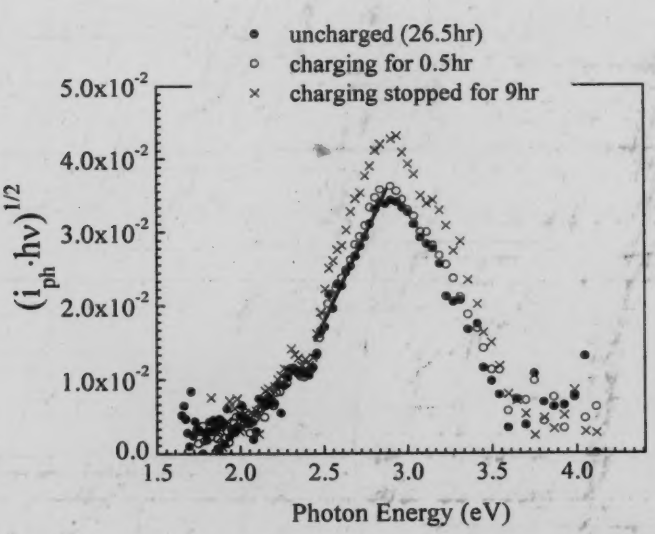

Figure 3-9. Evaluation of the E_g of the passive films formed at 0.6 V. After 26.5 hours passivation, hydrogen charging was started and then stopped 1.5 hours later.

To confirm the irreversibility of the hydrogen effect on the photocurrent of the passive film, another set of experiment was performed. Here, the specimen was pre-passivated at 0.6 V for 73 hours and hydrogen was charged into the other side of the specimen at 2 A/m^2 for 3 hours after which hydrogen-charging was stopped. I*n situ* passive currents under potentiostatic condition and photoelectrochemical measurements were conducted again concurrently on the test side of the specimen. Similar phenomena were observed with the results shown in Figure 3-10 and Figure 3-11. By extending hydrogen charging time in this set of experiment, the anodic current density of the specimen took a longer time period (about 12 hours) to return to the steady value before

the hydrogen charging, whereas the photocurrent peak value of the film first increased with time and then stayed at a high level at long last.

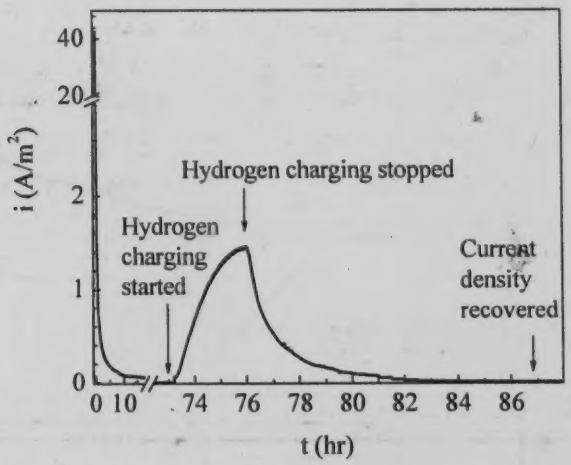

Figure 3-10. Variation of passive current density with time for the passive film formed at 0.6 V. After 73 hours passivation, hydrogen charging was started and then stopped 3 hours later.

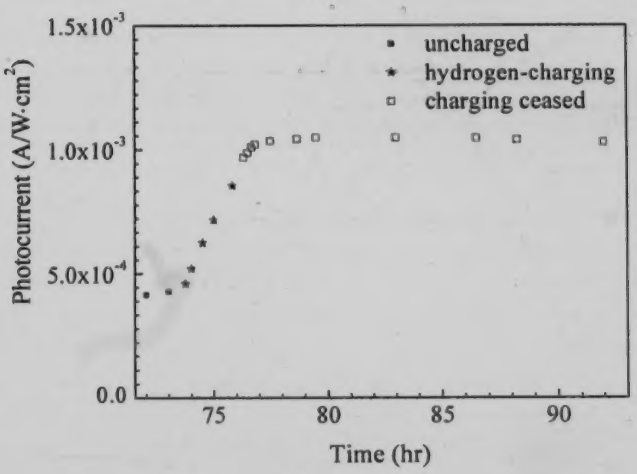

Figure 3-11. Variation of the photocurrent peak value for passive films with time. After 73 hours passivation, the hydrogen charging was started and then stopped 3 hours later.

A number of studies have been done to explore the growth of passive films on metals and alloys[20-26]. Although different approaches were used, certain conclusions were reached consistently: at a film formation potential, cations are injected into the film from the metal and move to the film/solution interface while oxygen vacancies are created at the metal/film interface, and then oxygen ions are injected from the solution into the film and move to the metal/film interface. The anodic passive current densities of passive films on metals and alloys are mainly related to the ionic transport and dissolution processes in the films. The enhancing effect of hydrogen on the anodic passive currents of the passive film may be attributed to two apparent processes: (1) the hydrogen atoms charged into the metal would be oxidized at the metal surface as they migrate out of the film by diffusion at a film formation potential; (2) hydrogen would accelerate the diffusion and dissolution of cations (Fe^{2+} and Fe^{3+}) and anions (O^{2-}) by decreasing the stability of the passive film. Previous research has shown that hydrogen can change the properties of the passive film on iron and stainless steel, e.g., increase the concentration of Fe^{2+} in film and decrease the thickness of the film[14]. All these factors would result in a high passive current density for the film on X70 micro-alloyed steel. After the cessation of hydrogen charging, the resumption of anodic current density of the passive film implies that the influence of hydrogen on the transport and dissolution process of cations and anions is recoverable and could be eliminated by the relative long time passivation.

The photocurrent of the film on X70 micro-alloyed steel is enhanced by hydrogen and might be ascribed to the following factors:

(1) Hydrogen atoms may be oxidized by photo-generated holes at the film/solution interface[27] as illustrated in the following reaction and consequently increase the photocurrent of the passive film:

$$H + h^{+} \rightarrow H^{+} \qquad [3.2]$$

(2) Several researchers have reported that a low mobility of photo-generated electrons and holes is observed in the passive film on several metallic materials. Hydrogen reduces the passive film thickness, therefore increases the electric field strength in the passive film under the same film formation potential. And a stronger electric field in

the film would result in a higher mobility of the holes or electrons. The increased mobility of photo-generated holes and electrons caused by hydrogen could lessen the probability of recombination of electrons and holes in the film, and therefore increases the photocurrent.

(3) As discussed earlier on, hydrogen could also result in an increase in the quantity of Fe^{2+} ions in the film, which might also be oxidized by the holes generated from the p-d transition, i.e., thereby making additional contribution to the photocurrent of the passive film.

$$Fe^{2+} + h^{+} \rightarrow Fe^{3+} \qquad [3.3]$$

However, the processes shown above could not be used to explain clearly why the photocurrent of the film on X70 micro-alloyed steel continually increases and ultimately keeps at a high level after the hydrogen charging is stopped while the concurrent anodic current resumes. Surprisingly, at the film formation potential, the extension of the time of subsequent passivation has no significant influence on the photocurrent of the film. Researchers[28, 29] have shown that passive films containing higher concentrations of protons (H^{+}) exhibit an amorphous structure. In amorphous film formation, the photo response of a passive film is strongly related to the localized states and vacancy distribution in the film. The irregularity observed in our experiments infers that the effects of hydrogen on the optical and electronic properties of a passive film are far more complex than what is currently thought. The existing mechanisms for hydrogen effects on passive films could not provide a satisfactory interpretation of such phenomena. The exact mechanism, responsible for such hydrogen effects, will be investigated in future work.

3.5 Summary

1) Passive films formed on X70 micro-alloyed steel are n-type semiconductors. The photocurrent of the passive film increases with the extension of film formation time, especially in the beginning 24 hours. The E_g of the passive film decreases slightly with the film formation time.

2) Hydrogen increases the anodic current density of the passive film, but this effect is reversible after hydrogen charging is stopped. Longer hydrogen charging time requires a longer recovery time for the anodic current density of the film.
3) Hydrogen also increases the photocurrent of passive films on X70 micro-alloyed steel, yet exhibits no effects on the value of the optical E_g and therefore, the nature of photo-induced generation of charge carriers in the passive film. Surprisingly, an increase in photocurrent of the passive film due to hydrogen charging is irreversible. Subsequent extension of the passivating time has no significant effect on the photocurrent of the film. This phenomenon is first discovered and infers a far more complex mechanism for the hydrogen effects on the optical and electronic properties of the passive film than what is currently thought.

References

1. M. Z. Yang, J. L. Luo, Q. Yang, L.J. Qiao, Z. Qin and P. R. Norton, *J. Electrochem. Soc.*, **146**, 2107 (1999).
2. G. Bianchi and A. Cerquetti, *Corros. Sci.*, **10**, 19 (1970).
3. A. D. Paola, D. Shukla and U. Stimming, *Electrochim. Acta*, **36**, 345 (1991).
4. N. Sato, in *Electrochemistry at metal and semiconductor electrodes*, Elsevier, Amsterdam (1998).
5. N. Sato, *Corros. Sci.*, **31**, 715 (1990).
6. S. I. Pyun, C. Lim and R. A. Oriani, *Corros. Sci.*, **33**, 437 (1992).
7. R. H. Song, S. Pyun and R. A. Oriani, *J. Electrodhem. Soc.*, **137**, 1703 (1990).
8. E. Becquerel, *C.r. hebd. Séanc. Acad. Sci.*, Paris **9**, 561 (1839).
9. K. Leitner, J. W. Schultze and U. Stimming, *J. Electrochem. Soc.*, **133**, 1561 (1986).
10. P. C. Searson, R. M. Latanision and U. Stimming, *J. Electrochem. Soc.*, **135**, 1358 (1988).
11. A. D. Paola, F. D. Quarto and C. Sunseri, *Corros. Sci.*, **26**, 935 (1986).
12. U. Stimming, *Electrochim. Acta*, **31**, 415 (1986).

13. A. M. P. Simoes, M. Da Cunha Belo, M. G. S. Ferreira and B. Rondot, *Portugaliæ Electrochim. Acta*, **5**, 59 (1987).

14. J. G. Yu, J. L. Luo, C. S. Zhang and P. R. Norton, *J. Electrochem. Soc.*, **150**, B405 (2003).

15. M. Grätzel, *Nature*, **414**, 338 (2001).

16. *Hydrogen Degradation of Ferrous Alloys*, R. A. Oriani, J. P. Hirth and M. Smialowski, Editors, Noyes Publications, Mill Road, Park Ridge, New Jersey 07656 (1985).

17. L. G. Haart and D. Blasse, *J. Electroanal. Chem.*, **132**, 2933 (1985).

18. C. T. Chen and B. D. Cahan, *J. Electrochem. Soc.*, **129**, 17 (1982).

19. J. S. Kim, E. A. Cho and H. S. Kwon, *Corros. Sci.*, **43**, 1403 (2001).

20. E. J. W. Vervey, *Physica*, **35**, 1059 (1935).

21. N. Cabrera and N. F. Mott, *Reports on Progress in Physics*, **12**, 163 (1948).

22. N. Sato and M. Cohen, *J. Electrochem. Soc.*, **111**, 512 (1964).

23. R. Kirchheim, *Electrochim. Acta*, **32**, 1619 (1987).

24. E. Sikora, D. D. Macdonald and J. Sikora, in *Proc. 7th Int. Symp. Oxide Films, Metals and Alloys*, PEC, p. 94 (1994).

25. L. Zhang, D. D. Macdonald, E. Sikora and J. Sikora, *J. Electrochem. Soc.*, **145**, 898 (1998).

26. D. D. Macdonald, *J. Electrochem. Soc.*, **139**, 3434 (1992).

27. G. Razzini, S. Maffi and G. Mussati, *Corros. Sci.*, **39**, 613 (1997).

28. B. D. Cahan and C. T. Chen, *J. Electrochem. Soc.*, **129**, 921 (1982).

29. M. Cohen, in *Passivity of Metals*, R. P. Frankenthal and J. Kruger, Editors, Princeton, N J (1978).

Chapter 4 Effects of Elastic Stress and Hydrogen on Passivity of Carbon Steel

4.1 Introduction

Results from our experiments indicate that hydrogen can cause deleterious effects on the corrosion behavior of X70 pipeline steel under stress-free conditions. However, carbon steels and micro-alloyed steels are often employed under stressful conditions in industry in addition to the hydrogen exposure (*e.g.* the pressure vessel). For this reason, it is very important to study the effects of hydrogen and stress on passive films.

Numerous studies have shown that mechanical stress above the σ_y, either in the form of directly applied stresses or in the form of residual stresses, induces major changes in the corrosion behavior of metals and alloys[1-8]. Intensive investigation has been dedicated to the notorious phenomenon of stress corrosion cracking (SCC) on stainless steels [9-21]. Iwanaga and Oki studied the effects of applied stress on the anodic polarization behavior and pitting corrosion of stainless steels[22], and found that the pitting potential decreases with an increase in applied stress while the passivity-maintaining current density increases with the stress. It has also been shown[23-27] that applied tensile stress can increase the pitting susceptibility while compression, on the other hand, has a strong capability to reduce the pitting susceptibility. The results indicate that the passive film composition depends on the nature (compression or tension) and the level of its stresses.

However, up till now, most of these studies have been carried out at a stress level around or higher than the elastic limit. Very little experimental research has attempted to analyze the passive film formed under an elastic stress field and the consequent corrosion susceptibility. Recently, it was reported[28] that an elastic stress might reduce the time for pitting in the case of a type 316 L stainless steel immersed in 0.5 M NaCl, pH 6.5, heated at 50°C. It appears that even very low levels of stress may affect the corrosion behavior of materials and lead to a decrease in the protectiveness of passive films against localized corrosion in certain electromechanical environments. Yang *et al.*[29, 30] found that with an increase in applied tensile stress, the critical chloride concentration for the breakdown of a passive film on Type 304 stainless steel decreases. However, the effect of elastic stress

on the corrosion behavior of structural steels is still not fully understood. At present, existing results can only demonstrate that elastic tensile stress increases the susceptibility of stainless steels to pitting, but have not ascertained how the stress affects the anodic dissolution of metallic material, in terms of the open circuit potential and polarization resistance. Moreover, as mentioned above, under the conditions of hydrogen exposure, it is often assumed that a synergistic effect of hydrogen and elastic stress may affect the properties of passive film and consequently enhance localized corrosion. Therefore, it is necessary to investigate the effect of hydrogen on the breakdown of passive films under elastic stresses.

Type A516-70 steel is typically utilized in medium tensile strength vessels under the condition of moderate and lower temperature (generally in a range from 38 °C to 370 °C). The objective of the work described this chapter was to identify the influence of hydrogen and elastic tensile stresses on the anodic dissolution and properties of passive films on A516-70 steel by various electrochemical measurements.

4.2 Experimental Details

4.2.1 Materials and Solutions

Type A516-70 steel specimens with a thickness of 0.0018 m were used in this study, whose geometry is shown in Figure 4-1. The chemical composition of type A516-70 steel is listed in Table 4-1. All of the specimens were wet ground down to a 600-grit finish, rinsed with distilled water, degreased with acetone and dried before the tests.

0.1 M NaOH solution was used to charge hydrogen at the desired cathodic current densities. During the galvanostatic hydrogen charging, the specimens acted as a cathode, and the anode, a platinum wire, was placed parallel to the surface of the specimen to guarantee a uniform distribution of current during the charging.

The electrolyte used in the electrochemical measurements was 0.5 M $NaHCO_3$ + 0.01M NaCl. A traditional three-electrode corrosion cell was employed, wherein a SCE acted as the reference electrode. All the solutions were prepared with analytical grade reagents and distilled water. All experiments were carried out open to the ambient air at room temperature, and were performed at least twice, in order to verify the

reproducibility of the results. The error bar/range of the experimental results shows the range of experimental data produced by different sets of experiment.

Table 4-1. A516-70/A516-70M-01 standard specification for pressure vessel plates, carbon steel, for moderate- and lower-temperature service (Grade 70).

Chemical Composition (wt%, Maximum)					Minimum Yield strength (MPa)	Tensile Strength (MPa)	Minimum Elongation (%)
C	Mn	P	S	Si			
0.31	1.0	0.035	0.04	0.15~0.30	262	485~620	25

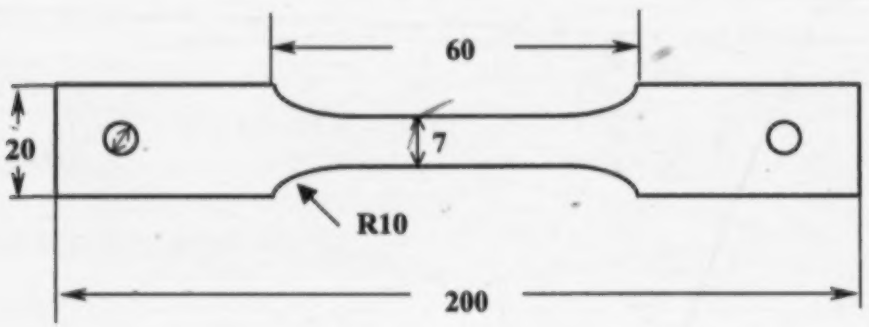

Figure 4-1. Shape and dimension (in 10^{-3} m) of specimens.

4.2.2 Tensile Tests

The mechanical properties of the specimen were first determined by tensile test using an INSTRON8500 machine. The testing conditions are as follows:

Sample Rate: 5 points/second Extensometer: Standard

Crosshead Speed: 0.0015 m per 60 seconds

Temperature: 23 °C Humidity: 50 %

Specimen Width: 0.0070 m Specimen Thickness: 0.0018 m

Ext. gauge length: 0.025 m Spec. gauge length: 0.030 m

wherein the polarization was applied in the anodic direction by successive steps of 0.002V/s. The peak-to-peak amplitude of the AC signal was 0.01 V.

To explore the possible synergistic effect of hydrogen and elastic tensile stress on the properties of the passive film, a set of specimens were first cathodically charged at 80 A/m^2 for 1 hour, then rinsed quickly using distilled water, and finally immersed in the test solution to perform those electrochemical measurements mentioned above for uncharged specimens.

4.3 Main Results and Discussions

4.3.1 Effects of Elastic Tensile Stress on Anodic Dissolution

In the tensile test, a stress-strain plot was made and is shown in Figure 4-3. The ultimate tensile stress and yield strength (σ_y) of the specimen were found to be 547.7 ± 5 MPa and 374.3 ± 5 MPa respectively. To investigate the effect of elastic stress on the properties of the passive film, two tensile stress levels lower than σ_y, *i.e.* 170 MPa (~ 45% σ_y) and 240 MPa (~ 64% σ_y), were applied to the specimens in the following experiments.

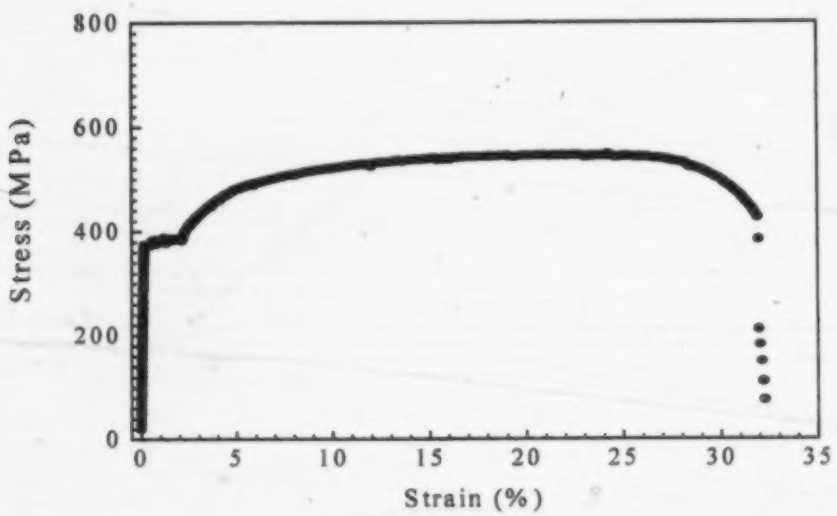

Figure 4-3. The stress-strain curve of the A516 steel specimen.

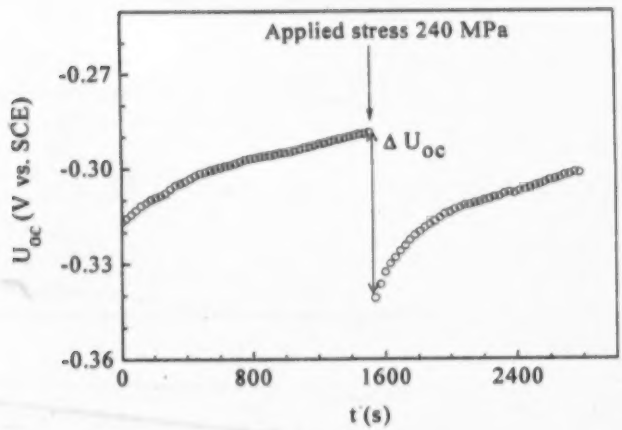

Figure 4-4. Open circuit potentials vs. time for A516 steel specimens in 0.5 M $NaHCO_3$ + 0.01 M NaCl solution.

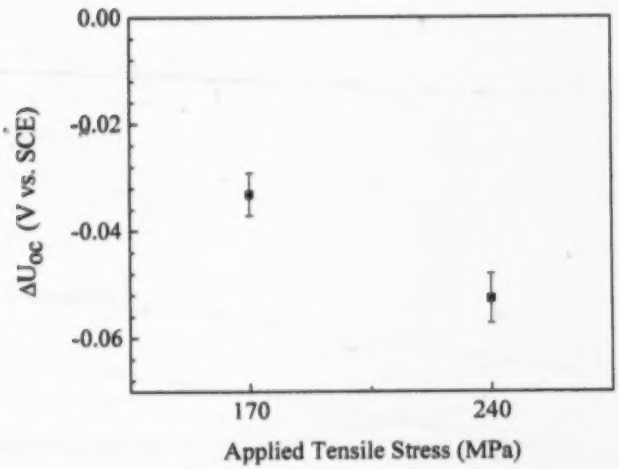

Figure 4-5. The changes of open circuit potentials caused by different applied elastic tensile stresses for A516 steel specimens in 0.5 M $NaHCO_3$ + 0.01 M NaCl solution.

The influence of applied elastic tensile stresses on the open circuit potential (U_{OC}) of the specimens is presented in Figure 4-4 and Figure 4-5. It was observed that in 0.5 M $NaHCO_3$ + 0.01 M NaCl solution, the U_{OC} of A516-70 steel slowly increased with

immersion time (see Figure 4-4), which can be ascribed to the formation of a very thin and porous deposit layer of corrosion products on the surface of the electrode. After 1530 seconds immersion time, the U_{OC} sharply deceased upon the gradually loading of an elastic tensile stress of 240 MPa and thereafter stayed at a lower potential level. Similar phenomena were also found when an elastic tensile stress of 170 MPa was applied to the electrode, however, with a smaller magnitude of U_{OC} decrease. Figure 4-5 shows the different decreases of U_{OC} caused by different applied tensile stresses, where the negative sign indicates the decrease of the U_{OC}.

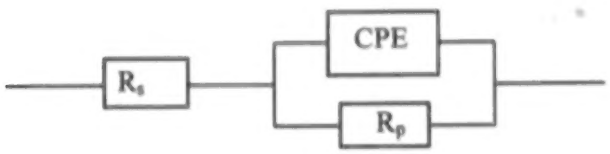

Figure 4-6. Equivalent circuit for A516 carbon steel at open circuit potential in 0.5 M $NaHCO_3$ + 0.01 M NaCl solution.

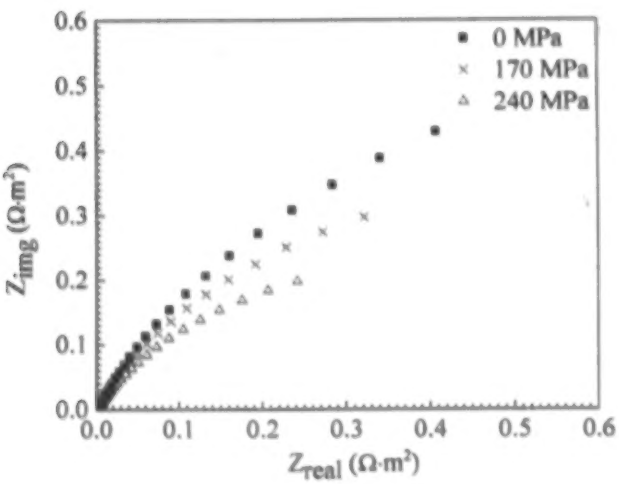

Figure 4-7. Impedance spectra for A516 carbon steel under various applied elastic tensile stresses in 0.5M$NaHCO_3$ +0.01MNaCl solution at open circuit potential.

In the beginning of immersion, the A516 carbon steel samples were under charge transfer control at open circuit potential in 0.5 M $NaHCO_3$ + 0.01 M NaCl solution, and the processes of anodic dissolution occurring at the metal/solution interface could be expressed by a simple equivalent circuit shown in Figure 4-6. Here, R_s is the resistance of the solution, R_p is the polarization resistance, which is inversely proportional to the corrosion current density i_{corr}, and CPE is related to the "double layer capacitor".

Impedance spectra for A516 carbon steel are shown in Figure 4-7. Using the equivalent circuit in Figure 4-6, the values of R_s, CPE, and R_p in Figure 4-7 were calculated and are shown in Table 4-2. It is observed that the R_p of the steel decreases and the capacitance of the double layer C_{dl} increases with the applied elastic tensile stress.

Table 4-2. The fitted values of R_s, R_p and CPE for different applied stresses.

Applied Stress Level (MPa)	R_s $\times 10^3$ ($\Omega \cdot m^2$)	R_p ($\Omega \cdot m^2$)	CPE	
			C_{dl} (F/m^2)	α
0	2.05	1.12	0.36	0.8
170	2.19	0.69	0.43	0.8
240	2.28	0.40	0.53	0.8

In an elastic stress field, a change in the volume per atom would arise from the deformation of a metallic material and the variation can be given by[31]:

$$\frac{r_s}{a_0} = \left(\frac{3V}{4\pi N a_0^3}\right)^{1/3} \qquad [4.1]$$

where N is the number of free electrons in the volume V, r_s is the radius of a sphere whose volume is equal to the volume per conduction electron, and a_0 is the Bohr radius ($\approx$0.0529 nm). Then the strain could be expressed as[27]:

$$\varepsilon = \frac{\Delta r_s}{r_s} \qquad [4.2]$$

Due to the change of localized volume per atom, a redistribution of the free electrons in the metal must occur in order to equilibrate their electrochemical potential[32, 33]. The redistribution of free electrons creates a macro-potential change in the metal, whose sign depends on the direction of applied stress. Since a tensile stress increases the volume per atom whereas a compressive stress decreases it, the electrochemical potential of a metal electrode would become more negative or positive when tensile/compressive force is applied[27, 33]. Our open circuit potential measurements are in agreement with the above theoretical analyses and indicate that the elastic tensile stress can result in a more negative U_{OC}. Furthermore, the impedance results also clearly show that the elastic tensile stress not only affects the U_{OC} of the A516-70 carbon steel, but also decreases the charge transfer resistance of the metal and thus enhances the anodic dissolution process.

4.3.2 Effects of Elastic Tensile Stress on Passivity

In order to determine the passivation potential domain, the potentiodynamic measurements, giving the anodic current density as a function of the applied potential, were made on the uncharged and unstained specimen at a scanning rate of 0.001 V/s.

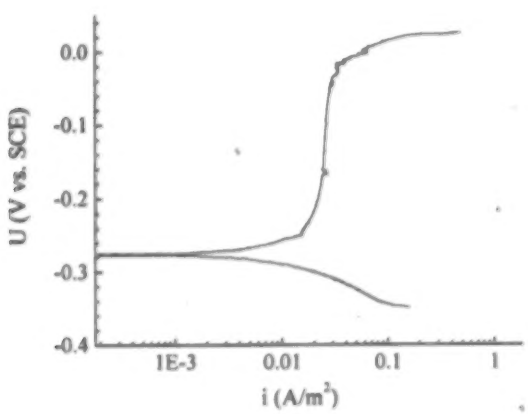

Figure 4-8. The polarization curve of the uncharged stress-free specimen in 0.5 M $NaHCO_3$ + 0.01 M NaCl solution.

The polarization behavior of the uncharged stress-free specimen in 0.5 M $NaHCO_3$ + 0.01 M NaCl solution is given in Figure 4-8. Passivity was exhibited in the potential range from about -0.25 V to nearly -0.02 V. In the subsequent processes, -0.1 V was chosen to be the passive film formation potential.

4.3.2.1 Influences of the Elastic Tensile Stress Applied Before Passivation

The current density vs. time curves for the samples at -0.1 V are shown in Figure 4-9. Comparing the curves obtained for the passive films formed under different stress levels, we can see that the anodic current density and the dissolution rate were slightly higher for elastically strained specimens than those for unstrained specimens. It was also observed that the anodic current density decreased slower for the stress-loaded specimens (170 MPa or 240 MPa) than that for the unstressed specimens at the beginning 1500 seconds of the passivation. These results confirm that the elastic tensile stress could enhance the anodic dissolution and retard the passive film formation. After the film grew thicker and less defective, however, the influence of the elastic tensile stress on passive current densities was not so pronounced as in the beginning of the film formation.

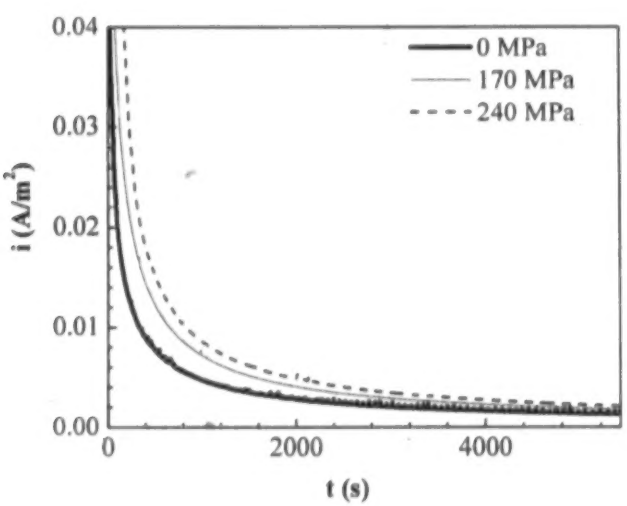

Figure 4-9. Current density vs. time curves for passive films on uncharged specimens passivated at - 0.1 V under different stress levels.

Figure 4-10 presents the Mott-Schottky plots obtained for the passive film formed on the specimens under different tensile stress levels. The results show that within the potential range of -0.2 ~ 0.1 V, the Mott-Schottky plots (*i.e.* the plots of $1/C^2$ vs. U) exhibit linear patterns, which correspond to semi-conducting behavior of the passive film. It is well known that the slope of Mott-Schottky plots is an indication of the conductivity type of the semiconductor. The positive slope of the lines in Figure 4-10 reveals that the passive film on A516 carbon steel is an n-type semiconductive film and the elastic stress does not change the conductivity type of the film.

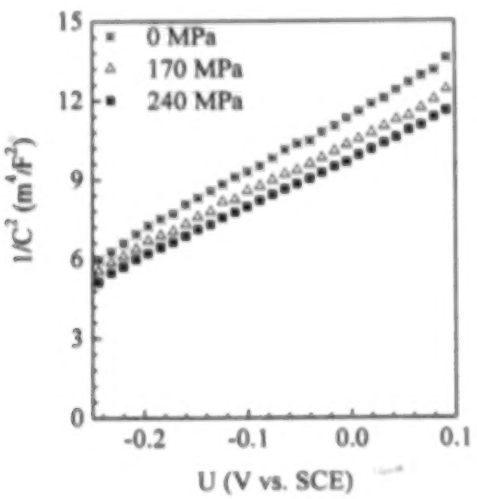

Figure 4-10. Mott-Schottky plots for the passive films formed at -0.1V for 1.5 hour where the specimens is under different stress levels.

For n-type semiconductor, equation [1.6] (see Chapter 1) applies:

$$\frac{1}{C_{sc}^2} = \frac{2}{\varepsilon_0 \varepsilon_r e N_D}(U - U_{fb} - \frac{kT}{e}) \qquad [1.6]$$

Here the dielectric constant of the passive film ε_r can be taken as 15.6 [34]. N_D can be determined from the slope of the experimental $1/C^2$ vs. U plots (Figure 4-10). The

calculated results are listed in Table 4-3. It can be seen that the presence of elastic tensile stresses results in a higher donor density in the passive films but the increment of N_D with the applied stress is not so pronounced.

Table 4-3. Calculated N_D for the passive films formed under different stresses.

Tensile Stress Level (MPa)	$N_D \times 10^{27}$ (/m^3)
0	4.1 ± 0.2
170 (~ 45% σ_y)	4.5 ± 0.3
240 (~ 64% σ_y)	4.9 ± 0.3

4.3.2.2 Influences of the Elastic Tensile Stress Applied During Passivation

During the experiment, the specimen was kept under potentiostatic control of -0.1 V. After 4000 seconds of passivation, when the steady-state passivation current was attained, a tensile stress of 170 MPa was applied to the specimen gently and slowly (attempting to avoid interference of the impact). The stressed specimen was continually passivated for 3600 seconds and then unloaded, to prepare for the application of another stress level. After that, passivation was continued for 1 hour and a tensile stress of 240 MPa was applied to the specimen, which was then passivated for another 1 hour. Figure 4-11 shows the changes of passive current density with time caused by the application of elastic tensile stresses.

Two interesting phenomena appeared in this experiment. First, a sudden increase in the current density was observed after loading the elastic tensile stress. The higher stress level caused a larger increase in the anodic current density. Secondly, the stressed electrode, especially at 240 MPa, displayed a higher passive current density at the stable stage than what would be produced by a stress-free specimen in the same passivation time.

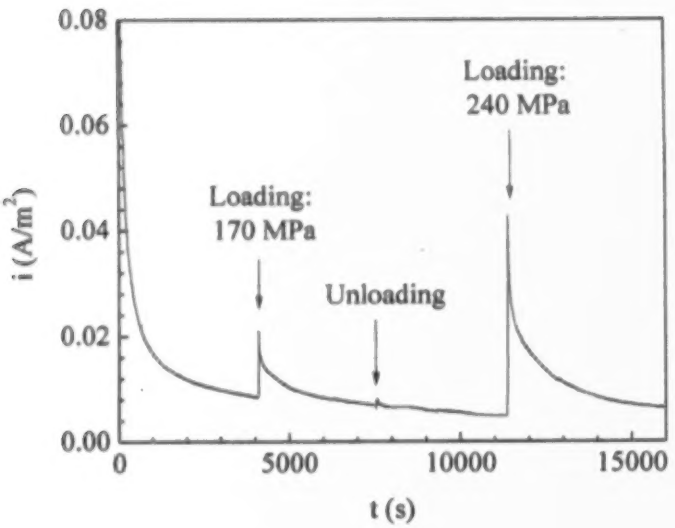

Figure 4-11. Passive current density vs. time curve for A516 carbon steel at -0.1 V in 0.5M $NaHCO_3$+0.01 NaCl solution. During passivation, elastic tensile stress was induced.

4.3.2.3 Influences of Elastic Tensile Stress on Passivity

In aqueous solutions, the competitive adsorption model[35] has been generally used to describe the formation and local breakdown of passive films on carbon steels. According to the model, aggressive ions (Cl^-) and inhibitive ions (HCO_3^-) compete for the adsorption sites on the metal surface. If the bicarbonate adsorption predominates, the following reactions could proceed:

$$Fe^{2+} + 2H_2O \longrightarrow Fe(OH) + 2H^+ \qquad [4.3]$$

$$Fe^{2+} + HCO_3^- \longrightarrow FeCO_3 + H^+ \qquad [4.4]$$

$$Fe(OH)_2 + HCO_3^- \longrightarrow FeCO_3 + OH^- + H_2O \qquad [4.5]$$

Therefore metastable films consisting of $FeCO_3$ and $Fe(OH)_2$ could form, and Fe^{2+} is finally oxidized to ferric oxide at the film formation potential.

The results from this experiment show that, with stresses applied before the film formation, the influence of the stress on the passivity of A516 steel was prominent in the beginning of the film formation process. As soon as the passive films attained the stable state, the effect became negligible. This can be explained as follows. At the initial stage of the film formation, the current densities of the electrode are mainly associated with the metal dissolution rate at the metal/solution interface. As discussed above, applied stress decreases the resistance of the metal to the anodic dissolution; therefore it could cause a noticeable increase in anodic current density in the beginning of the film formation process. Once the film has formed, the current densities of the electrode are now related to the transport rate of cations and anions in the passive film. Since the passive films are naturally formed on the stress-free and stress-loaded specimens at a constant film formation potential, it is safe to assume that the tensile stress applied before passive film formation only influences the chemical activity of the metal and the metal/film interface, and has little effect on the ion transportation rate in the passive film. Yet, another possibility may arise that the stress could result in a higher concentration of metal ions at the metal/film interface because the stress reduces the polarization resistance as shown in Table 4-2. This would lead to a small increment of current density and a higher donor (oxygen vacancies) density in the passive film, which is consistent with the experimental results obtained with the potentiostatic (Figure 4-9) and Mott-Schottky (Table 4-3) measurements.

With stresses applied during the passive film formation process, a noticeable influence of the stress on the passivity of A516 steel was also observed, as shown in Figure 4-11. However, the mechanism of such influence is different from that for the situation where stresses are applied before the film formation. After the formation of passive films, introduction of an elastic tensile stress caused a sudden increase in the current density, because the stress was also applied to the passive film as well as to the steel substrate at this time. For a passive film grown in 4000 seconds, a sharp increase in the passive current density means a local breakdown of the film. Previous research work[24, 36] showed that at a high tensile stress level, the applied stress affects the pitting

susceptibility through its influence on the mechanical integrity of the brittle protective films and the breakdown of passive films is a result of mechanical fracture or slip step emergence. Our experimental results initially show that even at a low elastic tensile stress level (~ 45% σ_y), the applied stress could cause local mechanical damage, or micro-breakdown, of the film. Moreover, the applied tensile stress would increase the quantity of point defects (*e.g.* vacancies) both in the metal and in the passive film on it, thereby facilitating the diffusion process. It was reported through thermodynamic analysis that, for vacancy type self-diffusion, the diffusion rate of ions and vacancies decreases with compressive stress and increases with tensile stress[37]. According to the point defect model (PDM), the n-type passive film on carbon steels belongs to the vacancy type self-diffusion. Therefore, a higher diffusion rate of ions in passive films would be present for the tensile-stressed A516-70 specimens than for the unstressed specimens. This simply accounts for the higher passive current densities observed at the steady state for the tensile-stressed specimens.

4.3.3 Effects of Elastic Tensile Stress and Hydrogen on Passivity

To study the possible synergistic effect of hydrogen and elastic tensile stress on the passivity of A516 steel, the specimens were initially charged with hydrogen at 80 A/m^2 for 1 hour and then the following measurements were performed.

4.3.3.1 Influences of the Elastic Tensile Stress Applied during Passivation

The current vs. time curves for hydrogen-containing passive films prepassivated at the potential of -0.1 V are shown in Figure 4-12. Compared with the current vs. time curves in Figure 4-9, it can be seen that hydrogen enhances the anodic current density greatly under all tensile stress levels. An increase of the passive current density with increasing applied stress level was again observed, similar to that of uncharged specimens, while a larger magnitude of increment appeared with the presence of hydrogen. The enhancing effect of elastic tensile stresses on the anodic current density for hydrogen-charged specimens after a long passivation time is more pronounced than that for the uncharged specimens. For example, at 5400 s, the increase of current densities for the charged specimen at 240 MPa is 0.007 A/m^2, while it is 7×10^{-4} A/m^2 for the uncharged specimen. It seems that a synergism of hydrogen and the elastic tensile

stress occurred. The results also imply that the synergistic effect become more noticeable with the increase in applied stress level.

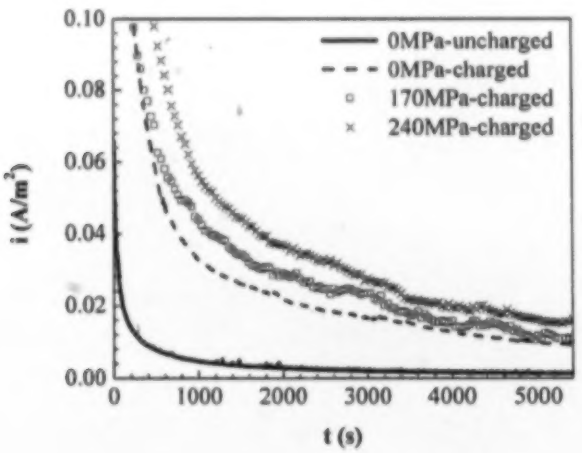

Figure 4-12. The current density vs. time curves for the passive films on charged and uncharged specimens passivated at - 0.1 V under various stress levels.

Figure 4-13 presents the Mott-Schottky plots obtained for the passive films formed on the hydrogen charged specimens under different tensile stress levels. The plots show linear dependence of $1/C^2$ on U within -0.2 ~ 0.1 V with positive slopes, indicating that the hydrogen-containing passive films are also n-type semiconductors. The N_D determined from the slope of the $1/C^2$ vs. U plots in Figure 4-13 are listed in Table 4-4. It is evident that for the hydrogen-containing passive films under all applied stress levels have a higher doping level than the hydrogen-free passive films, and an increase in N_D due to elastic tensile stresses is also observed. By comparing with the small enhancements induced by the elastic tensile stresses (see Table 4-3 and Table 4-4), the strong enhancing effect of hydrogen on the N_D overrules that of a relative low elastic stress level (*e.g.* 170 MPa). However, with a higher stress level, the N_D increased from 7.84×10^{27} m^{-3} in the absence of stress to 9.62×10^{27} m^{-3} for a stress of 240 MPa, indicating a synergistic effect of hydrogen and the elastic tensile.

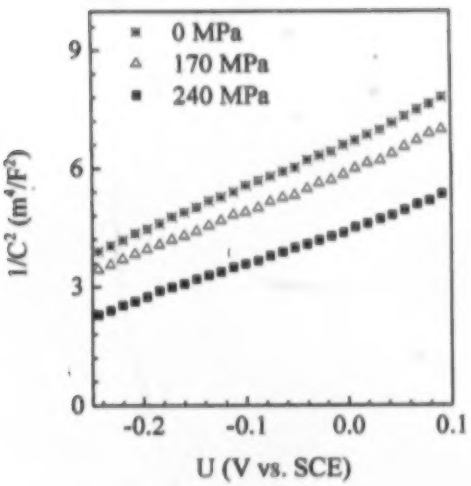

Figure 4-13. Mott-Schottky plots for the passive films on hydrogen-charged specimens formed at -0.1V for 1.5 h under various stress levels.

Table 4-4. Calculated N_D for the passive films on hydrogen-charged (80 A/m^2) specimens under different stresses.

Tensile Stress Level (MPa)	$N_D \times 10^{27}$ ($/m^3$)
0	7.8 ± 0.2
170 (~ 45% σ_y)	7.9 ± 0.4
240 (~ 64% σ_y)	9.6 ± 0.3

4.3.3.2 Influences of the Elastic Tensile Stress Applied During Passivation

Elastic tensile stresses were also applied to hydrogen charged specimens under potentiostatic control. Figure 4-14 shows the changes in the passive current density with time caused by the application of elastic tensile stresses for hydrogen charged specimens.

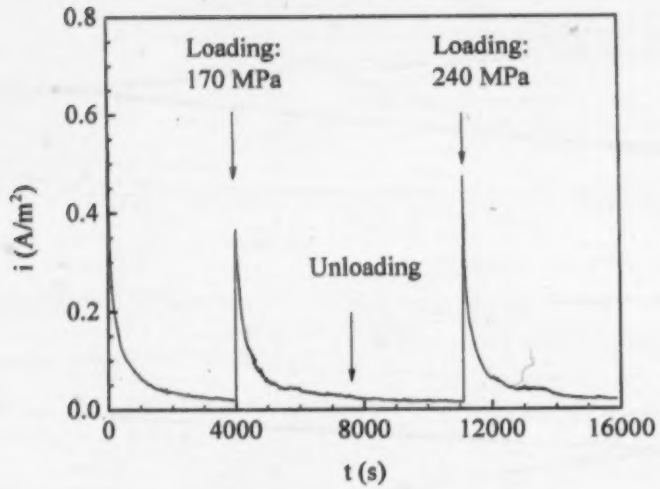

Figure 4-14. Passive current density vs. time for A516 steel sample (hydrogen charged at 80 A/m^2 for 1h) at -0.1 V in 0.5 M $NaHCO_3$+ 0.01 M NaCl solution.

It can be seen that a higher order of magnitude of the passive current density for hydrogen-charged specimens presented than that for the uncharged specimens. Sudden jumps in the current density were also observed, however, with a much larger magnitude than those for the uncharged cases, when the tensile stresses were applied gradually to the specimen. As shown in Figure 4-11 and Figure 4-14, a higher stress level caused a higher jump, and subsequently a higher steady state current value than that observed for an unstressed specimen with the same passivation time.

4.3.3.3 Influences of Elastic Tensile Stress and Hydrogen on Passivity

The enhancement of hydrogen to the passive current density of metals has also been found by other researchers[30, 38] and was already discussed in the preceding chapter. The enhancing effect may be attributed to the summation of the oxidation of hydrogen atoms migrating out of the passive film and the accelerated diffusion and dissolution of cations (Fe^{2+} and Fe^{3+}) and anions (O^{2-}) caused by hydrogen charging.

For charged specimen, as described in Chapter 1, hydrogen atoms would segregate around the surface defects in the metal, activating these regions. By applying elastic

tensile stress before passive film formation, some weak points on the surface of A516 steel could even experience micro-plastic deformation due to the internal stress caused by hydrogen. As a result, formation of more anodic active sites on the metal surface might occur, which eventually would enhance the oxidation ability of the steel. Moreover, the existence of hydrogen could cause a lattice expansion and thus fasters the diffusion of Fe^{n+} (n=2 or 3) ions and oxygen vacancies in the passive film formed on the pre-stressed specimens. Both the increased transport rate of cations and anions in the passive film and the increased oxidation rate of the metal, would contribute to the enhancement of the passive current density of the electrode. In other words, when applying elastic tensile stress before passivation, the synergism of hydrogen and stress results in a larger excessive concentration of Fe^{n+} (n=2 or 3) and oxygen vacancies at the metal/solution interface, resulting in a larger passive current density and a higher concentration of donor density in the passive film formed on the pre-stressed steel.

For a charged specimen with stresses applied after passive film formation, the influence of stress and hydrogen could be ascribed to the following factors. Firstly, a hydrogen-containing film would have less coherence force to the metal substrate and would more easily be damaged under the same stress level. This is the main reason for obtaining a much larger magnitude of sudden current jump as presented in Figure 4-14. Secondly, after film formation, an applied stress has a similar influence on the film to that of hydrogen, *i.e.* both hydrogen and stress enhance the oxidation ability of the metal substrate and the ion diffusion rate in the passive film. The combination of hydrogen and stress effect causes a higher current density than that observed in unstressed specimen with the same passivation time.

4.4 Summary

1) The applied elastic tensile stress could result in a more negative U_{OC} and a decrease in R_p of the electrode, and thereby increase the corrosion susceptibility of the A516 steel.
2) Before film formation, the application of elastic tensile stresses does not show a pronounced influence on the stable passive current density and donor density in the passive films. After film formation, the introduction of elastic tensile stresses could

result in a local breakdown of the passive film and consequently an increased current density.

3) A synergistic influence of hydrogen and applied tensile stress on the passivity of A516 steel has been observed. With increasing applied stress, the synergistic effect becomes more remarkable.

References

1. A. Desestret and R. Oltra, *Corros. Sci.*, **20**, 799 (1980).
2. M. Keddam and J. Vieira da Silva, *Corros. Sci.*, **20**, 167 (1980).
3. E. Smith, *Materials Science and Engineering*, **44**, 205 (1980).
4. C. R. Shastry, M. Levy and A. Joshi, *Corros. Sci.*, **21**, 673 (1981).
5. S. C. Tjong and N. J. Ho, *Surface and Coatings Technology*, **35**, 343 (1988).
6. J. R. Galvele, R. M. Torresi and R. M. Carranza, *Corros. Sci.*, **31**, 563 (1990).
7. R. N. Iyer and H. W. Pickering, *Annu. Rev. Mater. Res.*, **20**, 299 (1990).
8. R. M. Schroeder and I. L. Müller, *Corros. Sci.*, **45**, 1969 (2003).
9. A. W. Thompson, *Materials Science and Engineering*, **43**, 41 (1980).
10. Y. Hirose and T. Mura, *Engineering Fracture Mechanics*, **19**, 1057 (1984).
11. K. Sieradzki and R. C. Newman, *Journal of Physics and Chemistry of Solids*, **48**, 1101 (1987).
12. M. A. Eaglesham, J. U. Gaum and J. H. Bulloch, *Theoretical and Applied Fracture Mechanics*, **10**, 97 (1988).
13. R. C. Newman, *Corros. Sci.*, **33**, 1653 (1992).
14. D. D. Macdonald, *Corros. Sci.*, **38**, 1003 (1996).
15. M. R. Bayoumi, *Engineering Fracture Mechanics*, **54**, 879 (1996).
16. D. Delafosse and T. Magnin, *Engineering Fracture Mechanics*, **68**, 693 (2001).
17. A. Cigada, B. Mazza, P. Pedeferri, G. Salvago, D. Sinigaglia and G. Zanini, *Corros. Sci.*, **22**, 559 (1982).
18. R. L. Fullman, *Acta Metallurgica*, **30**, 1407 (1982).

19. M. P. Manahan Sr, D. D. Macdonald and A. J. Peterson Jr, *Corros. Sci.*, **37**, 189 (1995).

20. H. M. Chung, J. E. Sanecki, W. E. Ruther, A. Hins, N. J. Zaluzec and T. F. Kassner, *Journal of Nuclear Materials*, **239**, 61 (1996).

21. J. X. Li, W. Y. Chu, Y. B. Wang and L. J. Qiao, *Corros. Sci.*, **45**, 1355 (2003).

22. H. Iwanaga and T. Oki, *J. Soc. Mat. Sci. Jpn.*, **30**, 394 (1981).

23. S. J. Lennon, F. P. A. Robinson and G. G. Garrett, *Corrosion*, **40**, 409 (1984).

24. D. Chastell, P. Doig, P. E. J. Flewitt and K. Ryan, *Corros. Sci.*, **19**, 335 (1979).

25. F. Navaï, *J. Mater. Sci.*, **30**, 1166 (1995).

26. F. Navaï and O. Debbouz, *J. Mater. Sci.*, **34**, 1073 (1999).

27. F. Navaï, *Journal of Materials Science*, **35**, 5921 (2000).

28. V. Vignal, R. Oltra, M. Verneau and L. Coudreuse, *Materials Science and Engineering A*, **303**, 173 (2001).

29. Q. Yang and J. L. Luo, *Electrochimica Acta*, **46**, 851 (2001).

30. Q. Yang, J. G. Yu and J. L. Luo, *J. Electrochem. Soc.*, **150**, B389 (2003).

31. N. W. Ashcroft and N. D. Mermin, in *Solid State Physics*, p. 4, International ed., USA, (1990).

32. P. P. Craig, *Phys. Rev. Lett.*, **22**, 700 (1969).

33. A. Kiejna and V. V. Pogosov, *Phys. Rev. B*, **62**, 10445 (2000).

34. A. M. P. Simões, M. G. S. Ferreira, B. Rondot and M. da Cunha Belo, *J. Electrochem. Soc.*, **137**, 82 (1990).

35. E. McCafferty, *J. Electrochem. Soc.*, **137**, 3731 (1990).

36. R. B. Diegle and D. A. Vermilyea, *Corrosion (Houston)*, **32**, 411 (1976).

37. K. Tanahashi and N. Inoue, *J. Mater. Sci.: Materials in Electronics*, **10**, 359 (1999).

38. L. J. Qiao and J. L. Luo, *Corrosion*, **54**, 281 (1998).

Chapter 5 Conclusions and Future Work

5.1 Main Conclusions

The content of the previous chapters shows that the objectives stated in Chapter 1 have all been achieved. The main conclusions are summarized as follows:

1. The presence of hydrogen destabilizes the passive films on X70 and A516 steels and increases the susceptibility of the metals to localized corrosion.
2. The irreversible effect of hydrogen on the photoelectrochemical properties of the passive film on X70 steel has been discovered. Under the influence of hydrogen, the photoelectrochemical properties of the passive film on X70 steel may exhibit behavior different from what was indicated by other electrochemical responses of the system such as the passive current density. This implies that the effects of hydrogen on the optical and electronic properties of the passive film are very complicated and are not completely understood.
3. Tensile stresses lower than the yield strength have appreciable effects on the passive layer formation process and decrease the protectiveness of the film on the A516 steel. Synergistic effects of hydrogen and stress in the elastic deformation range on the corrosion behavior of the passive film on A516 steel were observed.

5.2 Suggestions for Future Work

1. The irreversible effect of hydrogen on the photoelectrochemical response of the passive film on X70 steel implies that the effects of hydrogen on the optical and electronic properties of passive film are really complex and puzzling. Future work is needed to find the mechanism of this effect.
2. Crucial mechanism responsible for the deleterious effects of hydrogen on the passive film on metals and alloys remains unsolved. A better knowledge is yet to be gained through further investigations on the synergism of hydrogen and stress, for example, by means of the photoelectrochemical measurements.

3. In light of the mechanism of hydrogen effects on the corrosion behavior of metals and alloys, efforts should be focused to find out effective methods to inhibit the hydrogen ingress into metals and alloys. Prospective techniques might be coatings or surface treatments that would impede the hydrogen evolution process.